Transactions

RRFM 2010

Marrakech, Morocco
21 -25 March 2010

organised in cooperation with:

IAEA
International Atomic Energy Agency
Atoms For Peace

© 2010
European Nuclear Society
Rue Belliard 65
1040 Brussels, Belgium
Phone + 32 2 505 30 54
Fax +32 2 502 39 02
E-mail ens@euronuclear.org
Internet www.euronuclear.org

ISBN 978-92-95064-10-2

These transactions contain all contributions submitted by 19 March 2010.

The content of contributions published in this book reflects solely the opinions of the authors concerned. The European Nuclear Society is not responsible for details published and the accuracy of data presented.

Poster Session

TRANSMISSION ELECTRON MICROSCOPY INVESTIGATION OF UAL_X BASED MTR FUEL

W. VAN RENTERGHEM, A. LEENAERS, S. VAN DEN BERGHE
Nuclear Materials Science Institute,SCK•CEN
Boeretang 200, B-2400 Mol, Belgium

ABSTRACT

High enriched, low density UAl_x dispersion fuel has been successfully used in research and test reactors for several decades. However, publications of detailed post irradiation examinations are limited. In this paper, a sample of a high enriched uranium fuel plate (90% ^{235}U enriched UAl_x fuel dispersed in an Al matrix), irradiated to a burn-up of 21% ^{235}U, is investigated with transmission electron microscopy. It is observed that the fuel became completely amorphous during irradiation. The Al matrix is found to remain crystalline and contains a large number of radiation induced defects. Neither in the fuel nor in the Al matrix, fission gas bubbles were observed.

1. Introduction

For high neutron flux conditions in research and test reactors like the BR2 reactor of SCK•CEN, high enriched, low density UAl_x dispersion fuel have been successfully used for several decades. The reason for their long-time use is the excellent behaviour of the fuel under irradiation [1]. Under normal reactor operating conditions, no significant deformations or swelling are observed in this type of fuel. However, very little has been published about the microstructure of irradiated fuel. More specifically, the fission gas behaviour is not described in detail.

UAl_x fuels are a mixture of UAl_2, UAl_3 and UAl_4 [1]. For a given uranium loading, UAl_2 would give the smallest volume of fuel particles, but it reacts at moderate temperatures with Al to form UAl_3 and UAl_4. UAl_3 will also react with Al to form UAl_4. Therefore the exact composition of the UAl_x fuel can change during fabrication and irradiation. The transformation to the UAl_4 phase results in a reduction of the volume and the formation of voids or porosities. It was reported that 4 - 11% of voids are formed in the fuel plate meat [1]. The fission of the U leads to a relative volume increase of $6.4\%/10^{21}$fiss/cm³, but it is reduced by the amount of meat porosity.

More recently, the aim of reducing the U enrichment to limit proliferation risks, triggered the development of high density fuels like U(Mo). It was, however, shown that the U(Mo)-Al dispersion fuel in flat plate configuration, is not stable under irradiation and that significant swelling occurs [2]. The cause of the swelling is related to the formation of an amorphous U(Mo)-Al interaction layer, which cannot retain the fission gas products and allows the formation of large voids [3,4] at the interaction layer (IL) and matrix interface.

For a better understanding of the fission gas and fuel behaviour, the microstructure of the well-behaving UAl_x fuels was investigated with transmission electron microscopy. The aim of the investigation is to determine how the fuel is affected by the irradiation and to understand why no agglomeration of fission gas into large bubbles at the IL-matrix interface occurs.

2. Experimental

The samples were retrieved from a high enriched Uranium fuel plate which was irradiated in the BR2 reactor of SCK•CEN during 3 irradiation cycles. The fuel reached a burn-up of 21% ^{235}U, which is 94.5% LEU equivalent burnup. The fuel consists of 90% ^{235}U enriched UAl_x ground fuel dispersed in an aluminium matrix. The meat is pressed between two layers of Al cladding. The uranium aluminide is fabricated from a melting and casting operation and as a result contains a mixture of UAl_3, UAl_4 and UAl_2. The exact composition was not determined, but, typically, it would be around 63% UAl_3, 31% UAl_4 and 6% UAl_2. As mentioned in the introduction, the UAl_2 phase is very reactive with Al and is probably transformed into a UAl_3 or UAl_4 phase during irradiation.

Due to a coolant flow blockage, two plates of a fuel segment had been locally exposed to a high temperature as described in [5]. For the current investigation, a section of the fuel plate was cut at a location away from the heat affected area and can be considered representative for the microstructural changes resulting from the irradiation of the UAl_x fuel. From the section, a thin slice was cut in cross-section and subsequently mechanically polished on SiC paper to reach a thickness of approximately 0.1 mm. Next, small specimens (length < 3 mm) were cut from the polished slice and glued on a golden grid. One of the specimens was electrochemically polished up to perforation.

After chemical polishing, the location of the holes was verified on a JEOL 6310 scanning electron microscope (SEM) equipped with an energy (EDS) and a wavelength dispersive X-ray spectrometer (WDS) for the determination of the local composition. Next the specimen was investigated with transmission electron microscopy (TEM) on a JEOL 3010 microscope.

3. Results

3.1 SEM-results

The specimen was first examined with SEM before and after electrochemical polishing. Figure 1a shows the specimen before electrochemical polishing. The small artefacts in the Al cladding, small particles and pits, result from the mechanical polishing. In the meat, a few voids or porosities are observed in the fuel kernels and at the kernel/matrix interface. Figure 1b shows an overview of the meat after electrochemical polishing and visualises the location of the holes. The mechanical polishing artefacts are removed. Two large and several smaller holes are formed in the meat, while the Al cladding remained largely unaffected. It cannot be excluded that the smaller holes correspond with the porosities observed in the fuel, but the two larger holes are definitely resulting from electrochemical polishing. The holes have preferentially formed within the UAl_x kernels, but at some locations also the Al matrix is present at the edges of a hole.

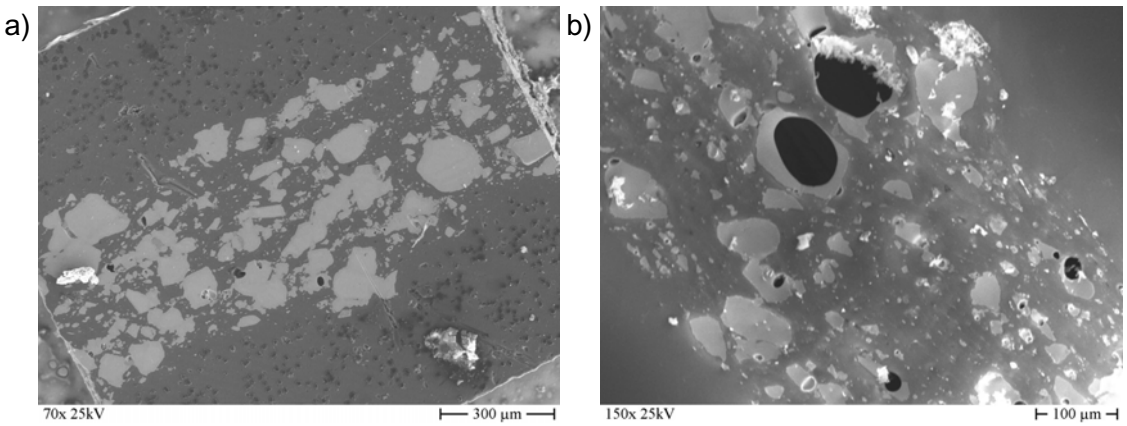

Fig. 1. SEM images of a) the specimen after mechanical polishing, showing the fuel kernels (light grey) in the Al matrix (dark grey) and b) the specimen after electrochemical polishing.

Figure 2 shows a secondary electron (SE) and a backscattered electron image (BSE) of one of the larger holes. The BSE image shows a lower intensity near the edge of a kernel compared to the middle of the kernel. This density contrast can be attributed to an increase in Al concentration. Leenaers et al. [5] reported that in the centre of the fuel kernel, the UAl_3 phase is dominant, whereas near the edge of the kernel, an interaction with the surrounding Al matrix has taken place, increasing the Al content to form the $U_{0.9}Al_4$ phase.

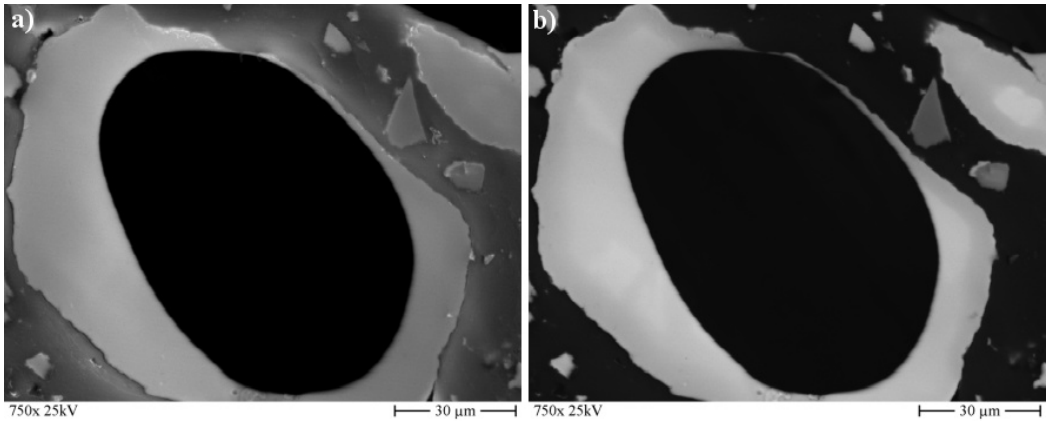

Fig. 2. a) SE image and b) BSE image of the UAl_x fuel kernel in which a hole is formed during electrochemical polishing.

The lateral distribution of the elements was verified qualitatively by EDS X-ray mapping. Apart from the main alloying elements U and Al, also the distribution of Xe was verified. Xe is one of the predominant fission products that tends to precipitate into fission gas bubbles which could induce swelling. Because of the relative low concentration and the overlap with peaks of other elements, the Xe X-ray map is obtained by WDS, which has a higher energy resolution and lower detection limit than EDS. The results of the mapping are shown in the false colour image of figure 3. The Al is shown in green, the U in blue and the Xe in red. The SE image is added to observe the correlation with the x-ray maps. From the elemental analysis, the results of the BSE image are confirmed: the core of the fuel kernel consists of U and Al and the matrix contains only Al. Near the interface between the fuel kernel and the matrix, an intermediate phase was detected containing a higher amount of Al. No quantitative data were recorded which allow the more precise identification of the different phases. Related to the Xe concentration, it was observed that in the core of the fuel kernel a fair amount of Xe is present, while a lower concentration was found in the interaction layer Around the fuel kernel, the typical fission product recoil zone can be observed and the halo at the interaction layer-matrix interface is also visible.

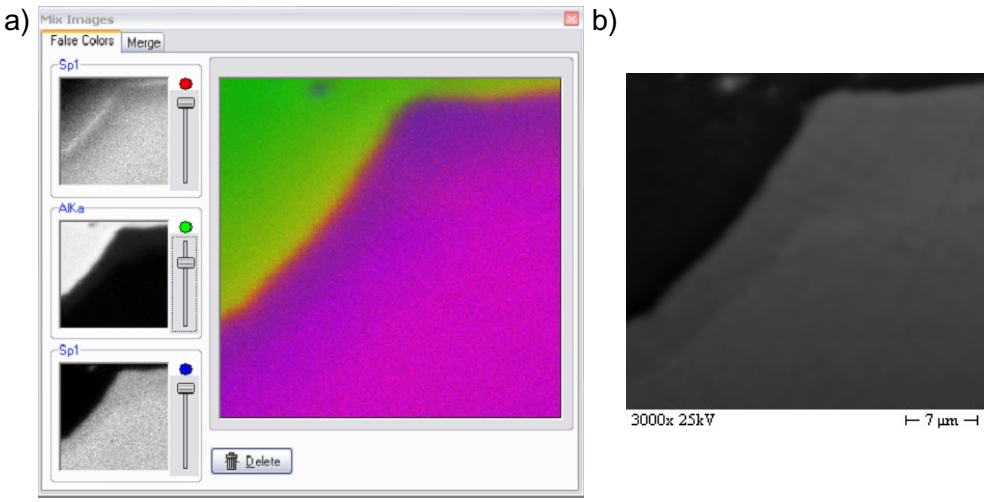

Fig. 3. a) False colour image showing the results of the EDS mapping of Al (green) and U (blue) and the WDS mapping of Xe (red). b) SE image of the analysed area.

The SEM results show that the fuel kernels remained intact under irradiation. The UAl_x phase is very brittle and the cracking of the fuel kernels in this fuel plate was reported [5]. It should be noted that the area with cracked kernels is located close to a defective area in the fuel plate which was exposed to temperatures up to 1000°C. Even though no indications of fission gas release were found there, thereby limiting the temperature below 560°C, the cracking can be related to thermal stresses resulting from heating to a temperature of a few 100°C. The SEM observations on this specimen prove that under normal operating conditions, where the temperature does not exceed 150°C, no cracks are formed in the fuel kernels.

3.2 TEM results

Figure 4a shows a typical dark field TEM image of the core of a fuel kernel and the inset shows the local diffraction pattern. Both the featureless nature of the dark field image and the diffuse ring in the diffraction pattern show that the core of the fuel kernel is amorphous. As the UAl_x alloy was crystalline before irradiation, these images prove that UAl_x becomes amorphous during low temperature irradiation.

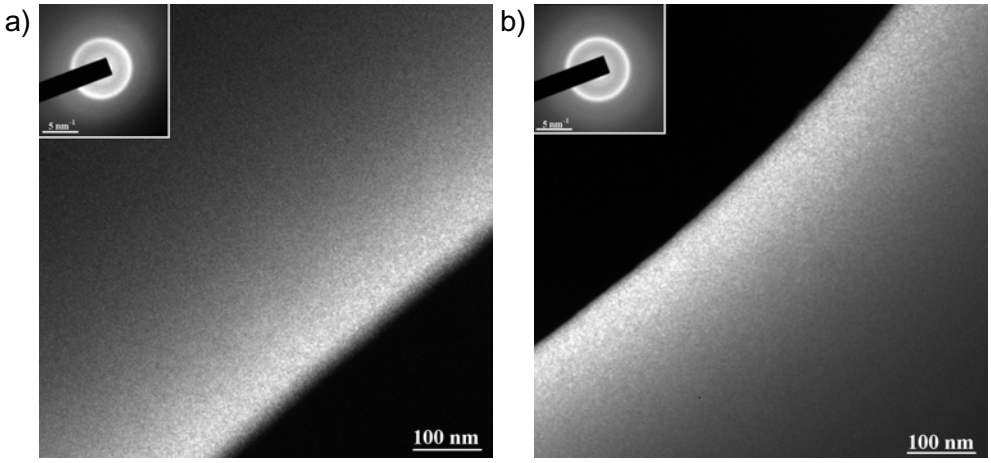

Fig. 4. Dark field images of a) the core and b) the edge of a UAl_x fuel kernel. The insets show the corresponding diffraction patterns, confirming the amorphous nature of the kernel.

Figure 4b shows a typical dark field TEM image recorded near the edge of the kernel well within the area attributed to the $U_{0.9}Al_4$ phase. The inset shows again the corresponding diffraction pattern. Again a featureless image is obtained and a diffuse ring is observed in the diffraction pattern. Similar to the core of a fuel kernel, also the interaction layer is amorphous.

Despite the amorphous nature of the material, the first ring in the diffraction pattern is still relatively sharp, indicating that even though the long-range order was destroyed, a high degree of short-range order remains. An estimate can be made about the nearest neighbour distance in the amorphous UAl_x fuel. The middle of the diffuse ring was taken as the average distance, limiting the precision of the measurement. For both the core of the fuel kernel and the interaction layer a value of 0.24±0.01 nm was obtained. If any variation of the nearest neighbour distance should occur in the fuel kernel, it is smaller than the precision of the measurement.

The transition of the core structure to the IL can not be retrieved from the TEM images. As both areas are amorphous, no changes in structure could be detected. Moreover, no contrast features were found in the bright and dark field images, even at the location corresponding with the intensity change in the BSE image.

The X-ray mapping of the specimen (figure 3) showed that fission gas products, like Xe, are still present in the fuel kernel. Because noble gases are insoluble in almost all materials, it was expected that the fission gases could be present in nanometer size bubbles, as has been shown to occur in irradiated U(Mo) dispersion fuel [3]. Figure 5 shows an under- and over-focus image from an area in the core of a fuel kernel. Small bubbles or voids are not visible in focused images, but give a Fresnel fringe when recorded out of focus. In the under-focus image, a bubble will show a white fringe and in over-focus, it will show a dark fringe. Similar images have been taken at different locations in the specimen, including areas in the interaction layer. No indications of the formation of nanobubbles could be found in any of the recorded images.

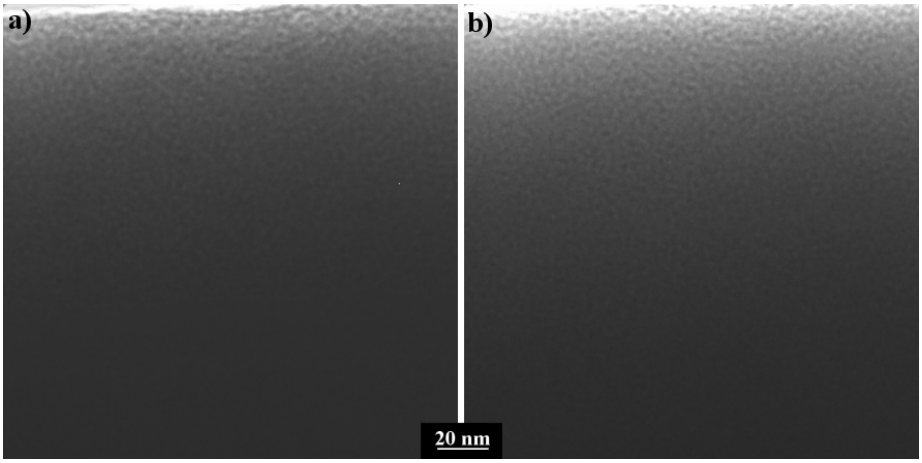

Fig. 5. a) Under-focus and b) over-focus bright field image of the core of a fuel kernel. No fission gas bubbles were observed.

In figure 6a, a dark field TEM image of the Al-matrix near the interface with a fuel kernel, i.e. in the recoil zone, is shown. Figure 6b shows the corresponding diffraction pattern of the matrix. It was found to agree with the crystal structure of Al oriented close to the [111] zone axis, which shows that the Al matrix remained crystalline. A large amount of radiation induced defects can be found. Because of their high number and the thickness of the crystal, most defects could not be characterized individually. However, the defects indicated by the letter D show a lobe contrast, which is typical for a dislocation loop. The defects that generally occur in irradiated crystals with a face centred cubic lattice are Frank loops, which have a Burgers vector of a/3⟨111⟩ and are lying in a {111} type of plane. Under the applied diffraction condition, the Frank loops with an a/3[111] or a/3[11-1] are extinct and only two sets of Frank loops are visible. The orientations of the lobe contrasts agree with loops lying in the (-111) and (1-11) planes.

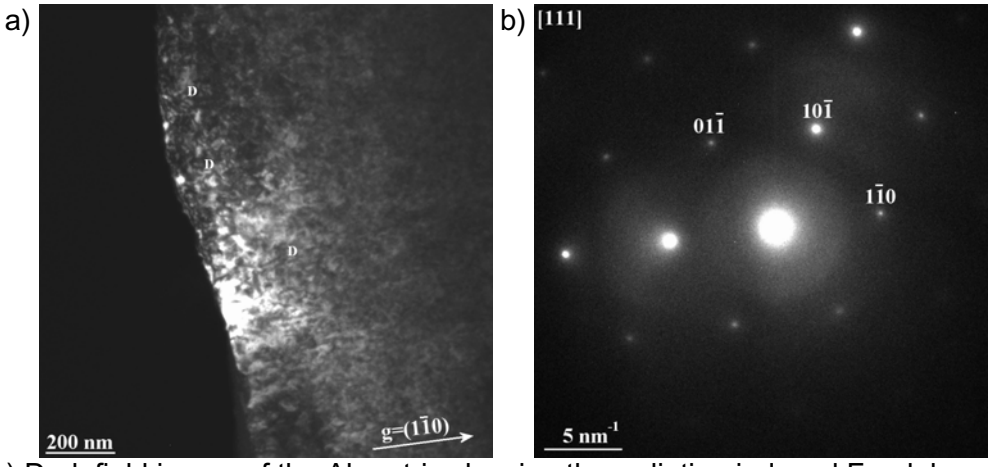

Fig. 6. a) Dark field image of the Al-matrix showing the radiation induced Frank loops (D). b) The corresponding diffraction pattern.

By recording out of focus images, it was verified if fission gas bubbles are present in the Al matrix. No bubbles could be found at any of the investigated locations.

4. Discussion

The main effect of the irradiation on the structure of the UAl_x fuel, is the amorphisation of the fuel kernels. Even though Hofman and Kim [6] mentioned that UAl_x would become amorphous under low temperature irradiation, these TEM results provide the first direct experimental evidence.

Many intermetallic compounds undergo amorphisation under low temperature irradiation, depending on the trade-off between the accumulation of radiation damage in the lattice and thermal annealing [7]. Once a critical dose is reached, the amorphisation is completed and the material remains amorphous under further irradiation. Whereas under thermal conditions the greatest degree of both short-range and long-range order, i.e. the crystalline phase, is the most stable phase, under irradiation it becomes progressively more difficult to maintain the long-range order and the greatest gain of energy comes from the establishment of short-range order. Therefore, a high degree of short range order is still expected in the amorphous material, which agrees with the still relatively narrow ring in the diffraction patterns of figure 4. The critical dose remains fairly constant with increasing temperature until thermal annealing processes are activated and the critical dose increases rapidly. Above the critical temperature, no amorphisation occurs anymore. Both the critical dose and temperature depend on the composition of the intermetallic, but also on the type of irradiation and dose rate.

In intermetallic fuels, the fission of U atoms and the resulting heavy ion bombardment of the material by the fission products (~80 MeV/ion) is an important source of radiation defects. Birtcher et al. [8] reported the amorphisation of U_3Si_2 fuel under low temperature irradiation conditions. They found a critical dose of 0.38 dpa (1.1×10^{23}f/m³) and a maximal irradiation temperature for complete amorphisation of 250°C. The critical dose and temperature were not reported for UAl_x, but the TEM investigation has proven that both the irradiation temperature and dose of this sample are well within the range of amorphisation.

The main question remains: what happened with the fission gas products. It is known that fission gases are not soluble in almost any kind of material and that the agglomeration of these gases induces the formation of bubbles which can cause breakaway swelling of the fuel plate. The X-ray analysis by WDS and EDS showed that Xe, which is the dominant fission gas, is homogeneously distributed in the core of the fuel kernel. In the interaction layer, where an increased Al content was stated, there was a slight decrease of the Xe signal and a local increase was measured again at the interface with the Al matrix (sweeping effect). It was found in the TEM investigation that no large nor nanosize bubbles were present. It can therefore only be concluded that the fission gases are still in solid solution in the amorphous fuel kernel.

He gas implantation experiments in glass samples have shown that noble gas bubbles are grown in amorphous materials, but only after a threshold concentration is reached [9]. Because both the noble gas and the matrix material are different, a comparison with the fission gas density is not exact, but it can be calculated that the fission gas density is indeed lower than this threshold. The authors explain this threshold by supposing that the gas bubbles only start to grow when the available void in the amorphous material is filled with fission gas. In the UAl_x fuel, the transformation of UAl_2 and UAl_3 to UAl_4 is accompanied by a volume reduction of 0.3% [1]. This volume reduction provides a large amount of empty space that can be filled with fission products thereby avoiding the formation of large fission gas bubbles.

The large amount of empty space is reflected in the swelling data. The swelling ($\Delta V/V$) due to the increased volume of the fission products is given by [1]:

$$(\Delta V/V)\% = 6.4\% F/10^{21} \text{ fiss/cm}^3 - V_p$$

Where F is the fission density (10^{21}/cm³ of meat) and V_p is the meat porosity (%). From swelling data from spent fuel elements an empirical relation was deduced:

$$(\Delta V/V)\% = 2.6\% F/10^{21} \text{ fiss/cm}^3$$

Even though fuel elements with more open porosity show lower swelling, there is no threshold fission density and swelling starts before the open porosities are filled with fission products. On the other hand, the much lower swelling rate in the empirical relation indicates that the gas atoms are not agglomerating and remain in solid solution.

This result is somewhat in contradiction with the observations in irradiated U(Mo) dispersion fuels [3,10]. In that kind of fuel, the fuel kernels remain crystalline, but an amorphous interaction layer between the fuel and the Al matrix is formed. In the fuel kernel a regular lattice of nanosize bubbles was observed, which is considered beneficial for the fuel swelling. The amorphous interaction layer, however, did not show good gas retention and the fission gases agglomerate in large porosities at the interface with the Al matrix. The bad swelling behaviour of the U(Mo) dispersion fuel is attributed to the amorphous nature of the interaction layer. Even though the composition of the interaction layer is, apart from Mo, comparable to the UAl_x fuel, the different formation mechanism apparently did not provide the necessary open volume to accommodate the fission gas products or the presence of Mo has an important influence on it. The latter is not impossible based on existing data on the dependence of metallic glass properties on composition, like, for example, the difference in swelling behaviour between U_3Si and U_3Si_2. On the other hand, the knowledge that nanometer size bubbles already exist in the crystalline U(Mo) also means that, as the U(Mo) is consumed by the formation of the interaction layer, the nanobubbles will have to be accommodated by the interaction phase. As they can no longer be maintained in an ordered lattice, due to lack of a host lattice, they may agglomerate into the voids observed at the interface IL/matrix.

5. Conclusions

A sample of a high enriched uranium fuel plate (90% ^{235}U enriched UAl_x fuel dispersed in an Al matrix), irradiated to a burn-up of 21% ^{235}U, was investigated with transmission electron microscopy. It is observed that the fuel has completely become amorphous during irradiation. Considering the irradiation dose and temperature and the general behaviour of intermetallics under irradiation, the amorphisation of the fuel could be expected. The short range order is well preserved and a nearest neighbour distance of 0.24 ± 0.01 nm was measured. The Al matrix remains crystalline and contains a large number of radiation induced defects.

Neither in the fuel nor in the Al matrix, fission gas bubbles were observed. This observation indicates that the fission gas products are still in solid solution in the amorphised fuel. The formation of porosities possibly resulting from the transformation of UAl_3 into UAl_4 probably accounts for the take-up of the fission gas thereby avoiding the formation of large fission gas bubbles, which would cause break-away swelling.

6. References

[1] J.M. Beeston, R.R. Hobbins, G.W. Gibson, W.C. Francis, Nucl. Technology, **49** (1980) 136-149.
[2] A. Leenaers, S. Van den Berghe, E. Koonen, C. Jarousse, F. Huet, M. Trotabas, M. Boyard, S. Guillot, L. Sannen, M. Verwerft, J. Nucl. Mater. **335** (2004), 39-47.
[3] S. Van den Berghe, W. Van Renterghem, A. Leenaers, J. Nucl. Mat., **375** (2008) 340-346.
[4] G. L. Hofman, M.R. Finlay, Y.S. Kim, in Proceedings of the 26th International meeting on Reduced Enrichment for Research and Test Reactors (RERTR), Vienna, Austria, (2004).
[5] A. Leenaers, F. Joppen and S. Van den Berghe, J. Nucl. Mater. **394** (2009), 87-94.

[6] G.L. Hofman, Y.S. Kim, Nucl. Eng. & Tech. **37** (2005) 299-308.
[7] A.T. Motta, J. Nucl. Mater. **244** (1997) 227-250.
[8] R.C. Birtcher, J.W. Richardson, M.H. Mueller, J. Nucl. Mater. **230** (1996) 158-163.
[9] G. Knuyt, M. D'Olieslaeger, L. De Schepper, L.M. Stals, Mater. Sci.& Eng. **98** (1988) 523-525.
[10] W. Van Renterghem, A. Leenaers, S. Van den Berghe, in Proceedings of the 31st International Meeting on Reduced Enrichment for Research and Test Reactors (RERTR), Beijing, China, (2009).

POWDERING DUCTILE U-Mo ALLOYS FOR NUCLEAR DISPERSION FUELS

M. DURAZZO, C.J. ROCHA, J. MESTNIK FILHO, R.M. LEAL NETO
Nuclear and Energy Research Institute - IPEN-CNEN/SP
Av. Prof. Lineu Prestes 2242, 05508-000 São Paulo – Brazil

ABSTRACT

For the last 30 years high uranium density dispersion fuels have been developed in order to accomplish the low enrichment goals of the Reduced Enrichment for Research and Test Reactors (RERTR) Program. Gamma U-Mo alloys, particularly with 7 to 10 wt% Mo, as a fuel phase dispersed in aluminum matrix, have shown good results concerning its performance under irradiation tests. That's why this fissile phase is considered to be used in the nuclear fuel of the Brazilian Multipurpose Research Reactor (RMB), currently being designed. Powder production from these ductile alloys has been attained by atomization, mechanical (machining, grinding, cryogenic milling) and chemical (hydriding-dehydriding) methods. This work is a part of the efforts presently under way at IPEN to investigate the feasibility of these methods. Results on alloy fabrication by induction melting and γ-stabilization of U-10Mo alloys are presented. Some results on powder production and characterization are also discussed.

1. Introduction

This research is part of the efforts under way at National Commission for Nuclear Energy (CNEN), and particularly at IPEN (Nuclear and Energetic Research Institute) for the construction of the Brazilian Multipurpose Research Reactor (RMB), currently been designed.

Gamma U-Mo alloys have been for long considered as fuel phase in research and test reactors using dispersion fuel in aluminium matrix [1]. Promising results concerning performance under irradiation tests of U-Mo alloys, especially with molybdenum content ranging from 6 to 10 wt.% Mo [2], have encouraged us to consider this fuel phase for the second stage of the reactor operation, since uranium silicide compound, U_3Si_2, already produced here, will be used at first.

As a fuel based on dispersion concept U-Mo alloys must be used in powder form. At least three main fabrication routes for U-Mo powders could be listed: atomization (mainly centrifugal atomization by rotating disk method [3] or even rotating electrode process [4], mechanical comminution, i.e., machining or grinding [5,6], and chemical comminution, i.e. hydride-dehydride process, also known by its acronym HDH [7-10]. HDH of gamma U-Mo alloys can be accomplished by heating the alloy at temperatures where it decomposes in two phases, i.e. alpha and gamma' (U_2Mo). Since alpha uranium is easily hydrated, generating a very fine powder, its content must be carefully controlled (changing soaking time) in order to obtain particles within the desired size range. A variation of the last route, named HMD, combines hydriding-dehydriding with milling process [11]. According to the authors, gamma U-Mo alloys can form a U-Mo hydride (A-15 structure) that embrittles the alloy, but not intensively, so powder could only be produced by interposing a milling operation, before dehydriding.

Each one of the previous routes are held by commercial or potential suppliers based on features like particle size range yield of the powder, costs, and the more important one, irradiation behaviour. Since there are some controversial arguments, an investigation at local process conditions is necessary to find the best technological solution.

The focus of this preliminary work is to compare the characteristics of U-Mo alloy powders (10 wt% Mo) fabricated by two routes: mechanical grinding and HMDH. In this particular case, HMDH stands for hydrogenation-milling-dehydrogenation, since a hydride phase was not formed. It was reported before that gamma U-Mo alloys (particularly U-10wt%Mo) suffered a loss of ductility when submitted to a hydrogen atmosphere, by incorporating hydrogen interstitially [12]. This fact was used here to provide enough brittleness to the alloy to allow comminution by high-energy ball milling. Details of both procedures are given elsewhere.

2. Experimental

Ingots of U-Mo alloy with 10 wt% Mo were induction melted into a magnesia-stabilized zirconia crucible. Metallic uranium and metallic molybdenum were used as raw materials. Metallic uranium was home produced through magnesiothermic reduction [13] and the metallic molybdenum was supplied with 99.95% purity, as small cylinders with 3 mm in diameter and 3 mm in height. Both materials were charged inside the zirconia crucible and heated by induction under high-purity argon atmosphere up to melting. Melting temperature was maintained for 3 minutes providing homogenization, than the furnace was turned off allowing the alloy to be solidified inside the crucible. The solid material was a cylindrical piece with near 40 mm in diameter and 50 mm in height, weighting around 1200 g with a density of 16,87 g/cm^3. The ingot was treated at 1000°C for 72 hours under pure argon and quickly cooled for retention of the gamma phase. It was cut in pieces for studding the two routes for powder preparation, namely mechanical grinding (MG) and hydrogenation-milling-dehydrogenation (HMDH).

For the mechanical grinding route, the powder was produced by using high-speed grinding (15000 rpm) with diamond abrasive wheel. The abrasive wheel was 4 mm in diameter, having impregnated diamond particles with mean diameter of about 100 μm. Grinding was accomplished inside a glove-box under protective argon atmosphere.

For the HMDH route, small pieces were taken from the U-Mo ingot (with approximately 10x50x5 mm in thickness) and were individually heated at 400°C for 3 hours under high purity hydrogen (99.9999%) at 3 bar. A Sievert type apparatus were used and no measurable hydrogen intake could be noticed, with the pressure gauge used (precision of 0.5 bar). At this temperature and time, alpha phase is not supposed to be formed, since about 40 hours would be necessary to start the gamma decomposition according to published TTT diagram [14]. Next the pieces were manually crushed in a stainless steel mortar. The resulting granules were 3 mm in length. For comparison, crushing of pieces not hydrogenated treated was carried out but not succeeded due to ductile behaviour of the parts. This was taken as an indication that some hydrogen intake must be occurred in former pieces. U-Mo granules were milled in a planetary ball mill at 400 rpm for 10 hours, with ball-to-powder weight ratio of 20:1. The vial and the balls were made from hardened steel. Loading and opening of the vial occurred inside a glove-box with protective argon atmosphere. After milling the powder was heat treated under vacuum at 400°C for dehydrogenization.

X-ray diffraction was conducted on pieces of the heat treated ingot using Cu-Kα radiation. Powder particles were characterized by SEM analysis and also optical microscopy using image analysis for size distribution. For optical microscopy powder samples were dispersed over a glass thin plate. The images were taken by transmitted light which allows enough

contrast for visualization. For each type of powder, measurements were carried out in 3 samples, accomplishing 24 image fields and at least 6000 particles. The smallest dimension between two tangents of the particles projection was considered for measurement (minimum Feret's diameter). This was done in order to reproduce the results that would be obtained by sieving analysis, since the powder mass produced was not enough to perform sieving in a reliable manner. By sieving, the second higher dimension of each particle is actually measured (which is able to pass trough the sieve openings), corresponding in this particular case to the minimum Feret's diameter (on doing this it is assumed that the thickness of the particles was not measured in projected images).

3. Results and Discussion

Figure 1 shows the diffraction pattern from U-Mo ingot after heat treatment. BCC gamma phase was the major phase with some unidentified peaks of minor phases. The relative intensity of the (100) reflection from gamma phase should be the highest one, which indicates that some texture is still present. In spite of that, the heat treatment was considered suitable for the purpose of this preliminary investigation.

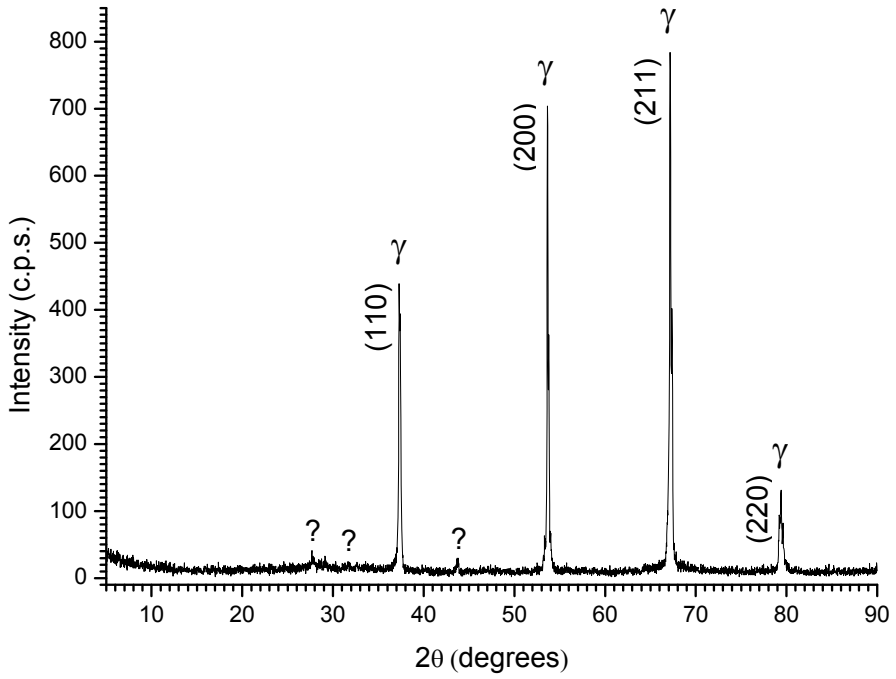

Figure 1 – Diffraction pattern of the U-10wt%Mo alloy showing BCC gamma phase.

Figure 2 shows the morphology of the powders prepared by both routes, mechanical grinding (MG) and hydrogenation-milling-dehydrogenation (HMDH). It was observed that the powder prepared by MG route (left column in Fig. 2) presents particles with acicular and flake shapes, while the particles from HMDH route (right column in Fig, 2) are more regular and equiaxial. Particle size distribution curves along with optical micrographs from both powder production routes are shown in Figure 3. The powder prepared by MG route presented particles sensibly larger than the ones prepared by the HMDH route. The mean particle size (50 wt%) was about 50 μm for MG powder and 100 μm for HMDH powder. Furthermore HMDH powder particles fits very well the size requirements of dispersion fuels,

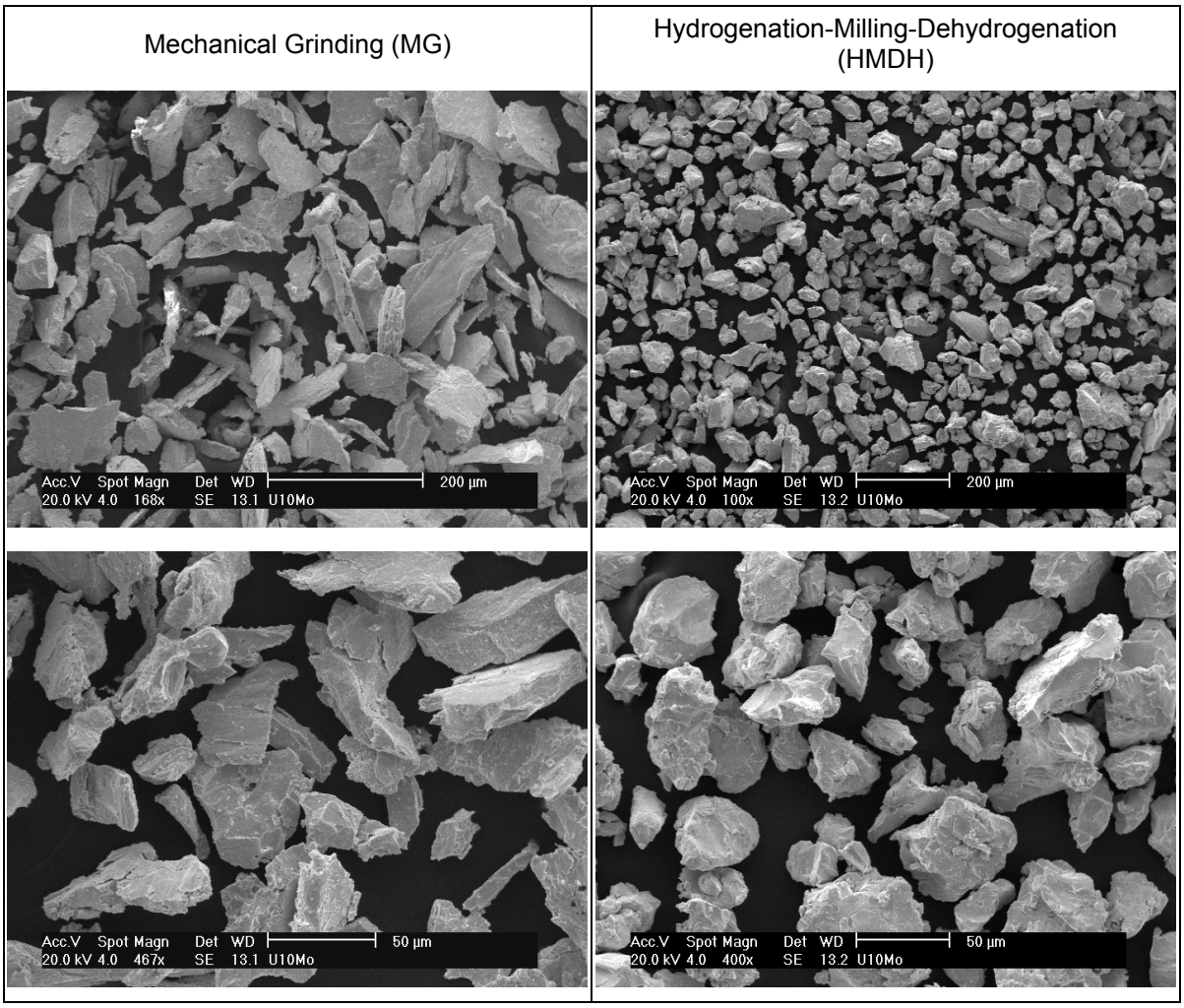

Figure 2 – Scanning electron micrographs of powder particles from both investigated routes.

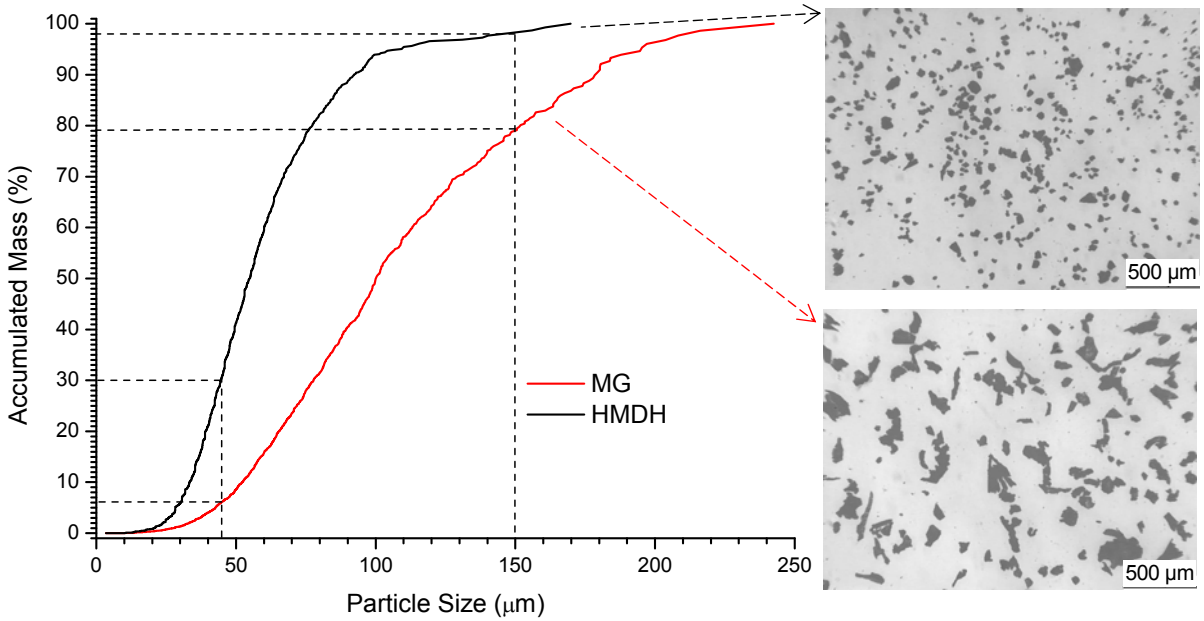

Figure 3 - Particle size distribution curves for the powders prepared by mechanical grinding route (MG – red curve) and hydrogenation-milling-dehydrogenation route (HMDH – black curve).

with practically 100 wt% below 150 μm and about 30 wt% below 45 μm, while MG powder particles were shown to be larger, with more than 80 wt% above 150 μm. Other important difference was the aspect ratio of the particles (maximum to minimum Feret's diameters). The aspect ratio reached 10 for the MG powder, much higher than the maximum ratio measured for HMDH powder, close to 4.

4. Conclusions

Despite the preliminary character of this work, the results indicate the technical feasibility for producing powders from both investigated routes. The control of variables of the MG route, as the size of the diamond granules of the abrasive wheel, the pressure of the tool under the alloy surface and the rotation of the grinding wheel machine, should promote the necessary adjustment in the particle size distribution. Powder produced by the HMDH present a particle size distribution compatible to be used as a dispersion fuel. Further work is necessary to increase the yields in order to evaluate both process routes as real technological alternatives for nuclear fuel powder production to research reactors.

5. Acknowledgements

The authors want to express their appreciation to the staff of IPEN for their cooperation during this phase of the project. The authors are also grateful to CNEN and FAPESP for the financial support.

6. References

[1] Snelgrove, J.L. *et al.*, "Development of very-high-density low-enriched-uranium fuels" Nuclear Engineering and Design, 1997, v. 179, pp. 119-126.
[2] Hofman, G. L. *et al.*, "Progress in development of low-enriched U-Mo dispersion fuels", RRFM Meeting, 2002.
[3] Kim, K. H. *et al.*, "Characterization of U-2 wt% Mo and U-10 wt% Mo alloy powders prepared by centrifugal atomization", J. Nuclear Materials, 1997, v. 245, pp. 179-184.
[4] Clark, C. R. *et al.*, "Production and characterization of atomized U-Mo powder by the rotating electrode process", RERTR Meeting, 2007.
[5] Clark, C. R. *et al.*, "Fuel powder production from ductile uranium alloys", RERTR Meeting, 1998.
[6] Vacelet, H. *et al.,* "Irradiation of full size UMo plates" RERTR Meeting, 1999.
[7] Balart, S. *et al.*, "U-Mo alloy powder obtained by a hydride-dehydride process", RERTR Meeting, 2000.
[8] Solonin, M. I. *et al.*, "Development of the method of high density fuel comminution by hydride-dehydride processing", RERTR Meeting, 2000.
[9] Oliveira, F. B. V. *et al.*, "Powder formation of γ uranium-molybdenum alloys via hydration-dehydration", RERTR Meeting, 2007.
[10] Olivares, L. *et al.*, "Powder production of uranium - molybdenum - metal alloys applying hydride - dehydride methodology" RERTR Meeting, 2008.
[11] Pasqualini, E. E. *et al.*, "Powder production of U-Mo alloy, HMD process (hydriding-milling-dehydriding)", RERTR Meeting, 2002.
[12] Powell, G. L. *et al.*, "Internal hydrogen embrittlement of gamma-stabilized uranium alloys", Corrosion-Nace, v. 32, n. 11, pp. 442-450, 1976.
[13] Durazzo, M. *et al.*, "Current status of U_3Si_2 fuel elements fabrication in Brazil". RERTR Meeting, 2007.
[14] Van Thyne, R.J. and McPherson, D. J., "Transformation kinetics of uranium-molybdenum alloys", Transactions of the ASM, vol. 49, pp. 598-619, 1957.

QUANTITATIVE DETERMINATION OF CRYSTALLINE PHASES IN THE SILICIDE FUEL BY THE RIETVELD METHOD

C.T.KNIESS[1], E.F.U.CARVALHO[1], M.DURAZZO[1], H.G.RIELLA[1,2,3],

[1] *Nuclear and Energy Research Institute - IPEN/CNEN*
[2] National Institute of Science and Technology for
Inovating Nuclear Reactor-INCT
Nuclear Fuel Center
Av. Prof. Lineu Prestes, 2242 – Cidade Universitária
CEP 05508-000, São Paulo – SP – Brazil

[3]*Chemical Engineering Department - Federal University of Santa Catarina*
Campus Universitário – Trindade
CEP 88040-970, Florianópolis – SC - Brazil

ABSTRACT

Uranium silicide has been used as nuclear fuel in modern research reactors. The nuclear fuel is based on a dispersion of uranium silicide and aluminum powder to form a fuel meat fabricated according to powder metallurgy techniques. The U_3Si_2 powder should attend technical specifications referring to the major crystalline constituent, which must be more than 80 wt% of U_3Si_2. IPEN/CNEN-SP currently produces the U_3Si_2-Al fuel to supply the IEA-R1 research reactor, which operates at 3.5 MW in order to produce primary radioisotopes used in nuclear medicine. The uranium concentration in the fuel should be increased from 3.0 gU/cm^3 to 4.8 gU/cm^3 in order to guarantee future fuel supplying for a new research reactor designed for radioisotope production, the Brazilian Multipurpose Research Reactor – RMB, which is planned to be constructed in the country. The new fuel will operate under much more severe conditions than the ones found currently in IEA-R1 reactor. So, the increasing of uranium concentration into the fuel requests urgent development of a new technology to qualify the uranium silicide powder produced by IPEN-CNEN/SP, referring to the characterization of crystalline phases. This paper describes a methodology developed to quantify crystalline phases in the silicide fuel powder, which is based in the Rietveld method for crystalline structures refinement.

1. Introduction

The IEA-R1 Reactor of IPEN/CNEN-SP is a pool type reactor operating since 1957. This reactor uses MTR type dispersion fuel element in a 5 X 5 core arrangement. The Nuclear Fuel Center of IPEN is responsible for the production of the necessary nuclear fuel to keep the continuous operation of the reactor. Development of new fuel technologies is also a permanent concern. The Nuclear Fuel Center had produced 77 fuel elements until now, including 14 control fuel elements.

The program for silicide fuel development at IPEN had great impulse after the approval of the IAEA TC BRA/4/047 “Fuel Improvement for the IPEN Research Reactor” in 1999. The primary purpose of this program was to develop the whole fabrication process of U_3Si_2-Al dispersion fuel plate (including 4.8 gU/cm^3), its irradiation test at the IEA-R1 reactor and post-irradiation analysis. This project proposal would give the necessary background to IPEN to produce and qualify its own U_3Si_2 powder and silicide based on dispersion fuel plates for the IEA-R1 fuel element fabrication. The project steps to achieve the objectives included the following steps:

a) to develop the process for producing UF_4 starting from UF_6;

b) to develop the process for producing metallic uranium starting from UF_4;
c) to develop the process for producing U_3Si_2 powder;
d) to produce miniplates with 20% enrichment for irradiation tests;
e) to irradiate miniplates at the IEA-RI reactor and to perform non-destructive analysis on the irradiated fuel miniplates inside the spent fuel pool.

Figure 1 shows a flow-sheet of the main project activities. More information of the project activities and results are available in the Project Progress Reports [1,2,3].

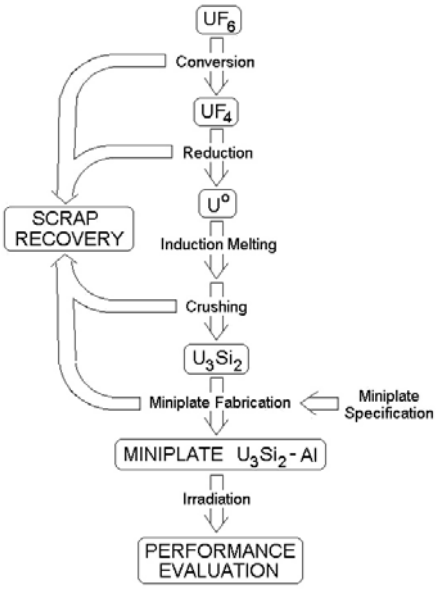

Figure 1: Main BRA/4047 Project activities.

Since 2000, the Nuclear Fuel Center of IPEN has been dedicating great efforts to achieve expertise in production of intermetallic alloy U_3Si_2. After facing some difficulties, as reported previously [4], in 2004 IPEN has arrived to the full experimental route to produce, in production scale, the necessary alloy for nuclear fuel.

From the produced uranium ingot, the metal was melted inside an induction furnace with silicon addition, with an adequate vacuum instrumentation and facilities for handling and melting uranium and uranium alloys. The zirconia crucible was specially designed to reach temperatures higher than 1750°C and to support the aggressive environment created by uranium chemical attack. The load arrangement inside the crucible was studied to help the sequence of melting in the several stages of that molten alloy, before reaching the final intermetallic composition, as shown in figure 1. More than 20 trials were carried out, using natural uranium, before the first LEU U_3Si_2 were successfully made. It was produced 3 enriched U_3Si_2 melting in 2005, which consisted the first own produced load of fuel plate fabrication in IPEN. In general terms, the quality of this intermetallic has fully met the needs postulated by the requirements for a routine nuclear material.

In relation to U_3Si_2 powder to IEA-R1 reactor fuel plate, technical specification requires that the bigger crystalline component of uranium silicide should be U_3Si_2 (>80% in weight). Inside this context, this paper aims to analyze uranium silicide nuclear fuel produced by IPEN/CCN in relation to recommended technical specifications, especially regarding crystalline phases percentage. To develop methodology to quantify uranium silicide fuel crystalline phases, the method developed by Hugo Rietveld will be used [5].

Rietveld developed a method to refine structures, based on the comparison between a calculated diffraction pattern and the observed one, which has been extended after to be

applied in the quantitative phases analysis and micro-deformation studies. The Rietveld Method considers crystallographic theoretical data (crystalline system, spatial group, atomic positions, system parameters, occupation number and isotropic temperature factor) of crystalline phases. The calculated pattern is obtained using the single cell as a basis. This calculated pattern is, so, compared to the observed pattern and the model parameters are adjusted by the minimum square method [6].

2. MATERIALS AND METHODS

U_3Si_2 powder analyzed was produced by Centro de Combustível Nuclear (CCN) of Nuclear and Energy Research Institute - IPEN/CNEN.

X Ray diffraction analysis of the silicide fuel were obtained with a Philips X´Pert equipment, (λ = 1,54 Å) through the powder method. Analyses were done with 0,01°/ 5s and 2θ from 10 to 90° (2 Theta).

Crystalline phases were identified based on JCPDS database [7]. In order to obtain the crystallographic data, necessary to the structural refinement through the Rietveld Method, it was used the ICSD [8].

The used refinement program was the DBWS 98. DMPLOT program made possible the comparison between the theoretical spectrum and the refined one.

3. RESULTS AND DISCUSSION

Figure 2 shows U_3Si_2 powder samples difracction. Identified crystalline phases were: U_3Si_2 (ICSD 31626) and $USi_{1,0147}$ (ICSD 81561). The Input data to the refinement by the Rietveld Method are presented in Table 1.

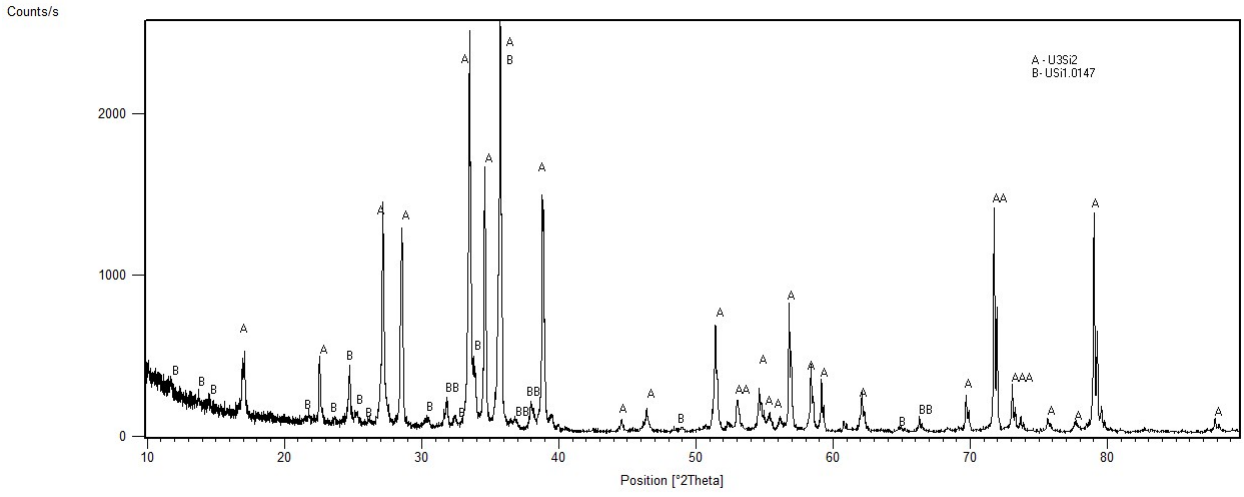

Figure 2: X ray patterns of U_3Si_2 powder.

Table 1: Crystallographic theoretical data of crystalline phase present in silicide fuel.

Crystalline Phases	Lattice parameters (Å)	Atomic Position	Occupation Number	Thermal Isotropic Factors (B_o)
	a = b = 7.3299	U1(2a), x = 0.0 y = 0.0, z = 0.0	U1 (2a) = 1.0	B_o (U1) = 0.5

U_3Si_2 ICSD 31626 P 4/m b m (127) Tetragonal	c = 3.9004 $\alpha = \beta = \gamma = 90$	U2(4h), x = 0.181 y = 0.681, z = 0.5 Si1(4g), x = 0.611, y = 0.111, z = 0.0	U2(4h) = 1.0 Si1(4g) = 1.0	B_o (U2) = 0.5 B_o (Si1) = 0.5
$USi_{1,0147}$ ICSD 81561 I 4/m m m (139) Tetragonal	a = b = 10.587 c = 24.310 $\alpha = \beta = \gamma = 90$	U1 (4e), x =0.0, y = 0.0, z = 0.2579 U2 (8f), x = 0.25, y = 0.25, z = 0.25 U3 (8j), x = 0.2652, y = 0.5, z = 0.0 U4 (16n), x = 0.0 y = 0.2594, z = 0.0617 U5(16n), x = 0.0, y = 0.3567, z = 01924 U6(16m), x = 0.3132, y = 0.3132, z = 0.1156 Si1 (2a) x = 0.0, y = 0.0, z = 0.10 Si2 (4c) x = 0.0, y = 0.5, z = 0,.0 Si3 (4e) x = 0.0, y = 0.0, z = 0.098 Si4 (4e) x = 0.0, y = 0.0, z = 0.43 Si5(8h) x = 0.234, y = 0.234 z = 0.0 Si6 (16n) x = 0.0 y = 0.259, z = 0.3037 Si7(16n) x = 0.0, y = 0.385, z = 0.399 Si8(16m) x = 0.125, y = 0.125, z = 0.1552	U1 (4e)= 1.0 U2 (8f)=1.0 U3 (8j)=1.0 U4 (16n)=1.0 U5(16n)= 1.0 U6(16m)=1.0 Si1 (2a) =0.5 Si2 (4c)=1.0 Si3 (4e)=1.0 Si4 (4e)=1.0 Si5(8h) =1.0 Si6 (16n)=1.0 Si7(16n)=1.0 Si8(16m)=1.0	U1 (4e)=0.0 U2 (8f) =0.0 U3 (8j)= 0.0 U4 (16n)= 0.0 U5(16n)= 0.0 U6(16m)= 0.0 Si1 (2a)=1.0 Si2 (4c)=2.0 Si3 (4e)=2.1 Si4 (4e)=1.3 Si5(8h)=0.5 Si6 (16n)=0.7 Si7(16n)=1.1 Si8(16m)=0.9

Figure 3 shows the comparison between U_3Si_2 powder experimental and simulate diffractions through Rietveld Method. It is possible to observe a good concordance between diffractions, with good definition to peaks intensities and positions. Refinement quality is verified through two statistical numeric indicators R_p and R_{wp}, comparative parameters between theoretical and experimental diffractions, which can be used to the model convergence following. R_{wp} waste considers the fault associated to each intensity value, related to counting numbers, using *w* (2θ) pondering factor. According to MCCUSKER, L. D. et al. [9], R_{wp} value to good results is 2-10%, while typical values obtained vary 10-20%. R_{wp} value found was 8.55%, in the best values range.

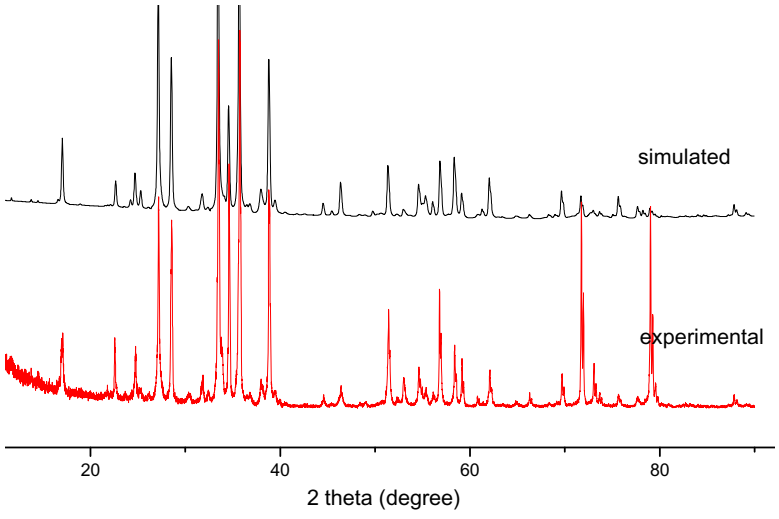

Figure 3: X ray patterns of U_3Si_2 powder: experimental and simulated by the Rietveld Method.

Table 2 shows quantitative percentage of each U_3Si_2 powder crystalline phase and the single cell parameters after refinement. It is possible to observe that U_3Si_2 powder have 90.31% of the U_3Si_2 phase and 9.69% of $USi_{1,0147}$, matching, so, established technical specifications (U_3Si_2 > 80%).

Table 2: Refined Lattice parameters and percentage of the crystalline phases calculated by Rietveld Method.

Crystalline Phases	Refined Lattice Parameters (Å)	Percentage of the Crystalline Phases
U_3Si_2	a = b = 7.3186 c = 3.9073	90.31
$USi_{1,0147}$	a = b = 10.630 c = 24.324	9.69

4. Conclusions

Methodology to silicide fuel crystalline phases quantification through Rietveld showed itself very apropriated. Rietveld Method, due to the fact of using all X ray diffraction profile in calculations, overcomes several compounds peaks superposition problem and turns possible to obtain results from all crystalline phases simultaneously, without the need of pattern samples and calibrations curves. It means an expressive gain in relation to other techniques to multiphase systems crystalline phases quantification through X ray diffraction.

Obtained results showed that U_3Si_2 powder produced by IPEN/CNEN matches technical specifications according to U_3Si_2 (90.31%) crystalline phase percentage.

5. References

[1] M. Durazzo, J.A. Perrota, “Fuel Improvement for the IPEN Research Reactor”. Semiannual Progress Report January-June 1999. IAEA Project Number BRA/4/047. IPEN, São Paulo, 1999.

[2] M. Durazzo, J.A. Perrota, “Fuel Improvement for the IPEN Research Reactor”. Semiannual Progress Report July-December 1999. IAEA Project Number BRA/4/047. IPEN, São Paulo, 1999.

[3] M. Durazzo, J.A. Perrota, “Fuel Improvement for the IPEN Research Reactor”. Semiannual Progress Report January-June 2000. IAEA Project Number BRA/4/047. IPEN, São Paulo, 2000.

[4] A.M. Saliba Silva, J.A.B. Souza, E.U.C. Frajndlich, J.A. Perrota, M. Durazzo, “First Results of U_3Si_2 Production and its Relevance in the Power Scale-up of IPEN Research Reactor IEA-R1m”. Proceedings of the XX International Meeting on Reduced Enrichment for Research and Test Reactors, Jackson Hole, Wyoming, 5-10 October 1997

[5] RIETVELD, H. M., A profile refinement method for nuclear and magnetic structures. *Journal of Applied Crystallographic*, v.2, p.65-71, 1969.

[6] RIETVELD, H. M. Line profiles of neutron powder-diffraction peaks for structure refinement. *Acta Crystallographica .* n.22, p.151-1152, 1967.

[7] JCPDS (Joint Committee of Powder Diffraction Standards). International Centre for Diffraction Data. Pennsylvania, USA., 1981.

[8] ICSD (Inorganic Crystal Structure Database). Gmchin-Intitut fur Anorganishe Chemie and Fachinformationzentrum FIZ. Karlsruhe, Germany, 1995.

[9] MCCUSKER, L. D.; VON DRELLE, R. B.; COX, D. e.; SCARDI, P. Rietveld refinement Guidelines. *Journal of Applied Crystallographic.* v. 32, p. 36-50, 1999.

REPROCESSING OF RESEARCH REACTOR NUCLEAR FUEL BASED ON PYROCHEMICAL SEPARATIONS TECHNIQUE

KEVIN NORBASH, STEVEN BAKHTIAR, DANIEL WACHS

Idaho National Laboratory, Idaho Falls, ID, 83415 USA

ABSTRACT

Treatment of spent nuclear fuel has received substantial attention over the last decade. At Idaho National Laboratory, pyrochemical separation is used to treat irradiated fuel elements from the Experimental Breeder Reactor-II (EBR-II). EBR-II, a sodium-cooled fast reactor at the Materials and Fuels Complex of the Idaho National Laboratory, was shutdown in late 1994 after 30 years of operation. It used uranium-10 wt% zirconium metallic fuel alloy enriched to 67-78% uranium-235. Pyrochemical technology is applied to discharged spent fuel to separate uranium from other fuel components. The experience and data obtained from this project may be used to treat newly designed high-density low-enriched uranium (LEU) research reactor nuclear fuel. This is consistent with the U.S. Department of Energy (DOE) Office of Nuclear Energy, Science and Technology goal to explore applications of pyrochemical separations to various fuel types. Therefore, pyrochemical processing of research reactor fuel is the focus of this paper.

Introduction

Research reactors are used for research, training, material testing and development, computer code validation, and the production of radioisotopes. Their main goal is to provide a neutron source for a wide variety of scientific experiments. There are many research reactor types with different designs and operating modes.

Unlike power reactors, research reactors need far less fuel, but more highly enriched uranium (HEU). Typically, they require about 90% U-235. HEU is needed to meet the reactor fissile-atom-density requirement. This allows for smaller cores, higher neutron fluxes, and longer times between refueling.

HEU has raised security concern among international community because of its potential for use in nuclear weapons. HEU may be very attractive to terrorist groups for making a crude atomic bomb. To guard against weapons proliferation from HEU fuels, in 1978 United States launched Reduced Enrichment for Research and Test Reactors (RERTR) program. Under this program, new LEU fuels with higher density have been developed. LEU is defined as less than 20% enrichment in uranium-235; these enrichment levels don't fall into the weapons grade material category. The LEU is offset by higher uranium density to meet the same fissile-atom density in the fuel. The RERTR program falls under DOE's National Nuclear Security Administration (NNSA) Global Threat Reduction Initiative (GTRI) to better manage fuel design with other nonproliferation programs.

In the United States, DOE's plan is to develop LEU fuel for civilian research reactors first. These include five high-performance research reactors (HPRR), namely 1) the High Flux Isotope Reactor (HFIR) at Oak Ridge National Laboratory (ORNL), 2) the Advance Test Reactor at the INL, 3) the National Bureau of Standards Reactor (NBSR) at the National Institute of

Standards and Technology (NIST), 4) the Missouri University Research Reactor (MURR) at the University of Missouri-Columbia, and 5) the MIT Reactor-II (MITR-II) at the Massachusetts Institute of Technology (MIT). The following table shows the current annual HEU fuel demand for these reactors:

Reactor	HEU/yr Kg	ΣHEU Kg	^{235}U/yr Kg	Σ^{235}U Kg
1. MITR	8		7.4	
2. MURR	24		21.9	
3. NBSR	13	250	12.1	232
4. HFIR	85		79.1	
5. ATR	120		111.6	

Although development of suitable LEU fuel that can be used in most of the world's research reactors is a challenge, management of spent nuclear fuel and scrap fuel is also a key component of this effort. The technology needed to safely and economically recycle LEU research reactor fuel in large scale is not yet at hand. Therefore, the pursuit of recycling technologies to save money and time must be considered as a worthwhile goal. This paper reports on pyroprocessing as a possible solution for dealing with research reactors spent nuclear fuel and scrap fuel. The goal is to have a technology validated for industrial deployment in the future. In fact the most recent LEU fuel developed by the RERTR program is an ideal candidate for assessing the feasibility of pyroprocessing.

Low-Enriched Uranium-Molybdenum Fuel

Since 1978, the RERTR program has been involved with the development of a novel nuclear fuel having significantly low-enriched uranium. In order to compensate for lower-enrichment fuel, higher density is necessary. Therefore, methods to fabricate plates containing higher loadings of uranium were developed. Work has continued to better understand the fabrication and fundamental behavior of these fuels. Currently, U_3Si_2 dispersed in alumina matrix with density of 4.8 g/cm^3 is the only fuel that has been licensed by Nuclear Regulatory Commission (NRC) for research reactor applications [1]. However, the most recent LEU fuel is based on uranium and 10 wt% molybdenum (U-10Mo) alloy in a monolithic form, clad in Al-6061. In this configuration the monolithic fuel consist of a single foil (~ 0.010 inch thick) of the fuel alloy with a much higher uranium density than dispersion-type fuel.

In order to mitigate detrimental fuel/clad interactions thin layer of zirconium is applied to the U-10Mo foil. This interlayer between the fuel matrix and cladding is necessary to achieve the desired performance during the fabrication process and during the reactor operation.

Wachs, Clark, and Dunavant [1] estimate that the HPRR LEU (U-10Mo alloy) demand will be about 4759 Kg per year (see below). This number includes all the fabrication process changes in going from HEU dispersion fuel to LEU monolithic fuel.

Reactor	LEU/yr Kg	ΣLEU Kg	^{235}U/yr Kg	Σ^{235}U Kg
1. MITR	233		46	
2. MURR	419		83	
3. NBSR	338	4759	67	940
4. HFIR	1589		314	
5. ATR	2180		431	

Spent Nuclear Fuel Management

Currently, US HPRRs produce more than 250 Kg of spent nuclear fuel per year. This nuclear fuel is no longer efficient in sustaining a nuclear chain reaction, but is highly radioactive. Spent fuel from nuclear research reactors has considerable U-235, plutonium, minor actinides, fission products, activation products and remnants of cladding. Of course, the exact composition of spent fuel depends on the initial enrichment and the amount of time fuel has been in the reactor. Separation of U-235 and Pu-239 from other components of spent fuel allows them to be used as reactor fuel. Therefore, spent fuel is eventually sent for reprocessing or final disposal.

The accumulated spent nuclear fuel must be stored as radioactive waste in disposal sites, either in a permanent repository or in temporary facilities (storage water pools). The strategy is to keep the nuclear waste isolated until its radioactivity drops to safe levels. A more responsible approach, one that avoids expanding geologic disposal areas and removes the uncertainty as to the long-term behavior of spent nuclear fuel or the geologic repositories is reprocessing. Nuclear reprocessing uses various technologies to separate spent fuel into its components. Recovery of fissile and fertile materials, such as uranium and plutonium, can provide feedstock for fresh fuel in future nuclear fuel rods, avoiding the waste of a valuable resource.

Separation and Recovery of Actinides from Fission Products

The separation and recovery of actinides and fission products of interest are carried out by aqueous or non-aqueous processes. In the aqueous process, spent fuel is dissolved with acid, and its various components are chemically separated. One of the most well-known aqueous process is PUREX (plutonium uranium extraction), in which fuel elements are dissolved in concentrated nitric acid, and uranium and plutonium are separated by solvent extraction. Next, the uranium and plutonium are added to the top of the fuel cycle for fuel fabrication.

The monolithic uranium-molybdenum alloy, with zirconium bonding layer, as nuclear fuel has shown potential to convert some of the targeted research reactors to low-enriched fuel. Argonne National Laboratory has conducted research to recover uranium from unirradiated fuel scraps [2]. To achieve this goal, lab personnel use a nitric acid dissolution technique for recovery of uranium from dissolved scrap material. In this process, one of the important considerations is formation of uranium-zirconium intermetallic compounds, which introduce a risk of explosive reaction [3-5]. However, the presence of excess hydrofluoric acid eliminates this. The explosive tendency of nitric acid dissolution of uranium-zirconium may not be an acceptable risk at an industrial scale. An explosion involving high-level liquid waste could contaminate hundreds of square miles and send people to hospitals. Thus, exploring other alternatives is a plausible effort.

Pyrochemical treatment of spent fuel (pyroprocessing) is one example of non-aqueous technologies being developed and implemented at the INL [6]. Pyroprocessing uses electrorefining techniques in which high temperature oxidation-reduction reactions in molten salt separate the actinides from the fission products. In this type of separation, thermodynamic stabilities of the compound govern the degree of separation. Pyroprocessing involves several stages. It starts with separating spent fuel elements from the fuel assembly in a hot cell. Then fuel elements are chopped into segments of 0.6 to 1.3 cm in length and the pieces are loaded into a steel basket. The steel basket is transferred into an electrorefiner containing a liquid salt solution. Using electrochemical process uranium is separated from the fission products. Cathode processor is used to remove residual salts and cadmium from the uranium. Salts and cadmium are recycled back into the electrorefiner while uranium is cast into fresh fuel. The two types of waste generated namely electrorefiner salt and cladding material are solidified for disposal. The advantages of pyrochemical technique are, 1) the solvents used are typically resistant to radiation damage which makes then ideal for handling high burnup fuel, 2) handling increased fissile material due to absence of water moderator, 3) incomplete separation of fissile material from fission products makes this technique non-proliferation friendly and 4) compact footprint allows for co-deployment of separation facility with the reactor complex which eliminates the need for the transportation and security of the hazardous waste. Therefore, this is an ideal technology for the treatment of HEU reactor fuels where radiation fields are high due to increased burnups.

Electrochemical Separation Technology

Electrorefining in a molten salt electrolyte is used to recover uranium and plutonium from spent fuel. The electrorefiner is a carbon-steel vessel, 1 m in diameter, that contains about 500 Kg of liquid LiCl-KCl electrolyte and dissolved actinide chlorides, such as UCl_3 and $PuCl_3$ [7]. The salt is heated to a temperature of approximately 500 ^{o}C in order to obtain a molten solution. In the electrorefiner, the steel basket with chopped fuel segments serves as an anode, and a steel mandrel and liquid cadmium serve as the cathodes. As a current is passed through the electrodes, the spent fuel is electrochemically dissolved from anode basket into the molten salt. The uranium is deposited on a steel cathode because the uranium has a less negative free energy change as compared to transuranic elements and fission products. The transuranics (plutonium, neptunium, americium, and curium) accumulate at the liquid cadmium cathode. Impurities with a more negative free energy than the desired product remain in the salt.

Planned Activities

Future work will explore monolithic fuel reprocessing on a demonstration basis. A Hot Fuel Dissolution Apparatus (HFDA), a laboratory scale electrorefiner, will be used for initial testing of the unirradiated RERTR low-enriched uranium-molybdenum fuel scrap to show the feasibility of technology. The HFDA, operated remotely in a hot cell, has a batch size of about 50 grams and a current capacity of 3.5 amps. Tests will be performed to measure fuel dissolution and current efficiencies.

Conclusions

Research reactors are used to produce neutrons for many different purposes. They are used in variety of different disciplines such as physics, chemistry, biology, information system, and nuclear medicine. The RERTR program is helping to convert research reactors from HEU fuel

to LEU fuel in the United States and throughout the world. Its goal is to reduce the amount of nuclear material available that may be used for malicious purposes. The RERTR program has developed U-10Mo monolithic fuels for research and test reactors with uranium densities of 15.3 g/cm^3.

Among the biggest challenges is dealing with spent fuel. Reprocessing is one possible solution where the volume of nuclear waste can be reduced and valuable elements from the spent fuel can be recovered. However, the zirconium used to provide an interface between the fuel and cladding causes a problem with aqueous processing of spent fuel. The uranium-zirconium forms an explosive compound in the presence of nitric acid. Therefore, non-aqueous technologies for recycle of spent nuclear fuel should be pursued.

One class of non-aqueous technology is pyroprocessing which may provide benefits over aqueous options. In pyroprocessing electrochemical process instead of chemical reagents is used to separate actinides from irradiated fuel. Research and development activities will be performed to access the pyrochemical processing of research reactor nuclear fuel.

Acknowledgements

The authors greatly appreciate the assistance of Steven Herrmann and Michael Simpson of the INL. This work is supported by the DOE, and National Nuclear Security Administration's Office of Defense Nuclear Nonproliferation.

References

1. Wachs, D. M., Clark, C. R., Dunavant, R. J., "Conceptual Process Description for the Manufacture of Low-Enriched Uranium-Molybdenum Fuel", INL/EXT-08-13840, February 2008.
2. Stepinski, D. C., Maggos, L., Swanson, J., Stevens, J., Vandegrift. G. F., "SCRAP Recovery Operations in the Fuel Fabrication Capacity", 30th International Meeting on Reduced Enrichment for Research and Test Reactors, October 2008.
3. Schultz, W. W., Scott, F. A., Viland, E. E., "Explosive Hazards in the Nitric Acid Dissolution of Uranium-Zirconium Alloy Fuel Elements", HW-32365, July 1954.
4. Schultz, W. W., Scott, F. A., Viland, E. E., "The Identification and Characterization of Explosive Residues Produced by Dissolution of Uranium-Zirconium Alloys", HW-32410, November 1954.
5. Culler, F. L., "Explosive Reactions During Reprocessing of Reactor Fuels Containing Uranium and Zirconium or Niobium", ORNL-58-11-31, November 1958.
6. Goff, K. M., Benedict, R. W., Howden, K. L., Teske, G. M., Johnson, T. A., "Pyrochemical Treatment of Spent Nuclear Fuel", INL/CON-05-00216, October 2005.
7. Goff, K. M., Simpson, M. F., "Treatment of Spent Nuclear Fuel with Molten Salts", proceedings of the 2008 joint symposium on molten salts, kobe, Japan, October 2008.

COOLING AND RADIATION SAFETY CONTROL REQUIREMENTS FOR SAFE STORAGE OF LEU WWR-M EXPERIMENTAL FUEL ASSEMBLIES

K.KONOPLEV, A.ZAKHAROV, S.ORLOV
Reactor Department, Petersburg Nuclear Physics Institute, RAS Gatchina, Leningrad district 188300, Russia.

T.TOTEV
Argonne National Laboratory, 9700 S. Cass Avenue, Argonne, IL 60439, USA

ABSTRACT

Two pin-type experimental fuel assemblies were tested in Petersburg Nuclear Physics Institute WWR-M reactor in support of development of LEU high-density fuel for some types of Soviet design research reactors. Pin fuel is being considered as a replacement of current standard tube type fuel. The experimental fuel assemblies contain pin type fuel elements (FE) with an aluminium matrix, containing either UO_2 or U-Mo fuel. Fuel assembly design, irradiation conditions and current status of these fuel assemblies are discussed. The LEU UO_2 and U-Mo fuel assemblies were irradiated up to 60% and ≈30 % burnup respectively, at a maximum power density of 277 kW/l.

The non-standard fuel design requires a revision of procedures for storage and further utilization of the spent fuel. The irradiated experimental fuel assemblies cannot be included in the existing fuel nomenclature, suitable for transportation to the Russian reprocessing plant Mayak. However, the basic principles for spent fuel management were observed to ensure safe storage of experimental fuel assemblies (EFAs). The paper describes the cooling and radiation safety control requirements for safe storage of the LEU WWR-M experimental fuel assemblies.

1. Introduction

Two pin-type experimental fuel assemblies were tested in the PNPI WWR-M reactor in support of demonstration of LEU high-density fuel for research reactors [1]. Pin type fuel offers several advantages compared to the tube type, and is considered an alternative for conversion of HEU fuel and replacement of standard tube type fuel elements. Pin fuel technology provides additional volume for fuel, but requires a fuel assembly shroud, which slightly increases parasitic neutron absorption.

The irradiated LEU experimental fuel assemblies were developed and fabricated by VNIINM Bochvar [2]. One of the irradiated fuel assemblies contains UO_2 and the other U-Mo fuel meat in aluminium matrix and cladding. Each of the fuel assemblies contains 37 pin elements (see Fig.1) inside of an hexagonal aluminium assembly shroud. The volume contents of fuel fission component in both type fuel elements are approximately identical (see Table 1). Main characteristics of the experimental fuel assemblies are presented in Table 2.

Table 1. Main Characteristics of the Fuel

No	Fuel composition	Average ^{235}U load per FE, g	Uranium concentration in fuel, g/cm^3	Length of fuel meat, mm	Volume share of fuel component, %
1	(U-Mo) + Al	2.54	5.3	500	33.9
2	UO_2 + Al	1.30	2.7	500	31.0

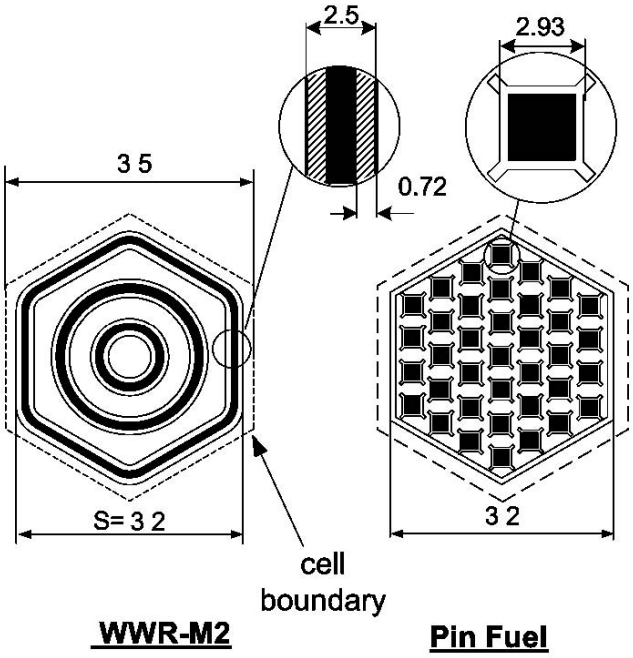

Fig .1. Pin and Tube type Fuel Assembly Designs

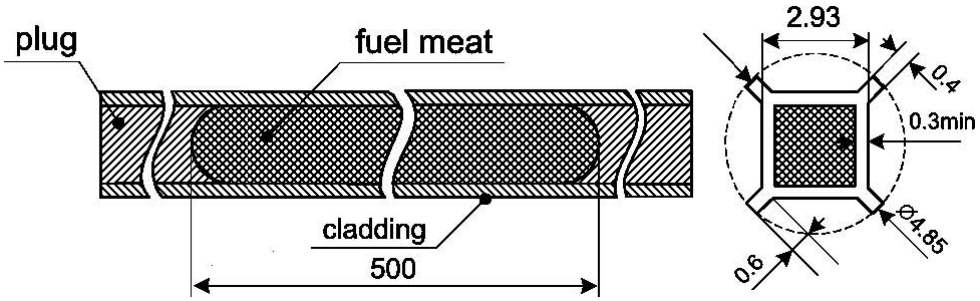

Table 2. Main Characteristics of the Fuel Assemblies

Characteristics of FA	Fuel UO_2+Al	Fuel (U-9%Mo) +Al
Quantity of FE in a FA	37	37
U-235 content in a FA, g	48.0	93.8
Water flow area, mm^2	467.3	467.3
Cooling surface, m^2	0.288	0.288
Hydraulic diameter, mm	2.74	2.74
Volume of fuel, cm^3	94.8	94.8
Volume share of water	0.523	0.523
Total length of FA, mm	748.5	748.5
Across the flats dimension, mm	32	32

Irradiated fuel assembles were loaded in WWR-M reactor active core and reshuffled several times in order to maintain the power, required by the experimental conditions (see Fig.3).

2. Irradiated fuel characteristics

The irradiation energy loading was nearly identical for both fuel assemblies with different uranium density of the fuel meat. The UO_2 and U-Mo type fuels were irradiated up to 60% and 30 % burn-up respectively. During the irradiation, the maximal power density of 277 kW/l was achieved, which is a typical value for Soviet designed pool-type research reactors.

The test program included measurements of the reactor loop radiation. The value of the pin fuel with UO_2 leakage parameter $1.3 \cdot 10^{-5}$, remained lower than the permissible value of $2 \cdot 10^{-5}$ in accordance with requirements of the test program. However, this value was 2.6 times higher comparing to maximum WWR-M2 energy release.

The leakage parameter is used as an operational indicator of fuel element non-integrity in WWR-M reactors. The criterion is defined as the ratio of the number of fission products released in the coolant to the number of fission product generated in the fuel [3,4]. The equilibrium activities of six nuclides: ^{85m}Kr, ^{87}Kr, ^{88}Kr, ^{135}Xe, ^{135m}Xe, ^{138}Xe were used to evaluate the of leakage rate (β) of the irradiated fuel assemblies. PNPI experience shows that the increasing of β from 10^{-7} to 10^{-6} is normal for dispersion fuel elements with aluminium matrix during fuel irradiation. Both types of experimental fuel assemblies have acceptable values of fission product leakage. However, comparisons of these values to the similar standard tube type WWR-M2 fuel assembly data shows slightly higher leakage of fission gasses from experimental fuel assemblies. Both difference and the fact that the cladding thickness of the experimental fuel element is less than the WWP-M2 standard tube fuel, were taken into account during planning of long-term storage of the test assemblies. The parameters of discharged fuel assemblies are presented in Table 3 before final reloading into the spent fuel pool (data on October 2006). Test results confirm the integrity of the fuel cladding.

Table 3. Irradiation characteristics of discharged fuel

#FA	Average burnup, %	Max power density of the core, κW/l	Max thermal flux, W/cm^2	Leakage parameter β, related units (max.)	Operating time at power, days
#11	61.3	252	55	$1.3 \cdot 10^{-5}$	321
#22	31.9	277	61	$6.7 \cdot 10^{-6}$	372

3. Storage process

The non-standard design of fuel requires a revision of procedures for storage and further utilization. The irradiated experimental fuel assemblies cannot be included in the existing fuel nomenclature, suitable for transportation of irradiated standard tube type fuel assemblies to the reprocessing plant at present time. However, the basic principles for spent fuel management were observed to ensure safe storage of experimental fuel assemblies (EFAs). The design and safety requirements for research reactor operation are established by the Russian Federal regulations [5]. Fuel management procedures are part of the safety analysis report of WWR-M reactor submitted to the National Regulator. Special attention was paid to:

a) coolability of the spent fuel
b) nuclear safety and particularly criticality of the spent fuel storage
c) coolability and water level of the storage
d) radiation safety
e) spent fuel storage water chemistry and radioactivity
f) physical protection and MC&A

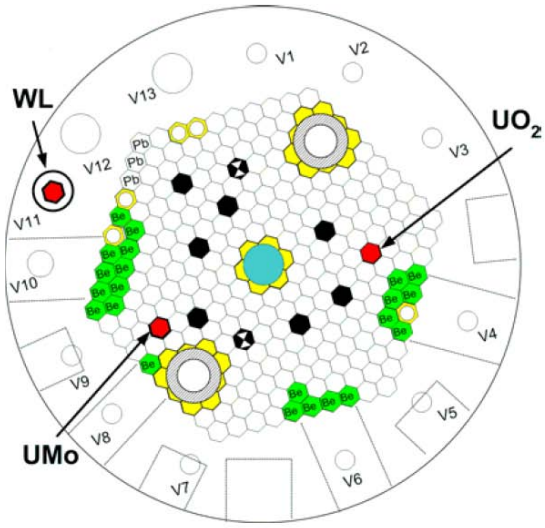

Fig.3. Experimental fuel assemblies arrangement during irradiation in reactor

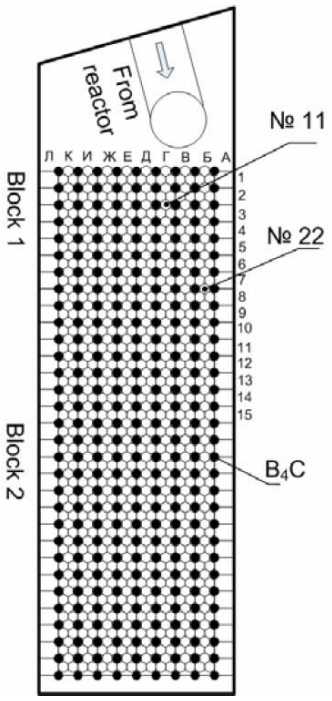

Fig. 4. Spent fuel storage No.1

From Fig.1 can be seen that EFAs have the same outer dimensions and shape as standard WWR-M5 and WWR-M2. This allowed EFAs to be loaded along with standard tube type fuel assemblies into spent fuel storage (SFS) No 1. The current arrangement of EFAs (on April 2009): in the Block No. 1 of SFS No 1: EFA No.11 with UO_2 fuel is located in cell No. B-8 (in Russian Б-8), EFA No.22 with U-Mo fuel is located in cell No.G-3 (Г-3) (see Fig. 4).

SFS No.1 is operational fuel storage and is used for reactor reloading in case of emergency situation. The SFS No 1 contains mainly intermediate burnup fuel and it will be used for formation of the reactor active core configuration. The operation procedure envisages transfer of spent fuel from SFS No. 1 to SFS No. 2 for long-term storage after achieving burnup limit. Aluminum alloy is used as material for the inner wall of the SFS double-walled casing and construction block for fuel assembly arrangement. SFS is equipped with a water purification system, including pump, ion-exchange filters and piping.

A Special inclined channel is used for the fuel transfer from reactor into SFS No.1. A Transport cask is used for fuel transfer between SFS No. 1 and SFS No.2. This operation is possible after reducing of the decay power below a certain level, because the fuel could be exposed in air for a prolonged time. Coolability assessment of FEAs' for these regimes and conditions was conducted.

The nuclear safety has been provided by arrangement of a system of B_4C control rods. The fuel cells are arranged between absorbing rods. The principle "one absorber for each one fuel cell" is used to determine the number of absorbers. All absorbers are welded with a block and cannot be extracted. This arrangement of the reactivity control secures maximum Keff =0.56 at limiting value of Keff <0.95.

Aluminium cladding corrosion of the stored EFA and associated water chemistry management are two main parameters, and have been closely monitored. The water chemistry in the ponds and its activity have been checked periodically. Water sampling is

provided by special equipment for activity measurement and gamma - spectra analyses. It is usual practice for fuel assemblies which exceed water activity limits not to be reloaded into reactor active core.

The water chemistry requirements for the primary coolant in the reactor core of pool-type research reactors are established by the Russian standard OST 95 10134-91. The following limits of coolant chemistry should be applied for WWR-M reactor operation: pH 5.5÷6.5 conductivity ≤ $2 \cdot 10^{-4}$ S/m (The limit is ≤ $4 \cdot 10^{-4}$ S/m), concentration Mg+Ca ≤ 3 μg-equivalent/kg, concentration Al, Fe or Cl ≤ 50 μg/kg. Water circulation within 2 hours accompanies each procedure of water sampling. The integrity of the experimental assemblies, based on results of water samples from EFAs and adjacent fuel assemblies was in the limits. The activity of water did not exceed $3 \cdot 10^{-6}$ Cu/l (approximately average background activity for other discharge fuel assemblies during measurements).

The cooling of EFAs has lasted more than 3 years after irradiation in accordance with the regulatory requirements and conducted assessment of FEAs power decay and coolability.
The conservative residual heat was estimated in accordance with cited references [6 and 7]. Estimated residual power with variation of the time and equal energy release was assessed to be in the range of 1.9 W and 2.3 W. These values are slightly lower compared to typical data based on ORIGEN calculation [8]. The estimates showed that for April 2009 the residual heat did not exceed 3 W for the each of the EFAs.

4. Conclusion

Cooling and radiation safety control requirements for safe storage of LEU WWR-M experimental fuel assemblies in the SFS No.1 are presented. Special attention is paid to coolability of the experimental fuel assemblies, pool criticality and coolant chemistry.

5. Acknowledgment

The authors would like to thank the U.S Department of Energy for funding this and any future work.

6. References

[1] A. Zakharov, G. Kirsanov, K. Konoplev, and A. Morozov. Test of Pin Fuel in WWR-M Reactor. The 27th International Meeting on Reduced Enrichment for Research and Test Reactors (RERTR). Boston, USA. November 6-10, 2005.
[2] A. Vatulin, I. Dobrikova, A. Morozov, and V. Suprun. Main Results of the Development of LEU Fuel for Russian Research Reactors, ibid.
[3] N.G. Badanina, Y.P. Saikov. Condition Comparison Criteria of Reactor Core Fuel Elements. Atomnaya Energia 24, (5), 429-432, 1968. (In Russian).
[4] N.G. Badanina, K.A. Konoplev, R.G. Pikulik, Yu.P. Saikov. Hermetic Sealing of WWR-M2 Fuel Elements During Operation. Leningrad Institute of Nuclear Physics preprint, No. 265, 1976 (In Russian).
[5] Safety rules for nuclear fuel on-site storage and transportation at nuclear power facilities. NP-061-05. Rostekhnadzor, 2005.
[6] A.D.Galanin. The introducing in the theory of nuclear reactors on thermal neutrons. M., Energoizdat 1990, 536p
[7] Shure K. Decay Rate and Decay Heat data from Fission Products. Nucl.Sci.Eng., 1981, vol.78 #l,.p.185.
[8] R. B. Pond and J. E. Matos, Nuclear mass inventory, photon dose rate and thermal decay heat of spent Research reactor Fuel Assemblies, (Rev. 1), ANL/RERTR/TM-26, ANL, USA, Dec 1996, pp. 34.

QUALIFICATION PROCESS OF DISPERSION FUELS IN THE IEAR1 RESEARCH REACTOR

D. B. DOMINGOS, A. T. SILVA, J. E. R. SILVA
Instituto de Pesquisas Energéticas e Nucleares (IPEN/CNEN-SP)
Av. Professor Lineu Prestes, 2242, Cidade Universitária, 05508-000 São Paulo, SP - Brazil

ABSTRACT

Neutronic, thermal-hydraulics and accident analysis calculations were developed to estimate the safety of a miniplate irradiation device (MID) to be placed in the IEA-R1 reactor core. The irradiation device will be used to receive miniplates of U_3O_8-Al and U_3Si_2-Al dispersion fuels, LEU type (19,9% of ^{235}U) with uranium densities of, respectively, 3.0 gU/cm^3 and 4.8 gU/cm^3. The fuel miniplates will be irradiated to nominal ^{235}U burnup levels of 50% and 80%, in order to qualify the above high-density dispersion fuels to be used in the Brazilian Multipurpose Reactor (RMB), now in the conception phase. For the neutronic calculation, the computer codes CITATION and TWODB were utilized. The computer code FLOW was used to calculate the coolant flow rate in the irradiation device, allowing the determination of the fuel miniplate temperatures with the computer model MTRCR-IEA-R1. A postulated Loss of Coolant Accident (LOCA) was analyzed with the computer code LOSS and TEMPLOCA, allowing the calculation of the fuel miniplate temperatures after the reactor pool draining. This paper also presents a system designed for fuel swelling evaluation. The determination of the fuel swelling will be performed by means of the fuel miniplate thickness measurements along the irradiation time.

1. Introduction

The IEA-R1 reactor of IPEN-CNEN/SP in Brazil is a pool type research reactor cooled and moderated by demineralized water and having Beryllium and Graphite as reflectors. In 1997 the reactor received the operating licensing for 5 MW. Since 1998, IPEN has been producing and qualifying its own U_3O_8-Al and U_3Si_2-Al dispersion fuels. The U_3O_8-Al dispersion fuel is qualified up to a uranium density of 2.3 gU/cm^3 and the U_3Si_2-Al dispersion fuel up to 3.0 gU/cm^3 [1]. The IEA-R1 reactor core is constituted of the fuels above, with low enrichment in ^{235}U (19.9% of U-235). IPEN has no hot cells to provide destructive analysis of the irradiated fuel. As a consequence, non destructive methods have been used to evaluate irradiation performance of the fuel elements [2]. For fuel qualification, complete fuel elements were irradiated in the IEA-R1 reactor core and the fuel element evaluation consisted of two items: i) monitoring the fuel performance during the IEA-R1 operation for the following parameters: reactor power, time of operation, neutron flux at the position of each fuel assembly, burnup, inlet and outlet water temperature in core, water pH, water conductivity, chloride content in water, and radiochemistry analysis of reactor water; ii) periodic underwater visual inspection of fuel assemblies and eventual sipping test for fuel element suspect of leakage. Irradiated fuel elements have been visually inspected periodically by an underwater radiation-resistant camera inside the IEA-R1 reactor pool, to verify its integrity and its general plate surface conditions.

Nowadays, IPEN-CNEN/SP is interested in qualifying the above dispersion fuels at higher densities. Ten fuel miniplates, five of U_3O_8-Al fuels and five of U_3Si_2-Al fuels, with densities of, respectively, 3.0 gU/cm^3 and 4.8 gU/cm^3, which are the maximal uranium densities qualified in the world for these dispersion fuels, were fabricated at IPEN-CNEN/SP. The miniplates will be put in an irradiation device, with similar external dimensions of IEA-R1 fuel

elements, which will be placed in a peripheral position of the IEA-R1 reactor core. In order to certify miniplate safety irradiation in the IEA-R1 reactor core, neutronic, thermal-hydraulics and accident analysis calculations were developed.

2. Neutronic, Thermal Hydraulics and Accident Analysis Calculation for the Irradiation Device

A special Miniplate Irradiation Device (MID) was designed for irradiation of the fuel miniplates in the IEA-R1 reactor. Figure 1 shows the MID. The MID has the external dimensions of the IEA-R1 fuel element. The miniplates will be allocated in a box with indented bars placed inside the external part of the MID. Figure 2 shows the transversal section of the MID.

Fig 1: Miniplate Irradiation Device – MID.

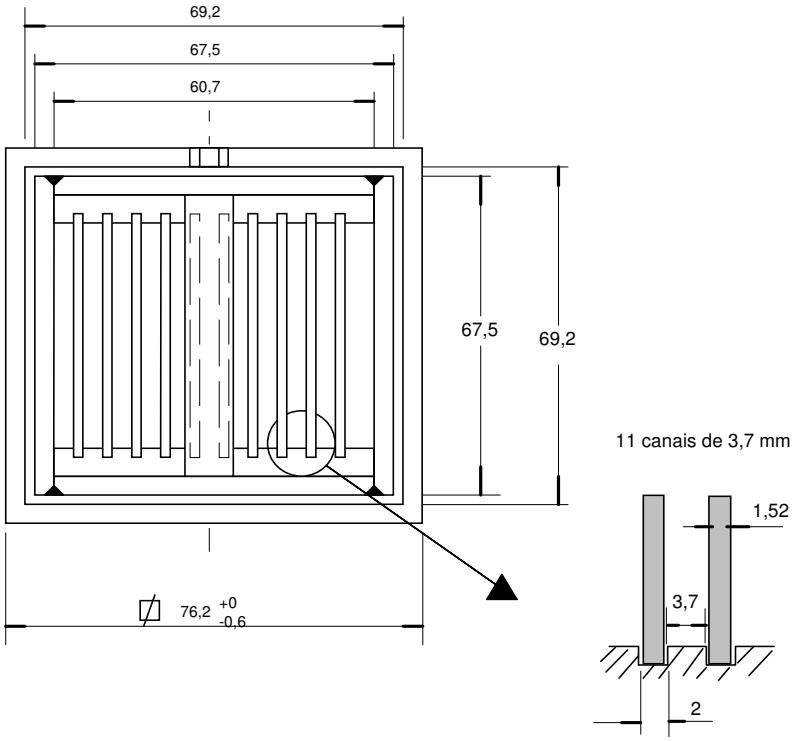

Fig 2: Transversal section of the MID (dimensions in mm).

As seen from Figure 2, up to ten miniplates can be placed in the box with indented bars inside of the MID. The qualification of the U_3O_8-Al and U_3Si_2-Al dispersion fuels with higher ^{235}U density will be made in use, which is based on the irradiation of the dispersion fuel miniplates in the IEA-R1 reactor followed by the use of non-destructive analysis techniques, mainly fuel miniplate visual inspections performed regularly with a radiation-resistant underwater camera [2].

A new special system [3] was designed for the fuel miniplate swelling determination. The fuel swelling determination will be performed by means of the fuel miniplate thickness measurement during the irradiation period in the IEA-R1 reactor. During the measuring period, the fuel miniplates will be transferred from the reactor core to the measurement system. Figure 3 shows the fuel miniplate thickness measurement system. It consists of a mobile metallic column held by an X-Y coordinate table system for miniplate thickness measurement. The table is supported by another metallic structure fixed at the border of the reactor pool. The thickness measurement is performed by eletronic probes (LVDT). The results are obtained through the instrumentation connected to the probes. The system is operated from the reactor pool border.

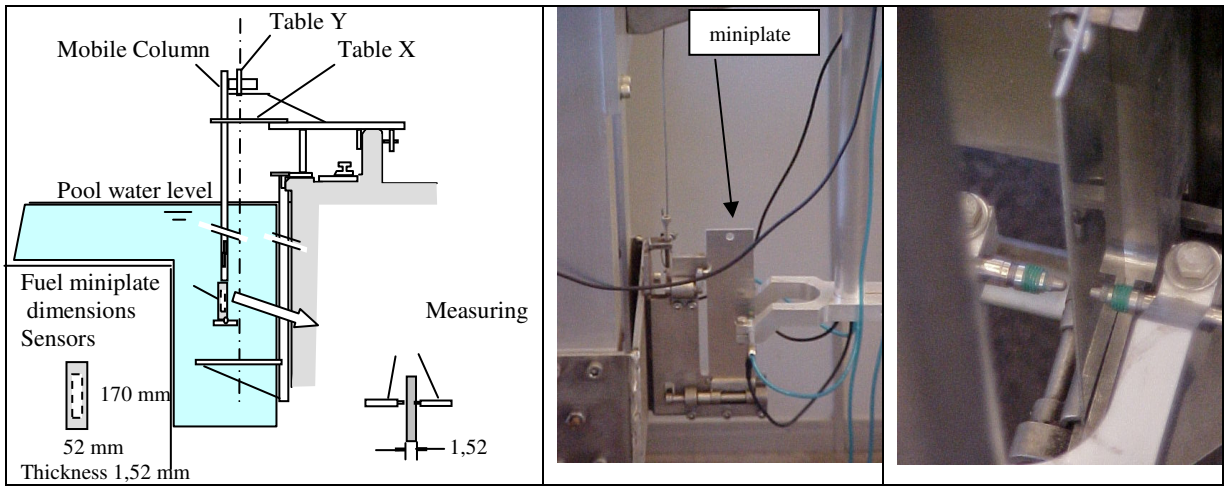

Fig 3: Fuel miniplate thickness measurement apparatus at IEA-R1: (A) schematic view at the reactor pool border; (B) lateral view; (C) profile view (thickness).

For commissioning the measurement system in the reactor pool area, two sets of measurements were made. The first set of measurements consisted of thickness measurements of an aluminum dummy miniplate, outside the reactor pool. These measurements evaluated the system performance in dry condition. The second set of measurements was performed for another dummy miniplate in the reactor pool. Dimensional results were in good accordance with those of the standards blocks supplied by TESA [4]. The results showed that the equipment was efficient and accurate, with measurement precision of 1 μm.

2.1 Neutronic calculation for the irradiation device

In the neutronic calculation, the computer code CITATION [5] was used for the three-dimensional core calculation and for burnup calculation. The cross sections were generated by the computer code TWODB [6]. The calculated radial and axial density curves were used as input data for the thermal-hydraulics reactor core and MID analysis. The core configuration number 236 of the IEA-R1 reactor [7] was used, with 24 elements, being 20 standard elements of U_3O_8-Al and U_3Si_2-Al dispersion fuels, four control elements, and one beryllium irradiation element in the central position of the core. In the calculation was considered that every fuel miniplate was made of U_3Si_2-Al with a uranium density of 4.8

gU/cm^3. In this situation will be generated the maximal power density in the miniplates, due to the maximal uranium density used. Three positions in reactor core matrix plate were given by the reactor operation to place the MID: 1) position 26; 2) position 37; and 3) position 36. In order to define the best position for the miniplate irradiation, calculations of the power densities were developed for three positions. The maximal power density was obtained for the position 36. In this position the miniplates will achieve the highest burnup in the shortest period of time.

2.2 Thermal-Hydraulics Analysis

A new thermal-hydraulics model MTCR-IEA-R1 [8] has been developed in 2000 at IPEN-CNEN/SP using a commercial program Engineering Equation Solver (EES). The use of this computer model enables the steady-state thermal and hydraulics core analyses of research reactors with MTR fuel elements. The following parameters are calculated along the fuel element channels: fuel meat central temperature (T_c), cladding temperature (T_r), coolant temperature (T_f), Onset of Nucleate Boiling (ONB) temperature (T_{onb}), critical heat flux (Departure of Nucleate Boiling-DNB), flow instability and thermal-hydraulics safety margins MDNBR and FIR. The thermal-hydraulics safety margins MDNBR and FIR are calculated as the ratio between, respectively, the critical heat flux and the heat flux for flow instability and the local heat flux in the fuel plate. Furthermore, the MTCR-IEA-R1 model also utilizes in its calculation the involved uncertainties in the thermal-hydraulics calculation such as: fuel fabrication uncertainties, errors in the power density distribution calculation, in the coolant flow distribution in the core, reactor power control deviation, in the coolant flow measures, and in the safety margins for the heat transfer coefficients. The calculated thermal-hydraulics core parameters are compared with the design limits established for MTR fuels: a) cladding temperature < 95°C; 2) safety margin for ONB > 1.3, or the ONB temperature higher than coolant temperature; 3) safety margin for flow instability > 2.0; and 4) safety margin for critical heat flux > 2.0.

The placement of the MID in the matrix plate of IEA-R1 reactor will deviate part of the reactor coolant flow to cool the fuel miniplates. The flow rate in the core of the reactor IEA-R1 is 3400 gpm which provides a flow rate of approximately 20 m^3/h per fuel element, sufficient to cool a standard fuel element. Results of the parametric tests developed with the program MTCR-IEA-R1 showed the need of a minimum flow rate of 10 m^3/h through the MID. The simulations have considered the MID with ten identical miniplates, with the same composition (U_3Si_2-Al), with the same uranium density (4.8 gU/cm^3), in order to analyze the most critical device configuration. The value of 12,3 m^3/h was defined for the coolant flow rate through the MID. It is sufficient to cool the miniplates and represent only a small deviation of the total coolant flow rate in the reactor core. A special flow restrictor was fabricated in order to maintain this coolant flow rate in the MID (see Figure 1).

No design limit was achieved for the analyzed irradiation device. The calculated cladding temperatures are below the value of 95°C, and the coolant temperatures are below the ONB temperature, indicating one-phase flow through the MID. The margins for critical heat flux (MDNBR) and flow instability (FIR) are well above the value of 2.0, admitted as design limit.

2.3 Accident Analysis

The Loss of Coolant Accidents (LOCA) in pool type research reactors are normally considered as limiting in the licensing process. For the IEA-R1 research reactor, a special Emergency Core Cooling System (ECCS) was constructed in order to avoid the core melting during a postulated primary coolant boundary rupture. With two redundant systems with passive action, the ECCS will be able to cool the reactor core after a reactor pool draining. However, the action of this system is limited to the boundaries of the reactor core and the ECCS is not able to cool the MID which is placed in a reactor core peripheral position. Two

computer codes LOSS [9] and TEMPLOCA [9] were used to calculate the temperatures achieved in the fuel miniplates during the core draining. The computer code LOSS determines the time to drain the reactor pool down to the level of the bottom of the core, and the computer code TEMPLOCA can calculate the maximal temperature to be achieved in the fuel miniplate during this transient. The calculations showed that about 7.5 min are necessary to drain the reactor pool during a postulated primary coolant boundary rupture accident. After the pool draining, the maximal fuel miniplate temperature achieved was 180 ºC, below the blistering temperature, which is the fuel temperature design limit [9]. At the blistering temperature the fuel miniplate will swell due to the fission gases released in the fuel and can close the fuel miniplate cooling channels with the fuel temperature increasing up to miniplate melting. The value of blistering temperature for dispersion fuels can vary between 350℃ e 600 ℃, depending on dispersion fuel type, fuel enrichment and burnup achieved.

3. Conclusions

The neutronic calculations showed that the inclusion of the MID in the IEA-R1 reactor core will not affect its operation, since the change in reactor reactivity will be irrelevant. The best reactor core position for miniplate irradiation is the core position 36, which will have the highest power density, allowing higher burnup in a shorter period of time. Through thermal-hydraulics calculations was determined that a flow rate of 12,3 m^3/h will be sufficient for cooling the fuel miniplates and will represent only a small deviation of the total coolant flow rate in the reactor core (600 m^3/h). The accident analysis concluded that there will not be done any damage to the miniplates in case of a postulated primary coolant boundary rupture.

4. References

1. A.T. Silva, L.A.A. Terremoto, J.E.R. Silva, C.T. Almeida, M.A. Damy, P.E.Umbehaun, M. Yamagushi, "*Qualification program of research reactor fuels manufactured at IPEN-CNEN/SP*", Progress in Nuclear Energy 50 (2008) 795-799.
2. J.E.R. Silva, A.T. Silva, L.A.A. Terremoto, "*Inspection experience with IEA-R1 spent fuel and non-destructive methods for qualification of high density LEU fuel (U_3Si_2-Al) at IPEN-CNEN/SP*", *In: RRFM 2009*, Vienna. Transactions RRFM 2009. Brussels, Belgium: European Nuclear Society, 2009. v. 1.
3. J.E.R. Silva, D.B. Domingos, A.T. Silva "*Fuel miniplate thickness measurement system for dispersion fuel swelling evaluation*", 2009 International Atlantic Conference - INAC 2009, Rio de Janeiro-RJ, Brazil, September 27 to October 2, 2009.
4. Manual of the module for Eletronic Length Measurements; TESA, model TESATRONIC TT60.
5. T.B. Fowler, D.R. Vondy, G.W. Cunninghan, – "*Nuclear Reactor Core Analysis Code: CITATION"*, Oak Ridge National Laboratory, ORNL-TM-2496, Ver. 2, July, (1971).
6. W.W. Little, Jr. and R.W. Hardie, 2DB, *"A Two-dimensional Diffusion Burnup Code for Fast Reactor Analysis"* BNW640, January 1968, Addendum and Errata, April 12, 1968.
7. D.B. Domingos, A.T. Silva, P.E. Umbehaun, J.E.R. Silva, T.N. Conti, M. Yamaguchi - "*Neutronic, thermal-hydraulic and accident analysis calculations for an irradiation device to be used in the qualification process of dispersion fuels in the IEA-R1 research reactor*", 2009 International Atlantic Conference - INAC 2009, Rio de Janeiro-RJ, Brazil, September 27 to October 2, 2009.
8. P. E. Umbehaun, – "*Metodologia Para Análise Termo-Hidráulica de Reatores de Pesquisa Tipo Piscina com Combustível Tipo Placa"* – Dissertação de Mestrado – São Paulo, (2000).
9. E. Maprelian, – "*Análise de Acidente de Perda de Refrigerante no Reator IEA-R1 a 5MW"* – Dissertação de Mestrado – São Paulo, (1998).

The authors are grateful for financial support from the Fundação de Amparo à Pesquisa do Estado de São Paulo (FAPESP) .

PERFORMANCE EVALUATION OF THE R6R018 FUEL PLATE USING PLATE CODE

PAVEL G. MEDVEDEV
Fuel Performance and Design
Idaho National Laboratory, P.O. Box 1625, Idaho Falls, Idaho 83415-6188, USA

ABSTRACT

The paper presents results of performance evaluation of the R6R018 fuel plate using PLATE code. R6R018 is a U-7Mo dispersion type mini-plate with Al-3.5Si matrix irradiated in the RERTR-9B experiment. The design of this plate is prototypical of the planned LEONIDAS irradiation test. Therefore, a detailed performance analysis of this plate is important to confirm acceptable behavior in pile, and to provide baseline and justification for further analysis and testing.

Specific results presented in the paper include fuel temperature history, growth of the interaction layer between the U-Mo and the matrix, swelling, growth of the corrosion layer, and degradation of thermal conductivity. The methodology of the analysis will be discussed including the newly developed capability to account for the formation of the interaction layer during fuel fabrication.

1. Introduction

The purpose of this paper is to present results of the performance evaluation of the R6R018 plate. R6R018 plate is a U-7Mo dispersion type mini-plate with Al-3.5Si matrix irradiated in the RERTR-9B experiment. The design of this plate is prototypical of the planned LEONIDAS [1] irradiation test. Therefore, a detailed performance analysis of this plate is important to confirm acceptable behavior in pile, and to provide baseline and justification for further analysis and testing.

2. Analysis methodology

Local performance metrics were calculated using PLATE fuel performance code [2]. The following empirical behaviour models were used in this analysis. Swelling due to fission products was calculated as a sum of swelling due to fission gas [3]:

$$\left(\frac{\Delta V}{V_0}\right)_g = 1.8\times10^{-21}\left(f_d\right), \quad \text{for } f_d \le 3\times10^{21}\ \text{f/cm}^3,$$

$$\left(\frac{\Delta V}{V_0}\right)_g = 5.4 + 2.2\times10^{-21}\left(f_d - 3\times10^{21}\right) + 0.51\times10^{-42}\left(f_d - 3\times10^{21}\right)^2, \quad \text{for } 3\times10^{21} \le f_d.$$

,

and swelling due to solid fission products:

$$\left(\frac{\Delta V}{V_0}\right)_s = 3.5\times10^{-21} f_d$$

where fd = fission density,

The interaction layer growth was calculated using the following power law [4]:

$$Y^2 = A\ F_r^{\ 0.5}\ \exp\left(-\frac{Q}{RT}\right) t$$

where:
Y = IL thickness (cm)
A = $7.5\text{x}10^{-18}$, pre-exponential factor
Fr = fission rate (f/cm^3-s)
T = temperature (K)
t = time (s)
Q = 8000 (cal/mol), activation energy

The PLATE code was modified to account for the as-fabricated interaction layer between the U-Mo particles and Al matrix. Previously, presence of the as-fabricated interaction layer was ignored in the PLATE fuel performance calculations. Formation of the reaction product during fuel fabrication results in the reduction of thermal conductivity of the fuel meat. In addition, since the reaction product contains fissile nuclides, it is subject to fission-induced degradation, which, in turn, is a function of the local fission density. The PLATE code tracks both the local fission density, and the extent of degradation. It is expected that the EOL fission density in the reaction product generated by the fabrication procedures would be higher than that in the reactor product formed in-pile. This may lead to earlier amorphization of the reaction product formed during fabrication as compared to the reaction product formed in-pile.

Corrosion of the cladding by the coolant is modelled according to the methodology proposed elsewhere [5].

3. Results

Calculated parameters included heat flux, peak temperature, temperature profile, fuel particle swelling, interaction layer thickness, plate thickness swelling, and corrosion layer thickness. The calculations were based on the nominal dispersion fuel plate design, plate as-built data, and on the power history calculated by Chang et al. [6,7].

Results of the evaluation of the R6R018 fuel plate at the end of life (EOL) using PLATE code are shown in Table 1. Results correspond to the plate transverse cross-section located at the axial mid-plane. As evident from Table 1, the temperature throughout the plate varies primarily due to variation of the local power and due to burnup-dependent thermal conductivity degradation of the fuel meat. The key reasons for meat thermal conductivity degradation are formation of the fuel cladding interaction layer and formation of the fission gas bubbles in the fuel particles and in the interaction layer. Formation of the corrosion layer on the waterside and its effect on the temperature is also modelled.

Table 1. Results of the evaluation of the R6R018 fuel plate at the EOL using PLATE code. Results correspond to the plate transverse cross-section located at the axial mid-plane. As-fabricated fuel-matrix interaction layer of 5 micron was used as an input parameter.

Node	Power factor from [7]	Fission density, $x10^{21}$ fissions/cm3			Local U-235 Burnup	Fuel particle swelling	Heat flux, W/cm2
		Meat	Fuel particle	Reaction product			
1 (hot edge)	1.907	7.155	10.99	3.333	0.521	0.618	488.038
2	1.553	5.829	9.086	2.755	0.433	0.508	393.687
3	1.358	5.095	8.018	2.431	0.383	0.446	342.106
4	1.218	4.573	7.245	2.197	0.347	0.402	305.806
5	1.107	4.154	6.626	2.009	0.318	0.366	276.870
6	1.004	3.769	6.052	1.835	0.291	0.333	250.383
7	0.939	3.526	5.689	1.725	0.274	0.313	233.815
8	0.884	3.317	5.377	1.630	0.259	0.295	219.557
9	0.837	3.140	5.11	1.551	0.246	0.280	207.588
10	0.791	2.968	4.855	1.472	0.234	0.265	195.901
11	0.779	2.861	4.3694	1.423	0.226	0.256	188.698
12	0.684	2.512	4.169	1.264	0.201	0.226	165.222
13	0.694	2.549	4.225	1.281	0.204	0.229	167.687
14	0.684	2.512	4.169	1.264	0.201	0.226	165.22
15	0.713	2.619	4.330	1.313	0.209	0.235	172.378
16	0.703	2.582	4.275	1.296	0.206	0.232	169.909
17	0.713	2.619	4.330	1.313	0.209	0.235	172.377
18	0.713	2.619	4.330	1.313	0.209	0.235	172.377
19	0.732	2.689	4.436	1.345	0.214	0.241	177.066
20 (cold edge)	0.760	2.791	4.590	1.392	0.221	0.250	183.984

Node	Power factor from [7]	Boehmite thickness, micron	Peak fuel temperature, °C	Plate surface temperature, °C	Interaction layer thickness, micron	Meat thermal conductivity, W/cm-s
1 (hot edge)	1.907	4.882	158.7	94.2	7.26	0.1075
2	1.553	5.534	156.8	99.5	7.11	0.1163
3	1.358	5.454	149.4	99.4	6.77	0.1226
4	1.218	5.132	141.5	97.5	6.45	0.1270
5	1.107	4.782	134.1	95.0	6.19	0.1310
6	1.004	4.472	127.3	92.5	5.98	0.1343
7	0.939	4.240	122.3	90.3	5.85	0.1360
8	0.884	4.066	118.3	88.6	5.75	0.1380
9	0.837	3.946	115.2	87.4	5.68	0.1395
10	0.791	3.889	113.2	86.8	5.63	0.1407
11	0.779	3.500	106.0	82.1	5.51	0.1410
12	0.684	3.454	102.5	81.6	5.45	0.1501
13	0.694	3.440	102.4	81.4	5.45	0.1489
14	0.684	3.434	102.1	81.4	5.44	0.1501
15	0.713	3.446	103.1	81.5	5.46	0.1467
16	0.703	3.437	102.7	81.4	5.45	0.1478
17	0.713	3.420	102.6	81.1	5.45	0.1466
18	0.713	3.366	101.6	80.3	5.44	0.1466
19	0.732	3.246	99.9	78.5	5.42	0.1444
20 (cold edge)	0.760	2.978	94.1	74.12	5.36	0.1410

PLATE code prediction of the EOL thickness of the fuelled portion of the R6R018 plate is shown in Figure 1. The plot shows thickness that is a sum of the cladding, meat and corrosion layer thicknesses at specific locations. Initial thickness of the plate is 1.4 mm. The PLATE thickness increase is due to formation of the interaction layer between U-Mo and Al and due to the swelling (solid and gaseous fission products) of the particles and the interaction layer. The maximum swelling is observed in the corners of the foil close to the reactor core, where maximum local power was predicted [7].

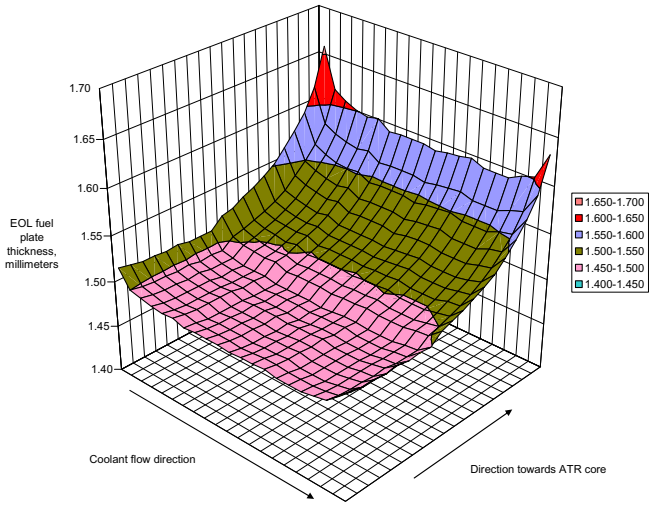

Figure 1. PLATE code prediction of the EOL thickness of the fuelled portion of the R6R018 plate. The plot shows thickness that is a sum of the cladding, meat and corrosion layer thicknesses at specific locations. Initial thickness of the plate is 1.4 mm.

PLATE code prediction of the EOL thickness of the interaction layer in the R6R018 plate is shown in Figure 2. Noting that the irradiation commenced with the as-fabricated interaction layer of 5 microns, it becomes obvious that very little generation of the reaction product occurred al the low-power side of the plate.

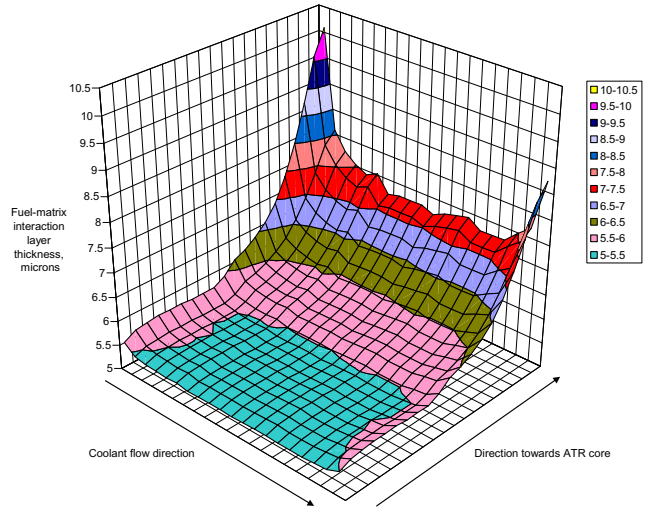

Figure 2. PLATE code prediction of the EOL thickness of the interaction layer in the R6R018 plate.

Peak fuel temperature distribution at the end of the second irradiation cycle is shown in Figure 3. Fuel temperature reached its highest value at the end of the second irradiation cycle.

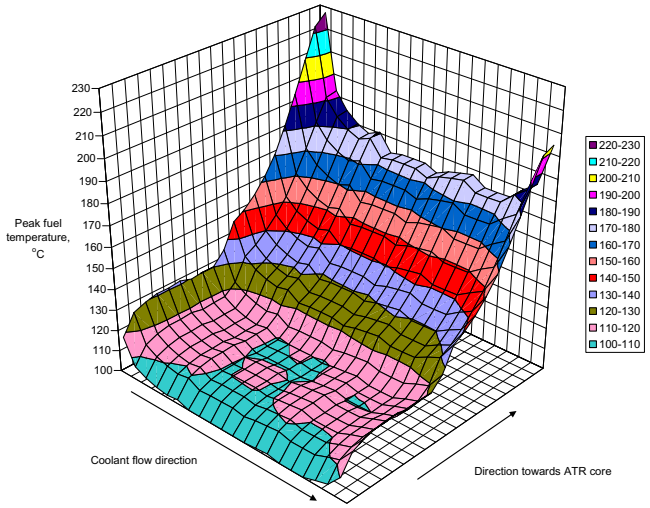

Figure 3. Peak fuel temperature distribution at the end of the second irradiation cycle. Fuel temperature reached its highest value at the end of the second irradiation cycle.

Temperature and interaction layer growth history in the peak power node are shown in Figure 4. The step changes in temperature are due to the changes in the local power history. The steady increase of the temperature between the step changes is due to the degradation of the thermal conductivity of the fuel meat.

The following effect of the as-fabricated interaction layer on the plate performance was noted from the simulation results. When the as-fabricated interaction layer is not present, the interaction layer growth is quite rapid in the beginning of life (BOL). The layer grows even faster on the high power side of the plate. When the as-fabricated interaction layer is present, the in-pile interaction layer growth is slow in the BOL and throughout the plate life. The effect is explained by the reduction of the surface area available for fuel-matrix interaction as the matrix phase is depleted due to formation of the as-fabricated interaction layer. In this context, formation of the as-fabricated interaction layer can be viewed as a passivation measure that leads to a more favourable in-pile performance.

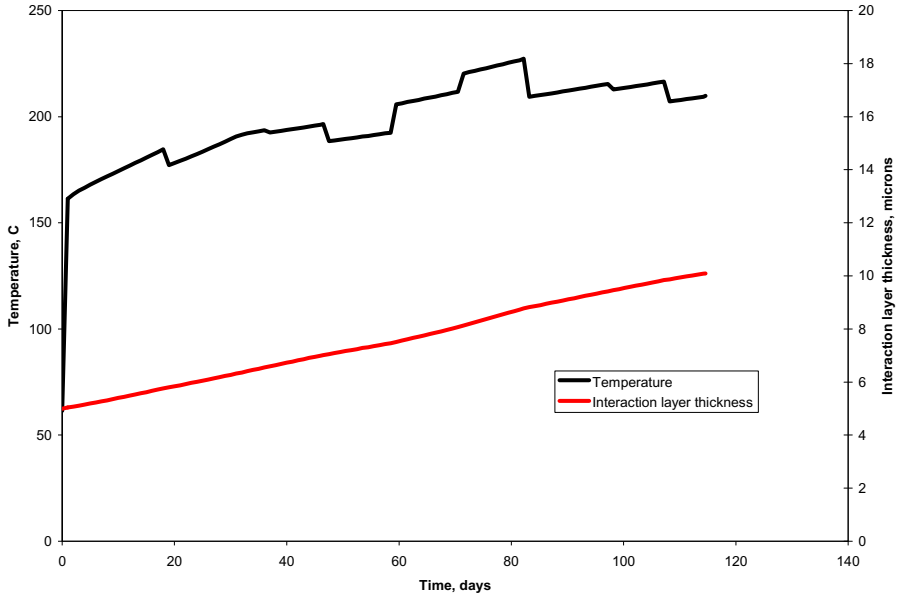

Figure 4. Temperature and interaction layer growth history in the peak power node.

4. Conclusions

PLATE code was used to obtain performance metrics for R6R018, a U-7Mo dispersion type mini-plate with Al-3.5Si matrix irradiated in the RERTR-9B experiment. The calculation results inform fuel developers about the changes occurring in the plate during irradiation. The calculation results could assist interpretation of the post irradiation examination data and help establish reference points to compare behaviour of the plates from this and other irradiation experiments.

Steep power gradients existing in the plate resulted in a wide range of irradiation conditions throughout the fuel foil. The plate featured both the low temperature and low burnup regions that exhibited little degradation, as well as highly degraded regions that were exposed to high power and high burnup. This information could be useful to guide PIE data collection.

A new methodology that accounts for as fabricated interaction layer was implemented in the code and successfully applied for the performance analysis of the present fuel plate. It was suggested that the EOL fission density in the reaction product generated by the fabrication procedures may be higher than that in the reactor product formed in-pile leading to earlier amorphization of the former. This observation can be further explored by performing parametric studies with the PLATE code. It was also noticed that presence of the as-fabricated interaction layer results in slower in-pile interaction layer growth rate at the beginning of irradiation.

Acknowledgements

This manuscript has been authored by Battelle Energy Alliance, LLC under Contract No.

DE-AC07-05ID14517 with the U.S. Department of Energy. The U.S. Government retains and the publisher, by accepting the article for publication, acknowledges that the U.S. Government retains a nonexclusive, paid-up, irrevocable, world-wide license to publish or reproduce the published form of this manuscript, or allow others to do so, for U.S. Government purposes.

The PLATE code was written by Dr. Steven Hayes of Idaho National Laboratory.

U.S. Department of Energy Disclaimer

This information was prepared as an account of work sponsored by an agency of the U.S. Government. Neither the U.S. Government nor any agency thereof, nor any of their employees, makes any warranty, express or implied, or assumes any legal liability or responsibility for the accuracy, completeness, or usefulness of any information, apparatus, product, or process disclosed, or represents that its use would not infringe privately owned rights. References herein to any specific commercial product, process, or service by trade name, trademark, manufacturer, or otherwise, does not necessarily constitute or imply its endorsement, recommendation, or favoring by the U.S. Government or any agency thereof. The views and opinions of authors expressed herein do not necessarily state or reflect those of the U.S. Government or any agency thereof.

References

[1] E. Koonen, H.Guyon, P. Lemoine, C. Jarousse, D. Wachs, J. Stevens The LEONIDAS and US Partnership for UMo Dispersion Fuel Qualification, 2009 International Meeting on Reduced Enrichment for Research and Test Reactors

[2]. S. L. Hayes, G. L. Hofman, M. K. Meyer, J. Rest and J. L. Snelgrove Modeling of High Density U-Mo Dispersion Plate Performance, 2002 International Meeting on Reduced Enrichment for Research and Test Reactors.

[3] Yeon Soo Kim, G. L. Hofman, Revision of the U-Mo Fuel Swelling Correlation, ANL Intra-Laboratory Memo, Jan. 15, 2009.

[4] Yeon Soo Kim, G.L. Hofman, P.G. Medvedev, G.V. Shevlyakov, A.B. Robinson, H.J. Ryu, 2006 International Meeting on Reduced Enrichment for Research and Test Reactors, Post Irradiation Analysis and Performance Modeling of Dispersion and Monolithic U-Mo Fuels, 2007 International Meeting on Reduced Enrichment for Research and Test Reactors.

[5] Yeon Soo Kim, G.L. Hofman, J. Rest, A.B. Robinson, Oxidation of aluminum alloy cladding for research and test reactor fuel, Journal of Nuclear Materials Volume 378, Issue 2, 31 August 2008, Pages 220-228

[6]. G. S. Chang, M. A. Lillo, As-Run Neutronics Analysis of the RERTR-9A/B Capsules in the ATR B-11 Position, Engineering Calculations and Analysis Report -231.

[7] G. S. Chang, M. A. Lillo, MCNP-Calculated Gradients Across RERTR-9 Miniplates Irradiated in ATR, Engineering Calculations and Analysis Report -689.

STRUCTURAL BEHAVIOUR OF MONOLITHIC FUEL PLATES DURING HOT ISOSTATIC PRESSING AND ANNEALING

HAKAN OZALTUN
Department of Mechanical Engineering, Ohio State University
201 W. 19TH Avenue, Columbus/OH - 43210, USA

PAVEL G. MEDVEDEV
Fuel Performance and Design, Material and Fuel Complex
Idaho National Laboratory, P.O. Box 1625, Idaho Falls/ID - 83415, USA

ABSTRACT

This article presents thermo-mechanical analysis of the monolithic fuel plates and their structural behavior during fabrication and thermal annealing performed by commercial FE solver COMSOL Multiphysics. The detailed 3D non-linear FEM analysis of the monolithic fuel plates has been useful not only for benchmarking the new model, but also for obtaining an in-depth understanding of fuel-cladding stress/strain characteristics. In particular, the 3D FEM analysis has revealed existence of stress gradients at the fuel/cladding interface region which could lead to structural failure. Large difference in the coefficient of thermal expansions between the U-10Mo foil and AL6061-TO cladding is the main reason for these gradients. During the thermal transient, thermo-mechanical behavior of the plate is driven by the significant mismatch between thermal expansion and basic mechanical properties of the foil and the cladding materials. By using elasto-thermo-perfectly plastic material models, it was shown that cladding material exceeds its yield limit; and therefore, deforms plastically; while the fuel foil remains below its elastic limit. In addition, it was observed that fabrication-induced residual stresses play major role in overall performance of monolithic fuel plates. The simulation results show existence of the critical temperature at which the normal and shear components of stresses change from compressive to tensile on both cladding and fuel. Furthermore, thermo-mechanical analysis of dispersion fuel mini-plates was presented. In order to properly identify three dimensional stress states over the dispersion particles and cladding material, micro-structure based finite element simulation was performed. It was shown that residual stresses in dispersion fuels cannot be neglected and should be included in proceeding simulations.

1. Introduction

Monolithic fuel plates comprised of uranium-molybdenum alloy foils encapsulated in aluminum alloy cladding are proposed for conversion of high performance research reactors to low enriched uranium fuel [1].

In this article, mechanical behavior of the monolithic plates during fabrication [2] by hot isostatic pressing (HIP) and during consequent thermal annealing is considered. The consequent thermal annealing is essentially the so-called “blister test” often performed on the fuel plates.

The process of fabrication of monolithic fuel mini-plates by HIP is as follows [3]. The foils are fabricated by arc-melting uranium and molybdenum feedstock in an inert atmosphere glove box, casting this alloy into a thin coupons and hot rolling at 650°C to the targeted thickness of 0.250 mm. Foils are further annealed at 650-675C for 30-120 minutes and assumed to be free of residual stresses before HIP process. Cladding material for the RERTR fuel plates was 6061Al-T6 alloy. After placing fuel foils between cladding materials, pressure and temperature are

gradually increased to 560°C and 104 MPa respectively. Specimens are held 90 minutes under constant pressure and cooled down to room temperature with the rate of 4.8 min/s while reducing the pressure gradually. Dimensions for final product are given in Figure 1.

The furnace annealing of the as-fabricated plates was assumed to proceed with a heating rate of 4.8 C/min to the temperature of 530C.

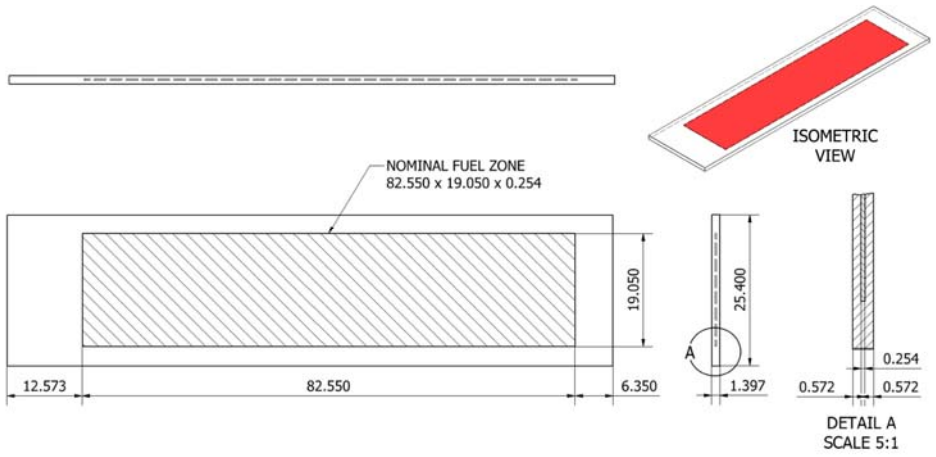

Figure 1 Nominal Dimensions (Millimeters) of the Monolithic Fuel Plate.

2. Modeling

2.1 Background

There are numbers of published works investigating thermal stresses in multi-layered structures. However, the modeling of mechanical behavior of the proposed monolithic fuel plates is still in its early development stages. This article will provide in-depth understanding of thermo-mechanical behavior of the fuel plates including residual stresses. Residual stresses are known to influence materials mechanical properties such as creep or fatigue life. Sometimes, the effect on properties is beneficial; other times, the effect is very deleterious. Therefore, it is important to be able to monitor and control the residual stresses. To provide an effective tool for assessment of thermal stresses in monolithic fuel plates, it would be more realistic to use a simulation model as close as possible to the actual product. Simulations demonstrated the importance of temperature dependence and material plasticity on analysis results. The failure would be caused by the difference in thermal expansion coefficient and mechanical mismatch between neighboring materials. A multiphysics simulation would consider heat transport, along with structural stresses and deformations.

2.2 Finite Element Model

General purpose commercial finite element solver COMSOL Multiphysics was utilized for this work to calculate the residual stresses in a monolithic fuel plate after the HIP process. Because of the symmetry, only one-half of the plate was modeled. Since eight-node hexahedral elements produce more accurate results than other elements, brick elements were used for discretization. Fuel was represented by using 3 layers totaling 3375 elements, while cladding contains 16200 elements. Total degrees of freedom solved for was 114660. Elasto-thermo-perfectly-plastic models were assigned to both cladding and fuel materials to simulate thermo-plasticity. One

node (lower left corner) of the model was constrained in three directions to prevent rigid body motion. Resulting symmetric FE model along with partial cut is presented in Figure 2.

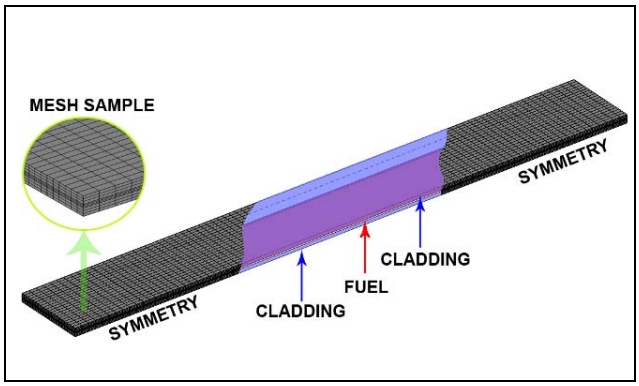

Figure 2 Corresponding FE Symmetric Model

Elasto-plastic parametric solver with reduced integration was used. Since amount of time under temperature is small, thermal creep was assumed to be zero. It was also assumed that complete mechanical bonding would be achieved at exact HIP temperature, and therefore 560C was assumed to be reference starting point for the HIP simulation. From 560C, 28 sub-steps were used to reach the room temperature. Solution was stored for every 20C temperature drop. Once residual stresses were identified in step 1 (HIP simulation), the same methodology was used to solve step 2 (furnace annealing simulation). Results from HIP simulation were considered as initial condition for step 2. Namely, normal and shear components were supplied to the solver. Same sub-stepping was chosen to reach from room temperature to desired annealing temperature (530C). For both simulations, yielding was defined according to Von-Mises criteria, formulated as,

$$\sigma_{eq} = \sqrt{\frac{1}{2}\left[\left(\sigma_{11}-\sigma_{22}\right)^2+\left(\sigma_{22}-\sigma_{33}\right)^2+\left(\sigma_{11}-\sigma_{3}\right)^2+6\left(\tau_{12}^2+\tau_{23}^2+\tau_{31}^2\right)\right]} \quad (1)$$

2.3 Material Properties

As the HIP temperature is 560C, material properties at such high temperatures are crucial to obtain more accurate simulation results. These properties and experimental details are available elsewhere [4-10]. For completeness, material properties used in thermo-plastic simulations are given in Table 1. The temperature dependence of the U-10Mo yield stress was derived from the U-10Mo hardness temperature dependence data [7].

Table 1 Material Properties

Cladding – [AL6061-TO]

Thermal Expansion [6]

[C]	[1/K]
100	23.60×10^{-6}
200	24.30×10^{-6}
300	25.40×10^{-6}

Modulus of Elasticity [6]

[C]	[GPa]
21	69.63
38	68.94
93	66.39
149	63.43
177	61.50
204	59.63
232	57.29
260	54.12
274	52.53
287	49.92

Yield Stress [6, 9]

[C]	[MPa]
24	55.15
38	55.15
93	55.15
149	55.15
177	51.71
204	44.81
232	36.54
260	27.57
288	22.06
315	17.92
371	12.41
560	6.89 (extrapolated)

Poisson's Ratio **(1)** [6]

[C]	[-]
23	0.33

Density

[C]	[kg/m^3]
23	2702

Fuel foil – [U10Mo]

Thermal Expansion [7]

[C]	[1/K]
50	11.81×10^{-6}
100	12.42×10^{-6}
200	13.63×10^{-6}
300	14.84×10^{-6}
400	16.05×10^{-6}
500	17.26×10^{-6}
600	18.47×10^{-6}

Modulus of Elasticity [7]

[C]	[GPa]
21	83.00
126	80.00

Yield Stress (Derived from hardness data [7])

[C]	[MPa]
20	734.00
100	644.73
200	549.73
300	464.82
400	424.58
500	306.53
600	295.08
700	181.35
800	115.17

Poisson's Ratio **(1)** [10]

[C]	[-]
23	0.25

Density [7]

[C]	[kg/m^3]
23	17200

Dispersion fuel meat [U7Mo–AL6061] (2)

Thermal Expansion (derived from [6,7])

[C]	[1/K]
50	18.40×10^{-6}
100	18.60×10^{-6}
200	19.30×10^{-6}
300	19.90×10^{-6}
400	20.60×10^{-6}
500	21.20×10^{-6}
600	21.80×10^{-6}

Modulus of Elasticity (derived from [6,7])

[C]	[GPa]
21	74.98
93	72.22
149	70.06
204	67.78
232	66.37
287	61.95

Yield Stress (derived from [6,7])

[C]	[MPa]
24	326.69
100	257.89
150	272.36
200	219.89
300	185.93
400	169.83
500	122.61

Poisson's Ratio **(1)** [derived from [4,5,6])

[C]	[-]
23	0.30

Density [4,5]

[C]	[kg/m^3]
21	6711

(1) Temperature dependent data for Poisson's ratio were not available. Poisson's ratio was assumed to be independent of temperature.
(2) Mechanical properties of the dispersion fuel meat were not available. Rule of mixtures was used to derive meat mechanical properties from known properties of U10Mo and AL6061TO.
(3) Properties at undefined temperatures were approximated by interpolation. Piecewise cubic formulation was used to interpolate between known values.

2.4 Constitution of the Continuum

Material properties were assumed to be independent of direction but dependent of temperature. Therefore, modulus of elasticity (E), Poisson's ratio (v) and shear modulus (G) were,

$$E_x = E_y = E_z = E(T) \tag{2}$$

$$\nu_{xy} = \nu_{yx} = \nu_{xz} = \nu_{zx} = \nu_{yz} = \nu_{zy} = \nu(T) \tag{3}$$

$$G_{xy} = G_{xz} = G_{yz} = G(T) \quad and \quad G(T) = \frac{E(T)}{2.\left[1+\nu(T)\right]} \tag{4}$$

Assuming the material of interest undergoes small strains, linearized form of the strain tensor can be expressed as,

$$\varepsilon_{ij}^{total} = \frac{1}{2}\left(\frac{\partial u_i}{\partial u_j} + \frac{\partial u_j}{\partial u_i}\right) \tag{5}$$

where, ε_{ij} and u strain tensor and displacements respectively. At each point of the plate, the total-strain components ε_{ij}^{total} are represented as the sum of the corresponding components of the elastic, plastic, thermal and initial ones. Such as,

$$\varepsilon_{ij}^{total} = \frac{1}{2}\left(u_{i,j} + u_{j,i}\right) = \varepsilon_{ij}^{el} + \varepsilon_{ij}^{pl} + \varepsilon_{ij}^{th} + \varepsilon_{ij}^{in} \tag{6}$$

Thermal strain tensor ε_{kl}^{th} is expressed by,

$$\varepsilon_{kl}^{th} = \alpha_{kl}(T) \times \Delta T \tag{7}$$

$\alpha_{kl}(T)$ is the tensor governing coefficient of thermal expansion, and ΔT is the temperature change from the reference point. The mechanical constitution of the plate was assumed to be in the following form:

$$\sigma_{ij} = D_{ijkl} \times \varepsilon_{kl}^{el} + \sigma_{ij}^{in} \tag{8}$$

where, D_{ijkl} is 6x6 temperature dependent elasticity matrix (i.e. $D_{ijkl}(T)$), ε_{kl}^{el} elastic strain tensor, and σ_{ij}^{in} is initial stress (i.e. residual stress). Substituting elastic strains from (6) into the mechanical constitution in (8) gives stress distribution on the plate expressed as,

$$\sigma_{ij} = D_{ijkl} \times \left(\varepsilon_{kl}^{total} - \varepsilon_{kl}^{pl} - \varepsilon_{kl}^{th} - \varepsilon_{kl}^{in}\right) + \sigma_{ij}^{in} \tag{9}$$

3. Results

In order to identify mechanical behavior during the specified thermal cycle, two-step simulation was performed. First, HIP simulation was performed to calculate the residual stresses. Once residual stresses were identified, they were used as initial condition for second step. HIP simulation started at the reference point (560C) and ended at the room temperature (21C). Annealing simulation started at the room temperature and ended at 530C. At the end of second step, elasto-plastic response was analyzed. Results for thermo-elasto-plastic simulations were discussed below. Due to the non-linearity, drastic shifts on the location of maximum stresses should be expected. Therefore, stresses presented in all graphs below were captured at wherever they were maximum regardless their location. However, for completeness, stress over the interface region was captured separately.

3.1 HIP simulation and residual stresses

Equivalent stress distribution with regional zoom is shown in Figure 3. Figure 4 presents contour plot for effective plastic strain on the domain. It seems cladding material over the fuel region deforms plastically while fuel does not go beyond its elastic limit.

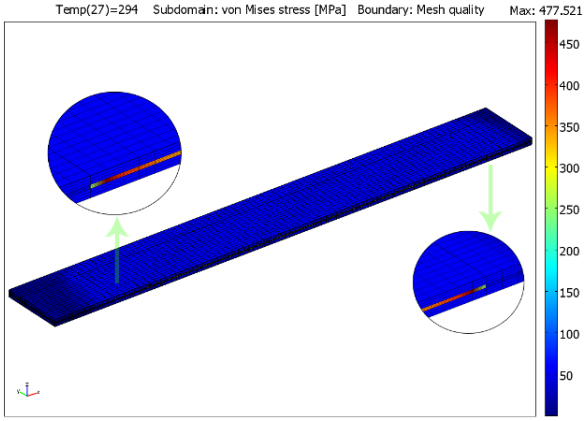

Figure 3 Equivalent Stresses

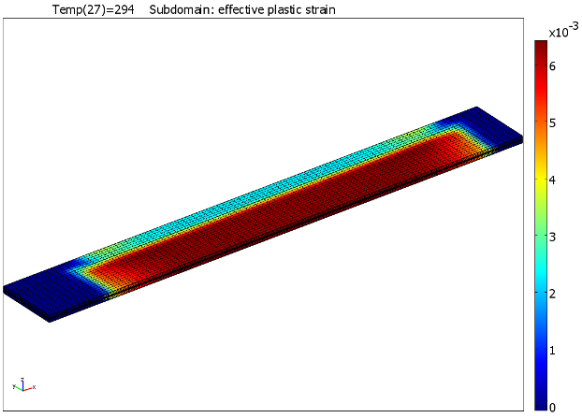

Figure 4 Effective Plastic Strain

Figure 5 and Figure 6 show normal and plastic strain history during cooling of the plate from 560C to room temperature. It seems that the cladding material manifests higher normal strains due to its higher compliance, while fuel shows more rigid behavior. Nearly 50% of total strain recorded by cladding is plastic deformation.

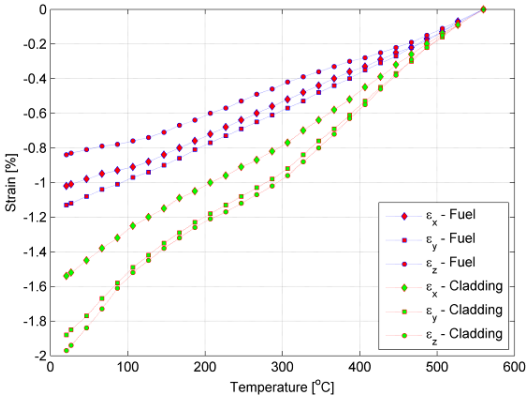

Figure 5 Normal strain history

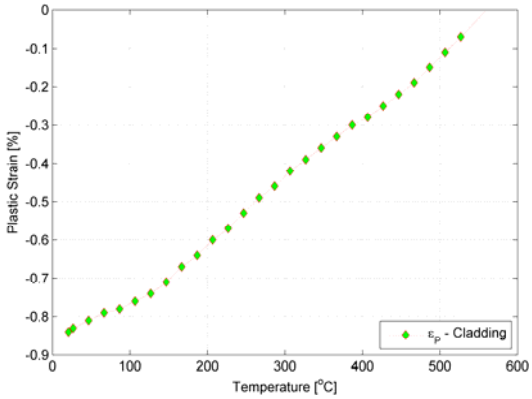

Figure 6 Effective plastic strain history

Figure 7 shows maximum equivalent stresses over the body including both cladding and fuel materials. Recorded stresses on the fuel are nearly 10 times higher than those on the cladding. This is due to property mismatch between the neighboring layers. The fuel has a much higher yield stress and somewhat higher modulus. Not surprisingly, this creates significant amount of stress gradient at the interface region and raises attention to survivability of the bond and its quality.

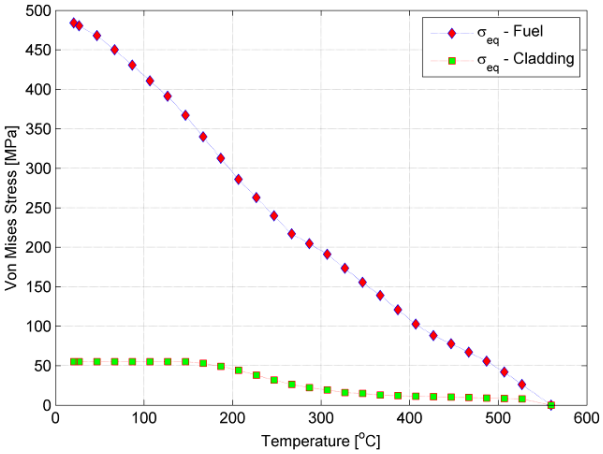

Figure 7 Equivalent stress history

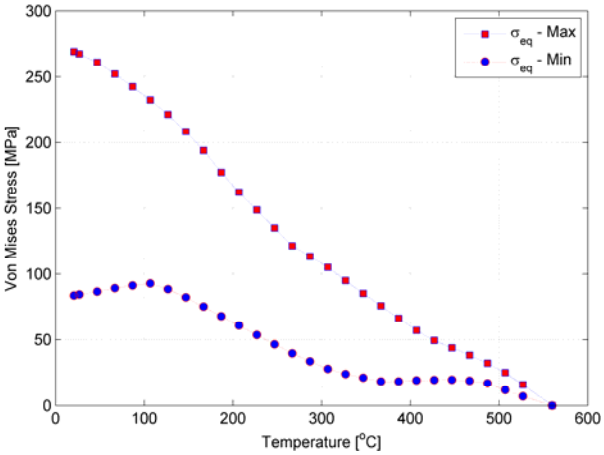

Figure 8 Stresses at the interface

Figure 8 shows equivalent stress history calculated for interface region including edges and corners. Maximum calculated stress at the interface is 275 MPa. If maximum equivalent stress theory is selected as the failure criteria, then acceptable bond strength should be higher than this value.

3.2 Annealing simulation and thermal stresses

By using the results shown in 3.1, behavior of the plate during annealing was calculated. Same sub-stepping was chosen to reach the annealing temperature (530C). Yielding was defined according to the Von-Mises criteria. Equivalent stress distribution is shown in Figure 9. Figure 10 presents contours for effective plastic strain on the plate. Similar to previous simulation, cladding material over the fuel region exhibits plasticity while the fuel still stays in the elastic region. However this time, it seems that plastic deformation on the cladding is significantly higher while equivalent stresses are much lower. Equivalent stresses on the fuel are more or less uniform, however, higher concentration was noted closer to the fuel ends (indicated by circle in Figure 9).

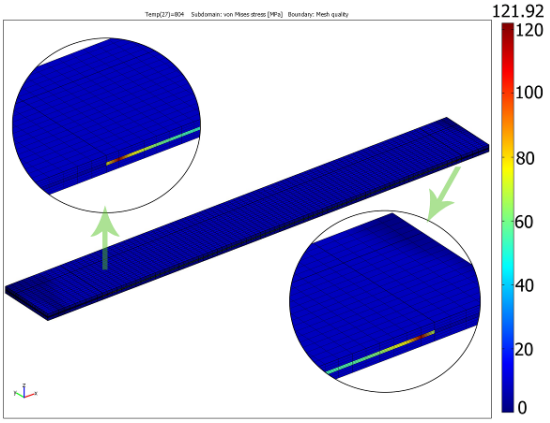

Figure 9 Equivalent stress

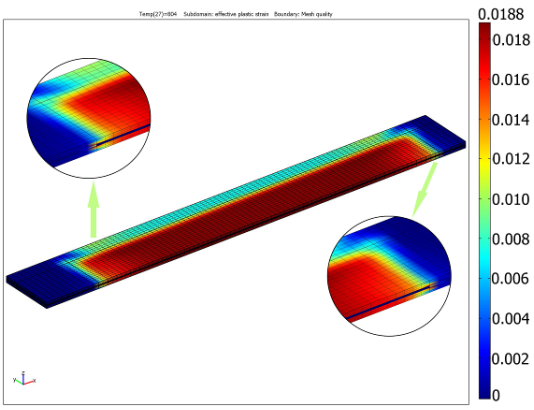

Figure 10 Effective plastic Strain

Figures 11 and 12 show normal and plastic strain history during the annealing of the fuel plate. Unlike HIP simulation, a clear transition temperature (approximately 300C) from compression to tension was noted. At this temperature (visible in Figure 11, at approximately 300C) plate would be free of any stresses. Similar to HIP simulation, cladding material manifests higher normal strains, while fuel still holds its rigidity. Total plastic strain is approximately 3 times of the plastic strain computed for the HIP simulation.

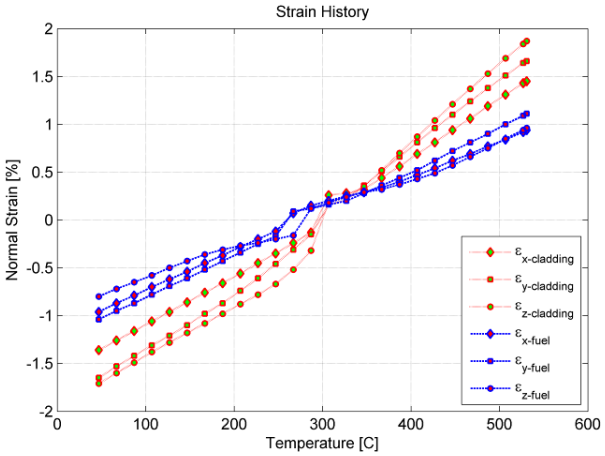

Figure 11 Normal strain history

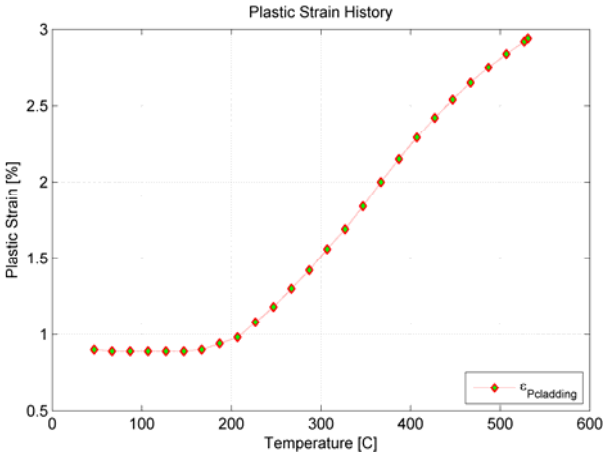

Figure 12 Effective plastic strain history

Figure 13 shows maximum equivalent stresses over the body including both cladding and fuel materials. It seems that annealing acts a stress relief on the plate. However, there is a bigger stress gradient between the cladding and fuel material. This time, maximum equivalent stress calculated for fuel is approximately 200MPa while it is approximately 7 MPa for cladding. Therefore, stress gradient between the two is nearly 30 times as opposed to 10 times as calculated for HIP simulation.

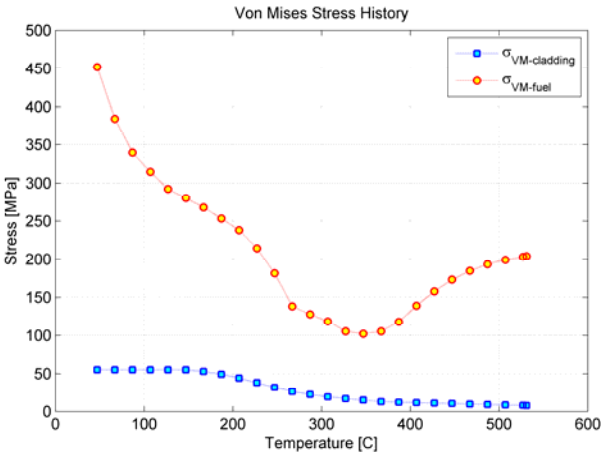

Figure 13 Equivalent stress history

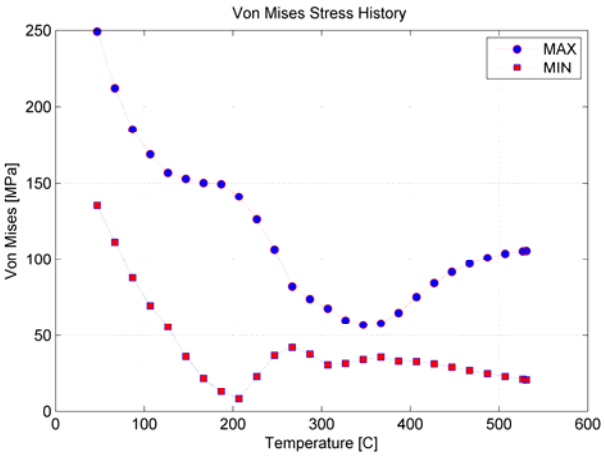

Figure 14 Stresses at the interface

Figure 14 presents equivalent stress history calculated for the interface region. It can be seen that stresses are relieved during the thermal annealing. Maximum residual stresses drop to 100 MPa which is significantly lower than 275 MPa as computed for the HIP. Assuming there are no significant microstructural changes that would hinder and defect the mechanical properties, it would be safe to postulate that if plate survives HIP process, it should overcome the thermal stresses raised during the annealing step.

3.3 Residual stresses in U7Mo-Al dispersion plates

To highlight the difference between the monolithic and dispersion fuel designs, a calculation of residual stresses induced in the dispersion plates by the hot rolling fabrication procedure was performed. The hot rolling temperature of 500C was adopted [11]. To construct the FE model of the dispersion fuel meat, a representative image of the U-Mo powder (Figure 15) taken from the reference [12] was selected. Resulting FE model is shown in Figure 16. The boundary conditions and the finite element solver settings were the same as described in Section 2 of the present paper. In order to identify residual stresses over the mechanical domain after the hot rolling, single step elasto-plastic simulation was performed. Hot rolling simulation started at the reference point of 500C assuming that mixture is free of residual stresses at this temperature. Parametric solver was used with 25C drop in each step until reaching to the room temperature (21C).

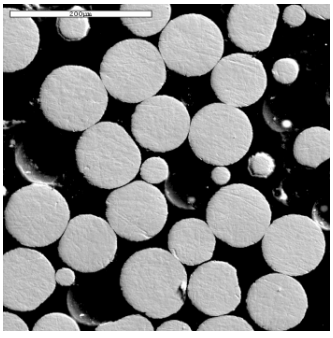

Figure 15 A representative micro-structure

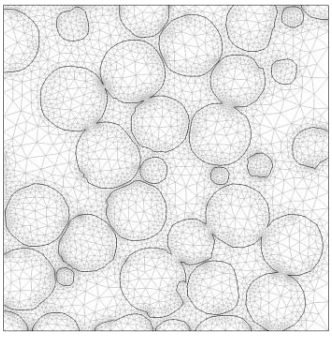

Figure 16 FE model of the micro-structure

Equivalent stress distributions over the domain and just on the particles are shown in Figure 17 and Figure 18 respectively. A complete plastic deformation of the matrix (Al6061TO) and high

compressive stresses on the particles (U7Mo) was observed. Existence of several hot spots is evident from Figure 18, while the stress in most particles remains below the yield point. It was concluded that although there are high local residual stresses around the particles the bulk of the fuel meat should have experienced residual stresses of approximately 55 MPa.

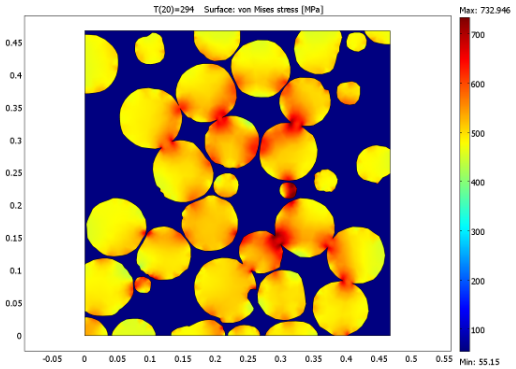

Figure 17 Stresses after Hot Rolling

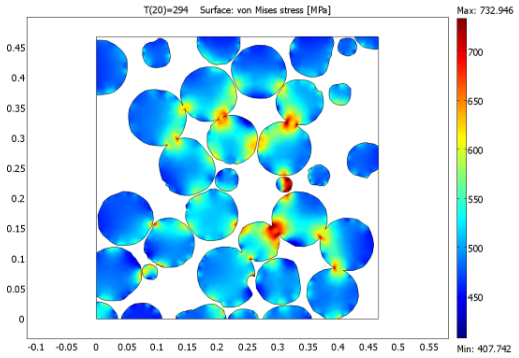

Figure 18 Stresses in the particles

4. Conclusions

Thermo-mechanical response of the monolithic fuel mini-plates during fabrication by hot isostatic pressing and consequent furnace annealing was investigated using commercial finite element solver COMSOL Multiphysics. The analysis demonstrated that large residual stresses are induced by fabrication. Residual stresses dominate the mechanical behavior of the monolithic plate during thermal annealing. Existence of the stress gradients at the interface region that could lead to the structural failure has been shown. This observation emphasizes the significance of the fuel-cladding bond strength on the structural integrity of the plate. It was noted, that during the analyzed thermal cycle, the cladding exceeds its yield point, while fuel foil remains in the elastic region. A transition temperature a clear transition temperature (approximately 300C) from compression to tension during annealing was noted. A micro-structure based finite element simulation was performed to identify the residual stresses and stress concentrations in the dispersion fuel plates.

The accuracy of the results presented in the paper relies on the availability and accuracy of the mechanical property data. Currently, such data is scarce. The model will be updated when mechanical properties become available. Until then the results of this work should be used with caution.

Acknowledgements

This manuscript has been authored under Contract No. DE-AC07-05ID14517 with the U.S. Department of Energy. The U.S. Government retains and the publisher, by accepting the article for publication, acknowledges that the U.S. Government retains a nonexclusive, paid-up, irrevocable, world-wide license to publish or reproduce the published form of this manuscript, or allow others to do so, for U.S. Government purposes.

U.S. Department of Energy Disclaimer

This information was prepared as an account of work sponsored by an agency of the U.S. Government. Neither the U.S. Government nor any agency thereof, nor any of their employees, makes any warranty, express or implied, or assumes any legal liability or responsibility for the

accuracy, completeness, or usefulness of any information, apparatus, product, or process disclosed, or represents that its use would not infringe privately owned rights. References herein to any specific commercial product, process, or service by trade name, trademark, manufacturer, or otherwise, does not necessarily constitute or imply its endorsement, recommendation, or favoring by the U.S. Government or any agency thereof. The views and opinions of authors expressed herein do not necessarily state or reflect those of the U.S. Government or any agency thereof.

References

[1] D. Wachs, RERTR Fuel Development and Qualification Plan, INL/EXT-05-01017, www.inl.gov/technicalpublications/Documents/3610331.pdf

[2] Daniel M. Wachs, Curtis R. Clark, Randall J. Dunavant, Conceptual Process Description for the Manufacture of Low-Enriched Uranium-Molybdenum Fuel INL/EXT-05-01017 http://www.rertr.anl.gov/ConcProcessDescFeb08.pdf

[3] Jan-Fong Jue, Blair H. Park, Curtis R. Clark, Glenn A. Moore, Dennis D. Keiser, " Fabrication of Monolithic Fuels by Hot Isostatic Pressing", Journal of Nuclear Technology, Accepted.

[4] S. H. Lee, J. C. Kim, J. M. Park, C. K. Kim, and S. W. Kim, Effect of Heat Treatment on Thermal Conductivity of U-Mo/Al Alloy Dispersion Fuel, International Journal of Thermophysics, Vol.24, No.5, (2003)

[5] S. H. Lee, J. M. Park, and C. K. Kim, Thermophysical Properties of U–Mo/Al Alloy Dispersion Fuel Meats, International Journal of Thermophysics, Vol.28, No.5, (2007)

[6] S.T. Polkinghorne, J.M. Lacy. Thermophysical and mechanical properties of ATR core materials. EG&G Idaho Inc., Internal Technical Report, PG-T-91-031, August 1, 1991.

[7] J. Rest, Y. S. Kim, G. L. Hofman, M. K. Meyer, S. L. Hayes. "U-Mo Fuels Handbook v.1.0", Argonne National Laboratory Internal Report. (2006)

[8] Totju Totev, Gerard Hofman, Mathew Looby, "AA-MATPRO-HANDBOOK, Aluminum Material Properties for Research Reactor", Argonne National Laboratory Internal Report, (2009)

[9] ASM Handbook http://products.asminternational.org/hbk/index.jsp

[10] Dr. Gerard Hofman, Argonne National Laboratory, personal communication.

[11] Dennis D. Keiser, Adam B. Robinson, Jan-Fong Jue, Pavel Medvedev, Daniel M. Wachs a, M. Ross Finlay, "Microstructural development in irradiated U-7Mo/6061 Al alloy matrix dispersion fuel", (2009)

[12] C. R. Clark, B. R. Muntifering, J. F. Jue, "Production and Characterization of Atomized U-Mo Powder by the Rotating Electrode Process", RERTR-2007 International Meeting on Reduced Enrichment for Research and Test Reactors September 2007.

Conversion of LVR-15 reactor to LEU

V. Brož, J. Ernest, M. Koleška, M. Vinš, J. Zmítková
Nuclear Research Institute Rez, Czech Republic

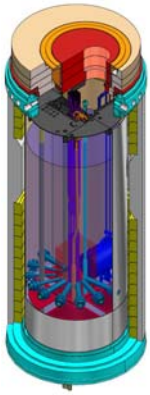

Fuel	IRT-2M, 36% ^{235}U	IRT-4M, 19,7% ^{235}U
Total length	882 mm	882 mm
Active length	580 mm	600 mm
Section square - head	71,5x 71,5 mm	71,5x 71,5 mm
Section square	67 x 67 mm	69,6 x 69,6 mm
Total mass of the assembly 4/8 tubes	3,7 kg	6 kg
3/6 tubes	3,2 kg	5,2 kg
Mass of ^{235}U 4/8 tubes	230 g	300 g
3/6 tubes	198 g	263,8 g
Tube wall thickness	2 mm	1,6 mm
Cladding thickness	2 x min.0,4 mm	2 x 0,3 mm
Fuel material	UO_2-Al	UO_2-Al
Fuel plate thickness	0,64 mm	0,7 mm

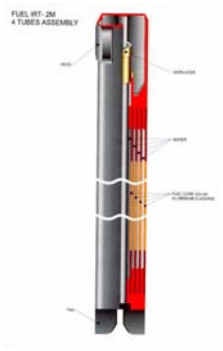

Reactor

- Thermal power: 10MW
- Fuel: 28 - 32 FAs
  - fabricated in NZCHK Novosibirsk
  - HEU, IRT-2M, enrichment 36 %
  - LEU, IRT-4M, enrichment 19,7%
- Max. fast neutron flux
  - In the core: 3 x 10^{18} n/m^{2}s
- Max. thermal neutron flux
  - In the core: 1.4 x 10^{18} n/m^{2}s
  - Irradiation channel in fuel : 1 x 10^{18} n/m^{2}s
  - Irradiation channel in reflector: 3-5 x 10^{17} n/m^{2}s

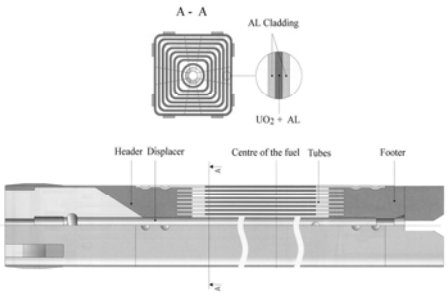

Conversion plan

- Trial irradiation
  - 2/2010 – 9/2010: 3 IRT-4M FAs in core
  - Irradiation time: 6 campaigns
  - Only IRT-2M FAs will be added into core
- Evaluation of tests
  - Performed since 6/2010
  - Visual inspection of FAs with under-water camera
  - Sipping tests
  - Primary circuit water activity observation
- Mixed cores planned since 10/2010
  - 16 mixed cores
  - only IRT-4M FAs will be added into core

Conversion is funded by US DOE

Conversion started with experiment 5. 2. 2010

Konfigurace : K116 - mix 01.01 HEU alias

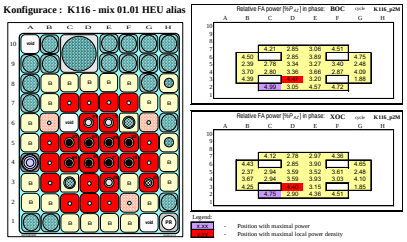

1) Operational core – HEU (K116_p2M)

- 5. 2. 2010
- 3 fresh IRT-2M FAs (B6, F2, G6)
- Critical state
  - HT: 680 mm
  - AR: 350 mm
  - KT: 300 mm (280 mm real)

Power extremes for configuration: K116_p4M								
Phase	Max. core power density			Max. power per FA			Power inequality	
	Position	Hom -[W/cm^3]- Fuel core		Position	[%P_{AZ}]	[kW]	PPF	DPF
BOC	D3	311	2484	C2	5.024	478	1.407	2.423
XOC	G6	307	2334	G6	4.817	458	1.349	2.390
EOC	G6	291	2212	G6	4.757	452	1.332	2.265

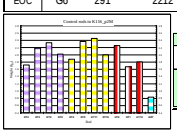

Average FA burn-up in configuration: K116_p2M					
Fuel type	Number of FAs	[%235U$_{fiss}$]		[MWd/kgU]	
		BOC	EOC	BOC	EOC
IRT-4M	-				
IRT-2M	28	32.86	32.86	97.83	97.83
Total	28	32.86	32.86	97.83	97.83

Konfigurace : K116 - mix 01.00 - Experiment HEU

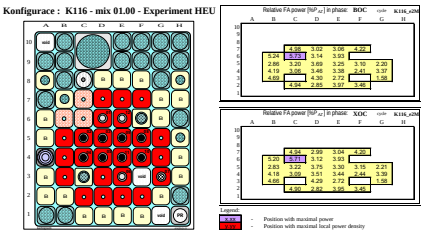

2) Experiment – HEU (K116_e2M)

- 5. 2. 2010
- 3 fresh IRT-2M FAs (B6, C6, C7)
- Operation – 4 hours, 5 MW$_{th}$
- Flux measurement using foils
  - fuel (C6)
  - beryllium reflector (B7, A8)
  - air(C8)
- Critical state
  - HT: 680 mm
  - AR: 350 mm
  - KT: 310 mm (287 mm real)

Power extremes for configuration: K116_e2M								
Phase	Max. core power density			Max. power per FA			Power inequality	
	Position	Hom -[W/cm^3]- Fuel core		Position	[%P_{AZ}]	[kW]	PPF	DPF
BOC	C6	211	1687	C6	5.733	287	1.605	3.102
XOC	C6	211	1684	C6	5.711	286	1.599	3.096
EOC	-			-				

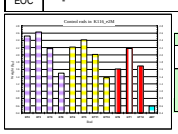

Average FA burn-up in configuration: K116_e2M					
Fuel type	Number of FAs	[%235U$_{fiss}$]		[MWd/kgU]	
		BOC	EOC	BOC	EOC
IRT-4M	-				
IRT-2M	28	32.86	32.87	97.83	97.88
Total	28	32.86	32.87	97.83	97.88

Konfigurace : K116 - mix 01.00 - Experiment LEU

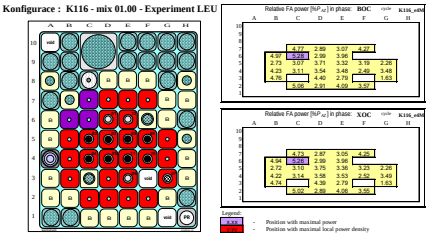

3) Experiment – LEU (K116_e4M)

- 12. 2. 2010
- 3 fresh IRT-4M FAs (B6, C6, C7)
- Operation – 4 hours, 5 MW$_{th}$
- Flux measurement using foils
  - fuel (C6)
  - beryllium reflector (B7, A8)
  - air(C8)
- Critical state
  - HT: 680 mm
  - AR: 350 mm
  - KT: 320 mm (317 mm real)

Power extremes for configuration: K116_e4M								
Phase	Max. core power density			Max. power per FA			Power inequality	
	Position	Hom -[W/cm^3]- Fuel core		Position	[%P_{AZ}]	[kW]	PPF	DPF
BOC	C6	169	1289	C6	5.280	264	1.478	2.508
XOC	C6	170	1293	C6	5.264	263	1.474	2.516
EOC	-			-				

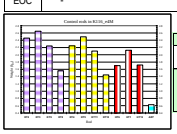

Average FA burn-up in configuration: K116_e4M					
Fuel type	Number of FAs	[%235U$_{fiss}$]		[MWd/kgU]	
		BOC	EOC	BOC	EOC
IRT-4M	3	0.00	0.02	0.00	0.03
IRT-2M	25	37.10	37.11	110.45	110.50
Total	28	31.77	31.79	84.53	84.57

Konfigurace : K116 - mix 01.01 provoz

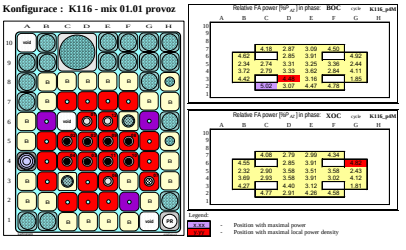

4) Operational core – LEU (K116_p2M)

- 9. 2. 2010
- 3 fresh IRT-4M FAs (B6, F2, G6)
- Critical state
  - HT: 680 mm
  - AR: 350 mm
  - KT: 295 mm (281 mm real)

Power extremes for configuration: K116_p2M								
Phase	Max. core power density			Max. power per FA			Power inequality	
	Position	Hom -[W/cm^3]- Fuel core		Position	[%P_{AZ}]	[kW]	PPF	DPF
BOC	D3	311	2485	C2	4.989	474	1.397	2.405
XOC	D3	297	2371	C2	4.752	452	1.331	2.294
EOC	-			-				

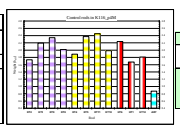

Average FA burn-up in configuration: K116_p4M					
Fuel type	Number of FAs	[%235U$_{fiss}$]		[MWd/kgU]	
		BOC	EOC	BOC	EOC
IRT-4M	3	0.00	4.15	0.00	6.43
IRT-2M	25	37.10	37.15	95.50	95.73
Total	28	31.79	35.84	84.57	95.43

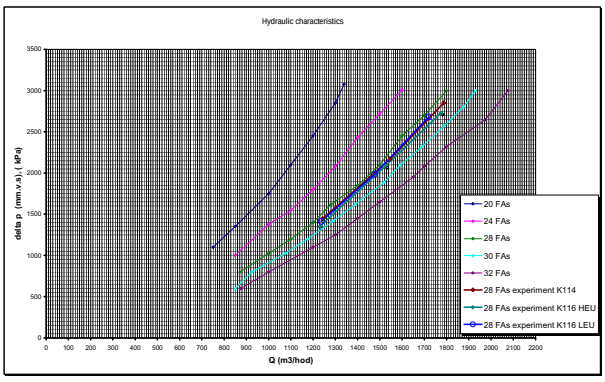

FULL INSTANTANEOUS TRAVERSAL RUPTURE OF THE PRIMARY LOOP PIPELINE.

Baytelesov S.A., Kungurov F.R.

Annotation

Accident, reflecting full immediate cross rupture of primary loop pipe of WWR-SM research reactor of INP AS RUz is observed in this paper. Calculations for accident situation and analysis for different reactor cores, formed from fully IRT-3M type high enriched fuel (36% enrichment on ^{235}U), first mixed core, compiled from 16 IRT-3M fuel assemblies and 4 IRT-4M type fuel assemblies with low enriched fuel (19,7% enrichment on ^{235}U) and the core fully formed from low enriched fuel are carried out.

Introduction

The process of conversion of a WWR-SM reactor of INP AS RUz from use of high enriched uranium fuel (HEU) on uranium-235 to low enriched uranium fuel (LEU) now has begun. It is the long-term process which is carried out in some steps. Calculations of various accidents for carrying out of conversion have been executed by us for the purpose of the analysis of safety of transfer of a reactor on use of low enriched fuel.

For thermohydraulic calculations of steady state and accidents we used the methods described in [1].

Following assumptions were made for the calculations:

- . Uniformity of spray is an assumption.
- . If the water does not fully vaporize, then a higher coolant flow rate will be required to remove the same amount of heat.
- . Vaporizing water (even some of it) produces steam which wants to flow upward and will inhibit the downward flow of liquid water between the fuel tubes. If steam up flow is sufficiently fast it can totally prevent down flow of liquid, a situation know as "flooding" or "counter current flow limitation". Supplying additional spray water does not necessarily eliminate this phenomenon.
- . In a transient analysis, the fuel could be allowed to heat somewhat during the early part of the LOCA as long as the fuel does not exceed its structural integrity limit and then show decreasing temperature as decay power decreases and coolant flow is maintained.
- . Residual energy release decreases in accordance with Wigner and Wei law.
- . The bounding analysis was performed for the peak FA assuming that all tubes have the peak power density.

Accident, presented in article, was calculated with PARET [2] code using two-channel model. The hottest and averaged fuel plates (the first and second channel) and the water fluxes related to them are chosen for calculations. As PARET allows to calculate only one type of the characterized fuel having certain geometrical parameters and a composition of materials entering into it, data for the mixed core gained separately for a FA of IRT-3M type and IRT-4M, then powers of an energy release were summed [3]. Following data were used as input parameters at calculations: accident occur on the nominal peak power (10 MW for HEU

core and 11 MW for the first mixed and LEU cores), reactor shutdown occurs on 12 MW. The delay time between excess of the peak power and the beginning of shim rod drop in a core is 0.1 seconds for both types of a FA. Reactor shutdown caused by three safety rods dip in a core (SR) from completely withdrawn position and six control rods (CR) from critical position. Insertion of SR rods on 0,6 m length occurs in 0,5 sec, control rod plunges into a core with constant velocity of 35 mm/sec.

Description of accident and its analysis

Accident with the full instantaneous traversal rupture of the primary loop piping of a reactor is one of the most dangerous accidents.

In the case of full instantaneous traversal rupture of the primary loop piping (inhausting or pressure head) out of a reactor tank, the reactor shuts down by emergency protection system because of a diversion from normal values of the following parameters:

- Pressure in primary loop is less, than 10%;
- Water flux rate in primary loop is less, than 20%;
- Water level in the reactor central tank is less, than 30 cm;
- Pressure drop in a core is less, than 20%.

At water level decrease in the central tank of a reactor to a mark of 2,7 m (less than 1 meter over core) special valves will open automatically and water delivery from tanks of a spare distilled water in a reactor tank through the spraying device of the core emergency irrigation system. Spare distilled water tanks volume is 40 м^3. Water flux rate through the spraying device - 15 m^3/h.

The water, leaking from a reactor tank, is collected in the gathering system channel of emergency leakings, located in a floor of a pump premise of the primary loop. As soon as the water level in the channel of system of gathering of emergency leakings will reach a point of 700 mm from a channel floor, one of two emergency pumps for return of water to the central tank of a reactor through system of an emergency irrigation of a core automatically will be turned on. Remaining heat release of the active core is tapped by an irrigation of fuel elements surface, preventing their heating to fusion temperature. At an emergency irrigation of a core the part of the water agglomerated in the channel of emergency leakings gathering system, partially vaporized. The volume of vaporized water will replenish automatically by operation of an emergency irrigation system (at delivery of the distilled water from tanks). If distilled water reserves are settled, then technical water from a water supply system or from the secondary loop moves in a core emergency irrigation system. There are also possibilities of delivery of technical water from a fire waterpipe or from a fire-engine.

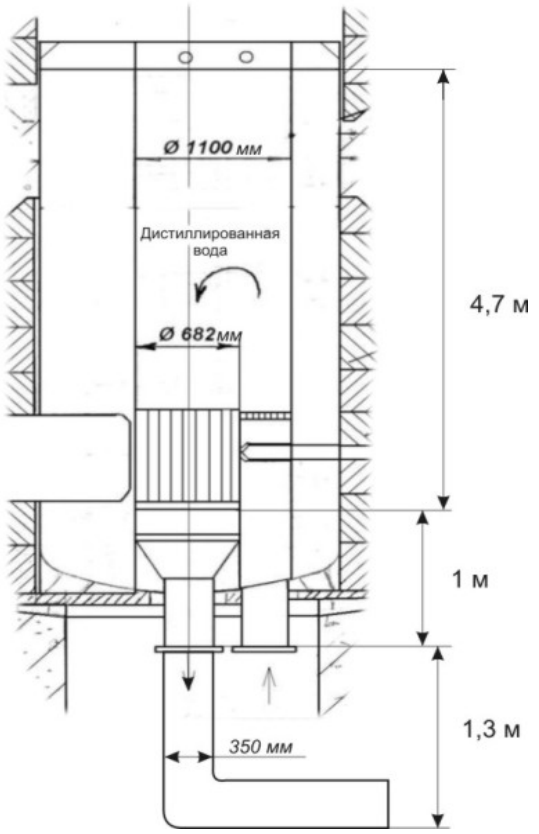

Fig. 1. Sideway view of a reactor tank.

PARET code cannot calculate a transient of water loss from a reactor tank in case of the full instantaneous traversal rupture of the primary loop pipeline. We yield an estimate of time of a devastation of a tank and an estimate of the underload of water flux rate through ызкфнштп device providing cooling of fuel elements of a FA in a core.

For an estimate of time necessary for the full devastation of a reactor tank, the tank is divided on 3 parts:

1 - diameter 1100 mm, height H_1=4,7 m and volume 4,464 m^3,

2 - diameter 682 mm, height H_2=1 m and volume 0,365 m^3,

3 - diameter 350 mm, height H_3=1,3 m and volume 0,125 m^3.

The full volume of a reactor tank - 4,954 m^3. The formula used by us:

$$V_i = \sqrt{2 \times g \times H_i}, \quad T_i = \frac{S_i \times HD}{S_3 \times V_i}$$

Where: V_i - velocity of water in pipe S_3, m/s, g - a free fall acceleration - 9,8 m/s^2, S_i - the second part, S_3 - $3{,}14 \times (0{,}175)^2$,

HD - a step on distance of 0,1 m.

Time estimated by us for operation of an irrigation system - 3,72 sec. Time estimated by us demanded for the full devastation of:

the first part - 4,92 sec,

the second part - 0,44 sec,

the third part - 0,42 sec.

Thus, the estimate time demanded for the full devastation of a reactor tank - 5,78 seconds.
After water losses, FA cooling is provided by water spraying which flows downwards on a surface of fuel elements. At functioning of this shower the temperature of fuel elements a little differs from water boiling temperature. At the insufficient water flux rate flowing downwards on a FA, it dries up, not reaching FA shaft. Thus, the dry part of fuel elements will be cooled only by steam and can heat up to higher temperature.
The necessary water flux rate at a residual energy release defined by equality of energy in a FA and a heat immersed by water, impinging on a FA. Water heating occurs at the expense of pinch of its temperature on an inlet in a FA to saturation temperature, at the expense of absorbing of the additional energy caused by a water dusting. Minimum water flux rate occurs in case of its full evaporation. The energy balance can be expressed in the form:

$$Q_{\min}^{FA} = \frac{P}{n(c\Delta t + r)}, \quad (1)$$

Where:
P - residual energy release in the core, calculated by Wigner and Wei formula:
$P(t) = 0{,}0622 \times P_0 \times (t^{-0,2} (t_0+t)^{-0,2})$
t_0 - reactor operation time on power P_0, t_0 = (20 days) ×(24 hours/days) ×(3600 seconds/hours)
t - time after a reactor shutdown, seconds
n - FA quantity in a core.
c - water heat capacity - 4,2 kJ/kg °K
Δt - a difference of saturation temperature and heated water or 105-45=60 °C
r - steam formation energy 2256 kJ/kg
$Q_{\min}^{FA}$ - minimum water flux rate for FA with a average residual energy release.

Analysis of a core with high enriched IRT-3M fuel

Calculated values for the full core combined from a IRT-3M type FA are the following: power in 1 sec - 6,2 % of 10 MW or 0,62 MW. 18 FA loaded in a core, average power of one FA - 0,034 MW for 1 sec (the same values as for the first mixed core). Calculated non-uniformity of an energy release is 1,39 for FA to FA and 1,16 - for pipe to pipe within FA, having the peak power; superimposition of two non-uniformities - 1,61. Therefore power which will be removed from one FA, taking into account non-uniformity, is equal to 0,0547 MW. Minimum water flux rate, necessary for cooling of one FA (formula 1) - 0,022 kg/sec or 0,082 m^3/h (the same values, as for the first mixed core). Delivered water flux rate in FA - 0,184 kg/sec or 0,245 m^3/h from a spare tank or the emergency pump, accordingly, as shown above. Therefore the excess factor of the actual water flux rate over the necessary flux rate in IRT-3M core is 2,2 or 3,0.

Residual power is known on a "decay" curve.

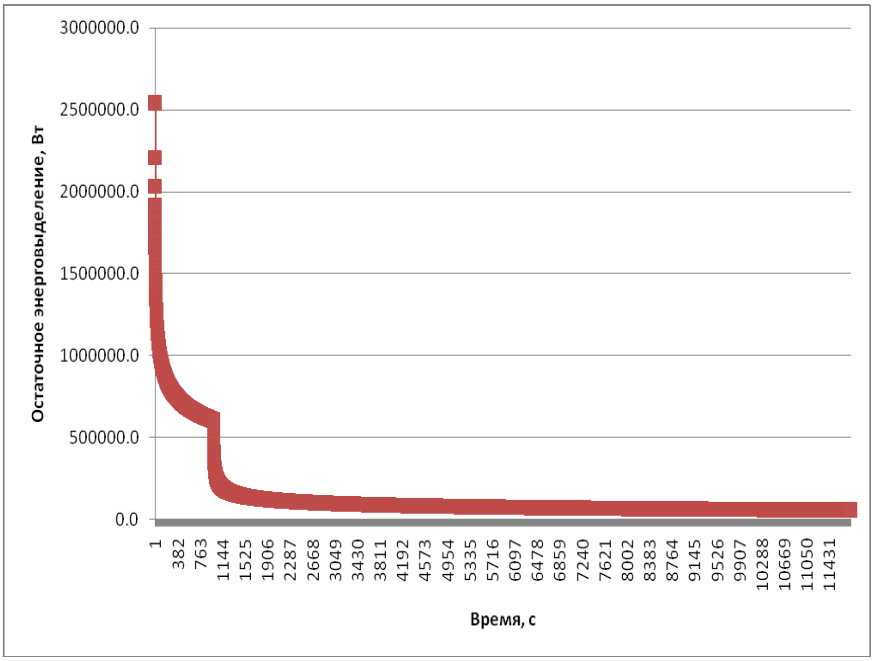

Fig. 2. Residual energy release calculated by Wigner and Wei formula.

After 1 second energy release reduction is approximately 6,2% or 0,682 MW if the reactor rated power was 10 MW, after 10 seconds the energy release is 3,3%, and after 2,2 hours - 1%.

Analysis of the first mixed core

Average power in FA is equal to the full power of a reactor divided into number of FA (18 FA for HEU or 20 FA for the mixed cores with HEU and LEU or completely LEU core), thus for the first mixed core is 0,034 MW after 1 second.

Combined non-uniformity in FA is 1,62 and it is used for definition of average power which should be removed from one FA which is, in the worst variant, - 0,0551 MW in 1 sec to prevent fuel heating. This power P is used in the formula (1) above.

Let's score, that the evaporation heat dominates over a denominator of the formula (1) because the full evaporation of water is supposed. For this core, the water flux rate at it spraying on one FA is 0,022 kg/sec or 0,082 m^3/h (at calculations water density is accepted equal to 960 kg/m^3).

Sprayed water from a spare tank is 15 m^3/h, and of the emergency pump - 20 m^3/h. The certain part of sprayed water as it is supposed, will flow by a reactor tank (because of a pulverization of splashes from a nose), that makes 20 % of total amount of sprayed water, and 80 % (or 12/16 m^3/h) sprayed water will begin to flow in a reactor tank.

Let's guess, that within a reactor tank water allocation is homogeneous at spraying; each FA gains that rate of water flux which falls on it (on the sides 71,5×71,5 mm or with the area 0,005112 $м^2$) concerning the full area of a reactor tank (the area of a circle in diameter of 0,652 m that makes 0,334 $м^2$) which is the factor of field 0,0153. Multiplication of this factor of field to the rate of sprayed water flux 12 m^3/h from a spare tank or 16 m^3/h from the

emergency pump in a reactor tank shows, that volume of the water flux rate, falling to one FA is equal to 0,184 or 0,245 m^3/h, accordingly. This value exceeds necessary water flux rate 0,082 m^3/h (calculated above) in 2,2/3,0 times.

Analysis of a core with low enriched IRT-4M fuel

Calculated values for a core with IRT-4M FA are the following: power after 1 sec is 6,2% from 10 MW that equal s to 0,682 MW. At a core with 20 FA, average power in one FA is equal to 0,034 MW after 1 sec (as well as for a core from IRT-3M FA and the first mixed core). Combined non-uniformity is 1,5. Therefore power which should be removed from one FA in a second at the worst variant is 0,051 MW. The underload water flux rate, necessary to cool one FA (the formula 1) is equal to 0,02 kg/sec or 0,076 m^3/h. Water flux rate on a FA will be 0,184 or 0,245 m^3/h from a spare tank or emergency pump, accordingly, as shown above. Therefore the water flux rate exceeds the necessary water flux rate in 2,4 or 3,2 times in a core completely loaded by an IRT-4M FA.

Conclusion.

Performed calculations and the accidents analysis, when there is the full instantaneous rupture of the primary loop pipeline of a WWR-SM reactor at reactor conversion on use of low enriched IRT-4M type fuel show, that the reactor safety system, including spraying, will cope with failure not causing melting of a core and not creating threat to the safety of the reactor personnel and associates.

Literature

1. **Baytelesov S.A., Dosimbaev A.A., Kungurov F.R., Salikhbaev U.S.** Neutron-physical and thermohydraulic calculations of WWR-SM with high- and low-enrichment uranium fuel assemblies. Atomic energy, v. 104, No 5, p. 339-343, 2008.
2. **Woodruff W., Smith R.** A Users Guide for the ANL Version of the PARET Code, ANL/RERTR/TM-16, 2001.
3. **Garner P., Hanan N.** Investigation of Approximations in Thermal-Hydraulic Modeling of Core Conversions, presented at 2007 International Meeting on Reduced Enrichment for Research and Test Reactors. Prague, Czech Republic, September 23-27, 2007.

APPLICATION OF THE MODIFIED NEUTRON SOURCE MULTIPLICATION METHOD FOR A MEASUREMENT OF SUB-CRITICALITY IN AGN-201K REACTOR

MYUNG-HYUN KIM
Department of Nuclear Engineering, Kyung Hee University
KHU Reactor Research and Education Center,
Yongin-shi, Gyeonggi-do, 446-701, Rep. of Korea

ABSTRACT

Measurement of sub-criticality is a challenging and required task in nuclear industry both for nuclear criticality safety and physics test in nuclear power plant. A relatively new method named as Modified Neutron Source Multiplication Method(MNSM) was proposed in Japan. This method is an improvement of traditional Neutron Source Multiplication(NSM) Method, in which three correction factors are applied additionally. In this study, MNSM was tested in calculation of rod worth using an educational reactor in Kyung Hee University, AGN-201K. For this study, a revised nuclear data library and a neutron transport code system TRANSX-PARTISN were used for the calculation of correction factors for various control rod positions and source locations. Experiments were designed and performed to enhance errors in NSM from the location effects of source and detectors. MNSM can correct these effects but current results showed not much correction effects.

1. Introduction

In this study, a theory of modified neutron source multiplication(MNSM) method[1] was tested in a small educational reactor, AGN-201K. This method is an improvement of correction to a conventional neutron source multiplication(NSM) method[2] using correction factors considering source location and detector locations. It has already been tested at Kyoto University Critical Assembly and a PWR plant core. A reactor tested in this study is a small core which has a sensitive effect of source location in a complex geometry.[3]
Generation of cross section library was developed and a S_N code, PARTISN was used for the evaluation of adjoint flux as well as real flux.
In order to investigate an effectiveness of correction, experiments for NSM method were designed to enhance the location effects of source as well as detector. Three kinds of correction factors were calculated in advance of experiment for all conditions of different control rod locations, source locations and detector locations.

2. Modified Neutron Source Multiplication Method

Conventional NSM method[2] is a straightforward and easy method to evaluate a control rod worth. This method is an economical one because expensive device is not required and only source and detectors are required. However, this method can be worked only for the steady state and cannot be used for the dynamic mode. Higher mode flux is not concerned and measured reactivity is highly dependent on the perturbations of sources and detectors locations. And also measurement is not reliable when the signal is weak and sub-criticality is very deep from critical condition. The basic formula for this method is as the following Eq. (1).

$$\rho_n = \rho_{ref}\left(\frac{M_{ref}}{M_n}\right) \qquad (1)$$

Here ρ_{ref} is a reactivity at a reference sub-critical state, ρ_n is a reactivity at n state, M_{ref} is a count rate at a reference state and M_n is a count rate at n state. MNSM method[1] applied three correction factors like as the following Eq.(2).

$$\rho_n = \rho_{ref}\left(\frac{M_{ref}}{M_n}\right)C_n^{ext}C_n^{im}C_n^{sp} \qquad (2)$$

Derivation of three correction factors were derived from kinetics equations in Ref.[1]. C_n^{ext} is an extraction correction factor which is defined as a ratio of fundamental mode extraction of reference state to n-state. C_n^{im} is an importance field correction factor which is defined as a ratio of importance weighted source intensity of n-state to reference-state. C_n^{sp} is a spatial correction factor which is defined as a ratio of detector signal from fundamental mode flux of n-state to reference-state. Those three correction factors are defined as ratios of weighted integral sum of eigenvalue fluxes or fixed source fluxes. In this problem weighting has been done by adjoint fluxes. Therefore, for each state of sub-criticality where control rod position are different, eigenvalue multi-group diffusion problems should be solved for normalized real fluxes and normalized adjoint fluxes. For each sub-criticality state, fixed source problems should be also solved for normalized fixed source fluxes. Therefore three kinds of problems should be solved in advance for all kinds of reactor conditions in order to solve three kinds of fluxes. These three kinds of fluxes should be put into formula for three correction factors as a energy-group weighted integrals as well as spatial node-volume adjoint-weighted integrals. At each reactor condition-n, three correction factors C_n^{ext}, C_n^{im}, C_n^{sp} are calculated as a ratio to the reference state. This is a drawback of this method, we should know exactly the reference state reactivity just below the critical state. This method needs an extensive calculation burden compared with the other method. However, once you have a proper calculation tool, computational cost is not a problem anymore at these days because of increased computing power. Once we prepared correction factor tables for each given conditions without measurement, all sub-critical reactor conditions can be evaluated as an interpolation scheme with computing automation.

3. Reactor AGN-201K

Research and Education Reactor, AGN-201K is a zero-power reactor which has been operated at Suwon campus of Kyung Hee University(KHU) since 1982. It was originally installed at Colorado State University in 1967 and was moved to Korea in 1976. It was dedicated for education for nuclear engineering students in KHU. Because of obsolescence, refurbishment project was carried out with government research fund during the period of 2004 through 2007. Reactor power was up-rated by 100 times and an old analog-type operational console and I&C parts were replaced. Additional shielding walls and a new digital-type console were also installed. The average thermal flux at the central hole is $3.0\text{x}10^8$#/cm^2-sec. The maximum thermal power of AGN-201K is 10 watt. Therefore there is no cooling system for a homogeneous reactor. Core is a cylinder of 25.6cm diameter and 24cm height and consists of 9 disks which is a homogeneous mixture of 19.5w/o UO_2 powders and polyethylene. There is a small diameter glory hole penetrating the core central zone which is utilized for neutron activation. There are 4 beam ports (8 in total in both direction) which penetrate a 20cm-thick graphite reflector zone outside of core. Reflector zone is surrounded by 10cm-thick lead for gamma shield and 55cm-thick water for neutron shield. Safety against nuclear transients and hypothetical radiation accidents was proved by accident analysis. [7], [8]

Two safety rods and one coarse control rod have a reactivity worth of 1.25% and one fine control rod has 0.3%. Neutron flux is measured at three locations outside of reflector zone in a biological shield water. Therefore flux measurement is very weak to see many effects from the reactor console. They are connected to reactor protection systems. Additional detector system is used for this study to investigate an location effects.

4. Calculation Tool & PARTISN Model

AGN-201K has water at the core boundary, graphite as a reflector outside of core and polyethylene as a homogeneously mixed moderator with fuel. Cylindrical geometry core is complex because of cylindrical shape holes and control rods. There is no proper calculation tools and cross section library for the calculation of flux, adjoint flux and fixed source flux in AGN-201K. In a previous study in 2006, PARTISN(PARallel, TIme-dependent SN)[5] and ZZ-KASHIL-199N[6] was chosen after a verification study in which results of PARTISN were compared with MCNP and DANTSYS for AGN-201K. PARTISN is a time-dependent, parallel processing, neutron transport calculation code developed at Los Alamos National Laboratory as a expanded version of DANTSYS. ZZ-KASHIL-199N library is a library (of 199-groups for total and 35 groups for thermal) developed for HELIOS code for LWR applications. was chosen to be the best.
The following Fig.1 is a cross-sectional view of AGN-201K and its PARTISN calculation model. Because of complex configuration, an approximate model was established where cylindrical control rod was approximated as a volume equivalent cylindrical node pieces. Total lengths were divided into 31 nodes in R-direction, 10 nodes in theta-direction, 66 nodes in Z-direction.

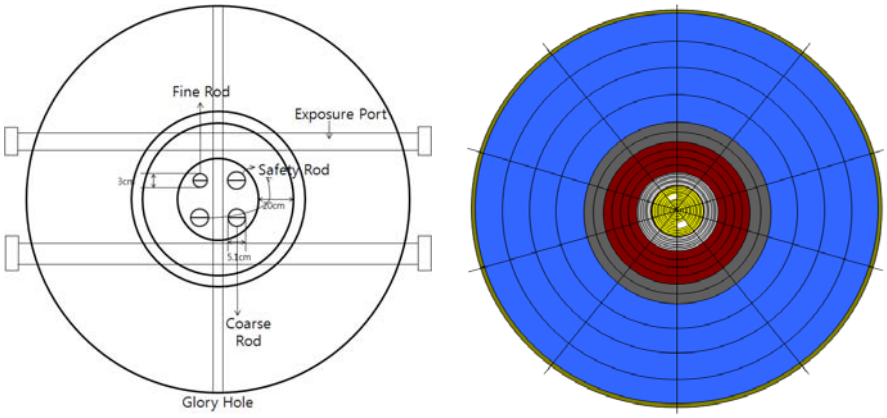

Fig. 1. Cross-sectional view of AGN-201K and mesh configuration for PARTISN

The following Fig. 2 and Fig.3 show normalized group-163(thermal) flux shapes and their adjoint flux shapes along the line passing two control rod and core center positions at the axially center plane. Fluxes were calculated at 5 sub-critical state of 5 coarse control rod(CR) positions. As we expected flux shape is quite symmetric except minor deviations in shape near the CR positions.
Fig.4 and 5 show normalized fixed source thermal (group-163) flux shapes along the line passing two control rod and core center positions at the axially center plane when the source is located at the core center and at the core boundary. There were no differences among different subcritical states, but big differences in shape as the source location moved.

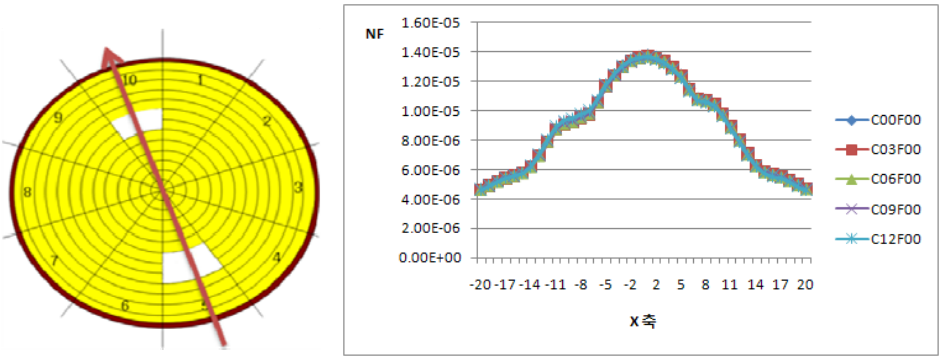

Fig. 2. Normalized real flux shape for group-163 along the center line

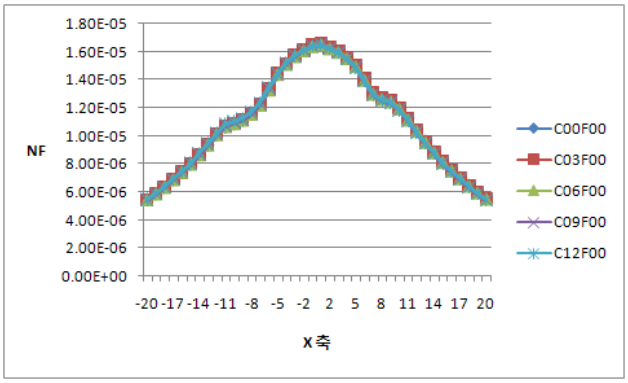

Fig. 3. Normalized adjoint flux shape for group-163 along the center line

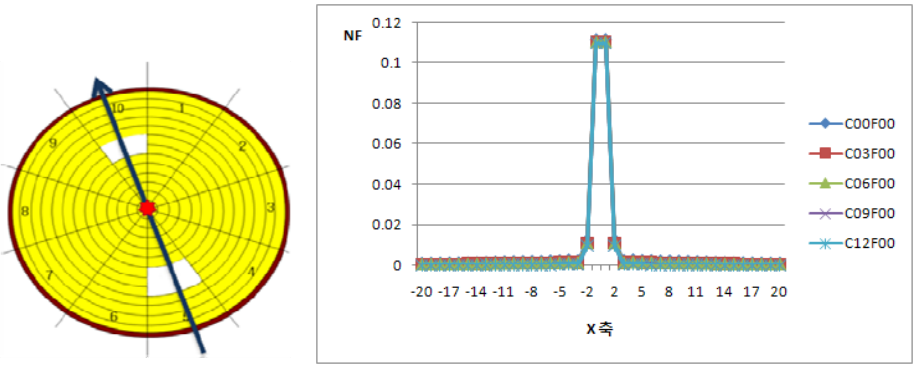

Fig. 4. Normalized fixed source flux shape for group-163 along the center line (with source at the center)

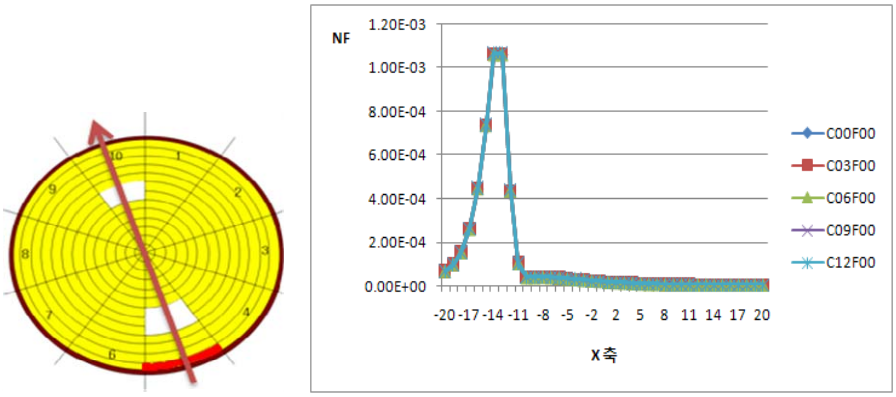

Fig. 5 Normalized fixed source flux shape for group-163 along the center line (with source at the core boundary)

5. Experimental Results

NSM experiment was done for the five subcritical state including one as a reference state. This experiment is a straightforward experiment with source and detectors. In order to check an effectiveness of correction factors. experiments were done for different source locations and detector locations.

5.1 Source Position Effect to Detector

Three different source location were tested for NSM experiment. Fig. 6 shows geometrical layout of source and detector in use. The case s0c0 has higher importance because source is located at the center and has a more capability of source multiplication before leakage. s1c0 and s2c0 has the same condition in source multiplication, but s2c0 case longer distance across the core between source and detector. Therefore source multiplication effect will be the highest in s0c0 and s2c0 and the lowest in s1c0. Fig. 7 & Table 1 shows this expectation is right. However control rod depth brought the same sensitivity along the positions. The differences in reactivity from the source location change is high and this should be corrected by the correction factors.

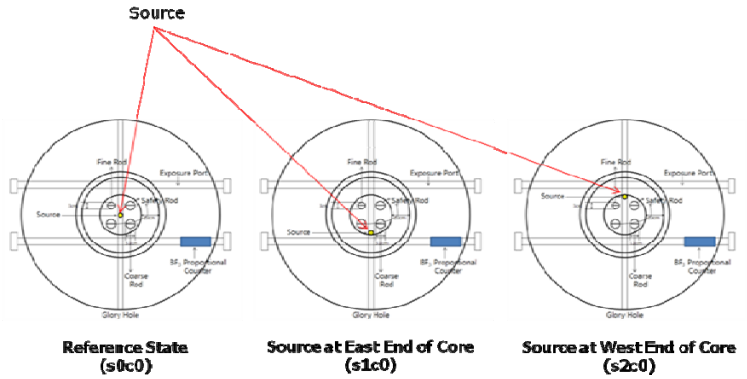

Fig. 6 Three different source location layout

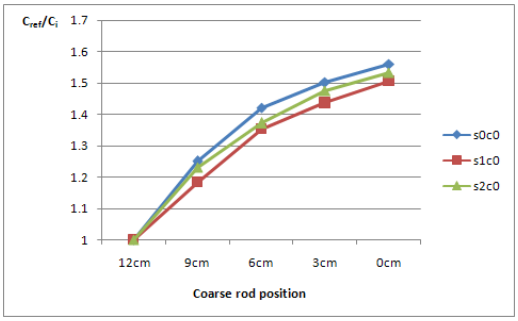

Fig. 7. Measured CR rod worth curve for different source locations

CR Position	s0c0	s1c0	s2c0
12cm	1	1	1
9cm	1.25	1.18	1.23
6cm	1.42	1.35	1.37
3cm	1.50	1.44	1.48
0cm	1.56	1.51	1.53

Table 1: Measured CR rod worth for different source locations

5.2 Detector Position Effect to Source

Four different detector location were tested for NSM experiment. Fig. 8 shows geometrical layout of source and detector in use. The case s0c0, s0c1, s0c2 have the same importance of source multiplication because detector is located with the same distance from the source at the center. However sensitivity from CR depth is different from each other. CR is located at the middle between source and detector in s0c0, at the shifted location to the side between source and detector in s0c1, and at the other side location between source and detector in s0c2. Therefore sensitivity would be high in the order of s0c0, s0c1, s0c2. In case of s0c3, detector is located outside of water tank and signal is very weak enough to make experimental measurement wrong. Fig. 9 & Table 2 shows this expectation is not right every case. Sensitivity of control rod depth did not show the same order. The differences in reactivity from the detector location change didn't show any differences.

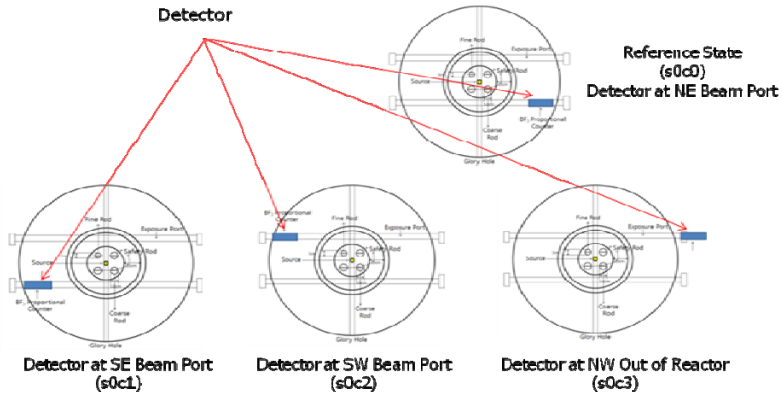

Fig. 8 Four different detector location layout

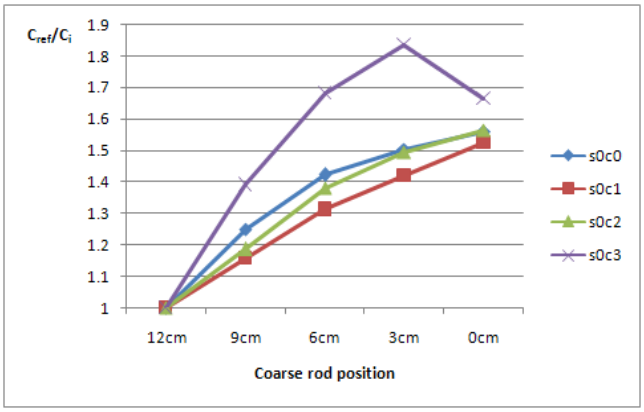

Fig. 9. Measured CR rod worth curve for different detector locations

CR Position	s0c0	s0c1	s0c2	s0c3
12cm	1	1	1	1
9cm	1.25	1.16	1.19	1.39
6cm	1.42	1.31	1.38	1.68
3cm	1.50	1.42	1.49	1.83
0cm	1.56	1.52	1.56	1.67

Table 2: Measured CR rod worth for different detector locations

6. Correction Effects

Three correction factors were calculated for five CR positions for three source locations. Following figures shows the calculated correction factors, but magnitudes of them are almost unity even though trend of change are reasonable. The maximum deviation from the reference state were less than 1%. Therefore correction was not done effectively as shown in Fig.13.

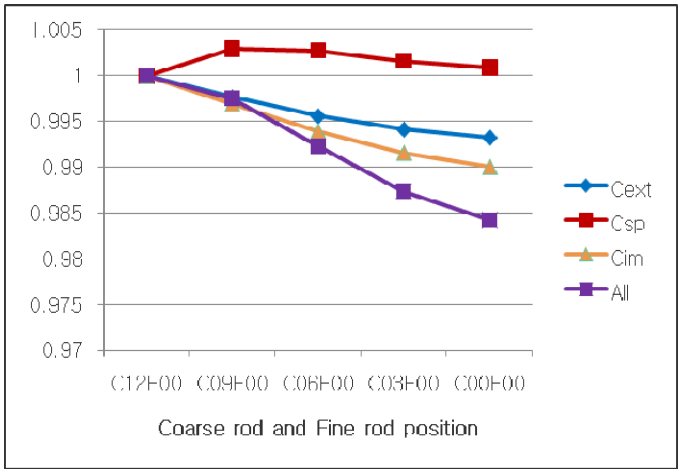

Fig. 10 Calculated correction factors of s0c0 layout

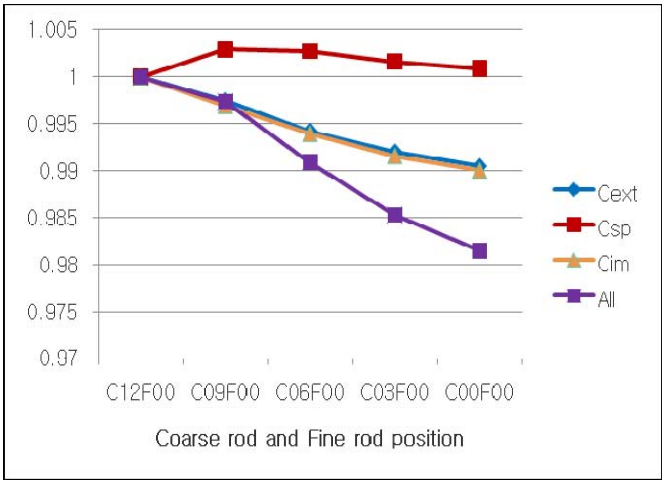

Fig. 11 Calculated correction factors of s1c0 layout

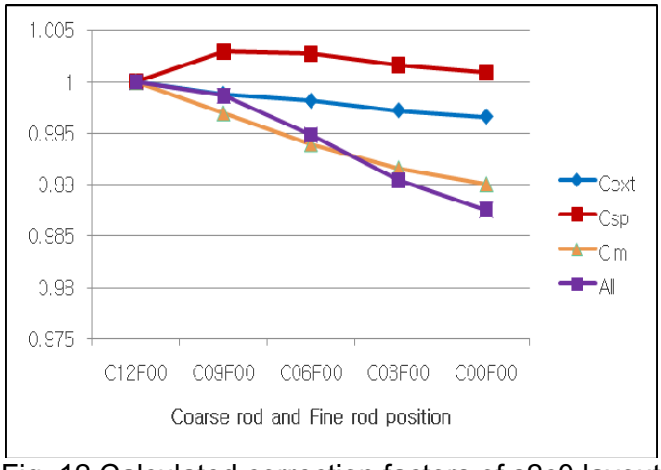

Fig. 12 Calculated correction factors of s2c0 layout

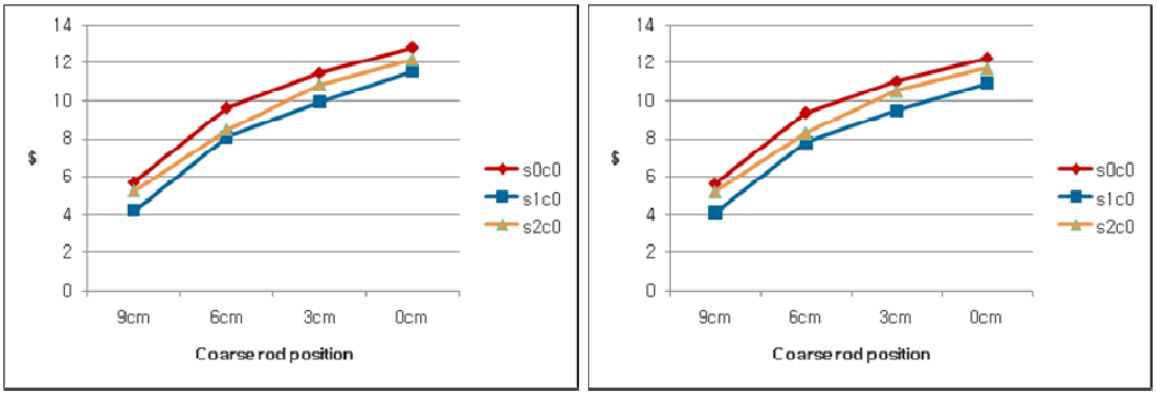

Fig. 13 Integral rod worth before and after the correction

7. Conclusions

The whole procedure of MNSM method was done for a educational small zero power reactor, AGN-201K and NSM experiments showed a relatively large effect in source location changes in sub-criticality measurement. For an evaluation of correction factors, approximated core model was solved for fluxes , adjoint fluxes and fixed source fluxes. Even though flux shapes are dependent on source locations, calculated correction factors are very insensitive. The maximum differences in correction factors are less than 1%. Therefore correction in sub-criticality measurement was not done effectively. More analysis should be done in order to explain this result.

References

[1] M. Tsuji, et. al., "Subcriticality Measurement by Neutron Source Multiplication Method with a Fundamental Mode Extraction," J. Nucl. Sci. and Tech., vol. 40, 158-169 (2003)
[2] E. Greenspan, "A Generalized Source Multiplication Method," Transaction of the American Nuclear Society, vol. 14, No. 29 (1971)
[3] Safety Analysis Report, Educational & Research Reactor AGN-201K, Kyung Hee University, Sep. (2007)
[4] Win Naing, et. al., "The Effect of Neutron Source Distribution on Subcriticality Measurement of Pressurized Water Reactors Using the Modified Neutron Source Multiplication Method," J. Nucl. Sci. and Tech., vol. 40, 951-958 (2003)
[5] R. E. Alcouffe, et. al., "PARTISN: A Time-dependent, Parallel Neutral Particle Transport Code System," LA-UR-05-3925, Los Alamos National Laboratory (2005)
[6] C. S. Gil, "KASHILL199N: A Multi-group Library for Thermal Reactor Design and Analysis Based on ENDF/B-Ⅵ," Korea Atomic Energy Research Institute (2005)
[7] Myung-Hyun Kim, "Reactor Upgrade of AGN-201 in KHU, Korea," Research Reactor Fuel Management(RRFM-2008), Hamburg, Germany, March 2-6, (2008)
[8] J.Y Lim, M.H.Kim, “Evaluation of Occupational Exposure Dose under a Hypothetical Radiational Severe Accidents of AGN-201K,” HANARO Symposium 2007, Daejon, May 4, (2007)

NEW TRENDS IN NUCLEAR FUEL EXPERIMENTAL IRRADIATION. MODERN CONTROL AND ACQUISITION OF THE IRRADIATION DATA

MARIN PREDA, MARIN CIOCANESCU, EMIL MUGUREL ANA
Institute for Nuclear Research Pitesti,
Campului Str. No. 1, 115400, Romania

ABSTRACT

With the irradiation devices used in the irradiation tests, the following experiments have been performed in TRIGA-SCN reactor :
a) In capsule-type irradiation devices
- fission gases composition determination
- dimensional measurements
- fission gases pressure measurement
- power pre-ramp and ramp
- power cycling
- structural materials testing

b) In loop-type irradiation device
- power ramp
- multiple power ramps
- overpower

Aiming to develop irradiation tests for advanced nuclear fuel elements, it is mandatory to increase the maximum neutron flux in the core with about 20%. This will lead to reactor power increase up to 21 MW.
This objective can be reached through:
- increasing the number of fuel clusters in the reactor core
- using the 6x6 fuel cluster to replace the present 5x5 clusters
- relocation of the control rods

In this context, the new control system and the data acquisition system operates online and allows real-time data evaluation.

Our TRIGA reactor was commissioned in 1980 (first criticality has reached on November 17th 1979).
During time the experimental facilities were used to perform the following test types:
a) Loop A:
- overpower type tests on fuel element,
- power ramp type tests on fuel element,
- corrosion and mechanical behavior studies on structural materials used in CANDU pressure tubes,
- LOCA type tests and on line and off line water chemistry control: pH 6÷10,5; conductivity: O_2 – 20÷100ppB; H adition; solid residues.

b) Capsule C1, C2:
- Fuel element dimensional measurement
- Fission products pressure – on line
- Power ramp
- Short-time irradiation for residual deformation of the cladding determination
- Central temperature measurement in the fuel element
- Fission gases release effects on the measured temperature during irradiation
- Fission gases composition for fuel element
- Densification - fuel element

c) Capsule C5:
- Structural materials irradiation tests in inactive environment: Zircalloy-4, steel 403-M, Zr-2,5%Nb until $2,3X10^{22}$ nvt
- Irradiation and tensile test of Chorpy standard minisamples – maximum 30 samples per irradiation campaign

d)Capsule C6:
- Thermomecanical behavior of CANDU type fuel element in fast power transients
- Analysis of fuel elements clad failure limits and mechanisms for pellet clading interaction
- Determination of energy level for fuel element failure depending on its geometry and microstructural characteristics
- Studies on clad-fuel mechanical interactions
- Database development regarding fuel element behavior in transient regimes

e) Capsule C9:
- Cycling tests on fuel elements that should confirm the fuel capacity to support a wide range of power cycling that occurs in normal operation of a CANDU reactor during power load following.

All irradiation devices are equipped with digital control system.
The irradiation data are on line gathered and processed.
C6 irradiation device is equipped with fast data acquisition system for fast transient processes.
In fact, as it could be seen in the Figure 1, the TRIGA reactor consists in two reactors:

✓ A Steady State Reactor, 14MWt.
✓ An Annular Core Pulsing Reactor of 20.000MWt.

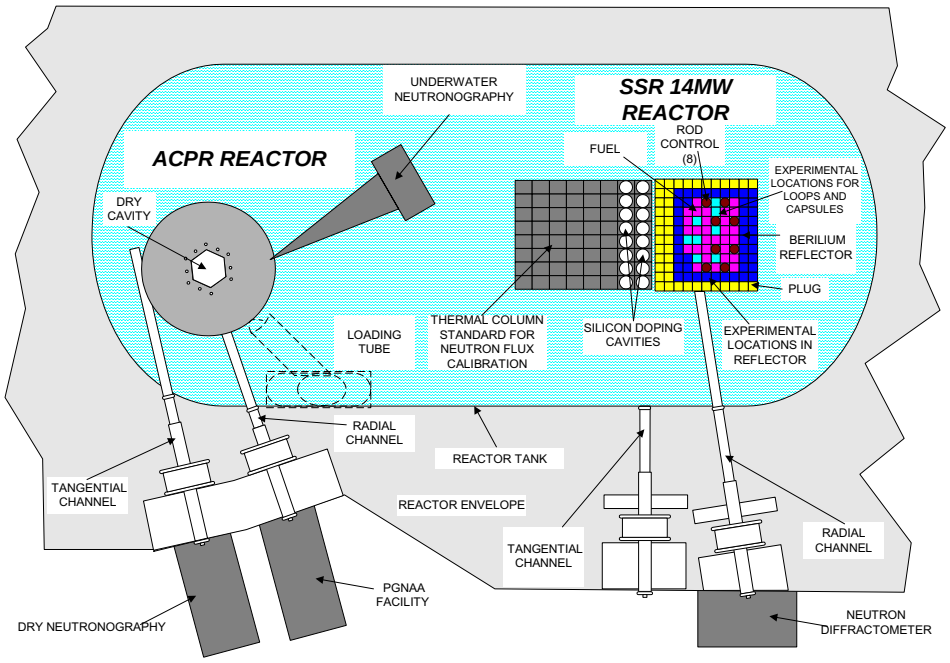

Figure1 TRIGA reactor pool arrangement

All data acquisition systems are connected to a server that gathers and display in real time the main parameters of irradiation devices in reactor control room taking to the reactor operator to act adequately.
Aiming to develop irradiation tests for advanced nuclear fuel elements, it is mandatory to increase the maximum neutron flux in the core with about 20%. This will lead to reactor power increase up to 21 MW.
This objective can be reached through:
- increasing the number of fuel clusters in the reactor core
- using the 6x6 fuel cluster to replace the present 5x5 clusters
- relocation of the control rods

The optimal solution seems to be the one with 6x6 fuel cluster, which results in:
- maximum neutron flux increase from 2,9E+14n/cm2s to 4,1 E+14 n/cm2s
- Keff increase from 1,139 to 1,164

- the overall size of the fuel shroud remains unchanged
- the core configuration remains unchanged
- the thermal–hydraulic regime is preserved: an analysis performed with PARET code shows that using 6x6 fuel clusters the maximum value for fuel temperature is 729 degrees at 20 MW, below the maximum temperature of 750 degrees allowed by fuel manufacturer.

The following figures illustrate the actual core configuration emphasizing the irradiation devices position and sample results of data acquisition and processing during tests:

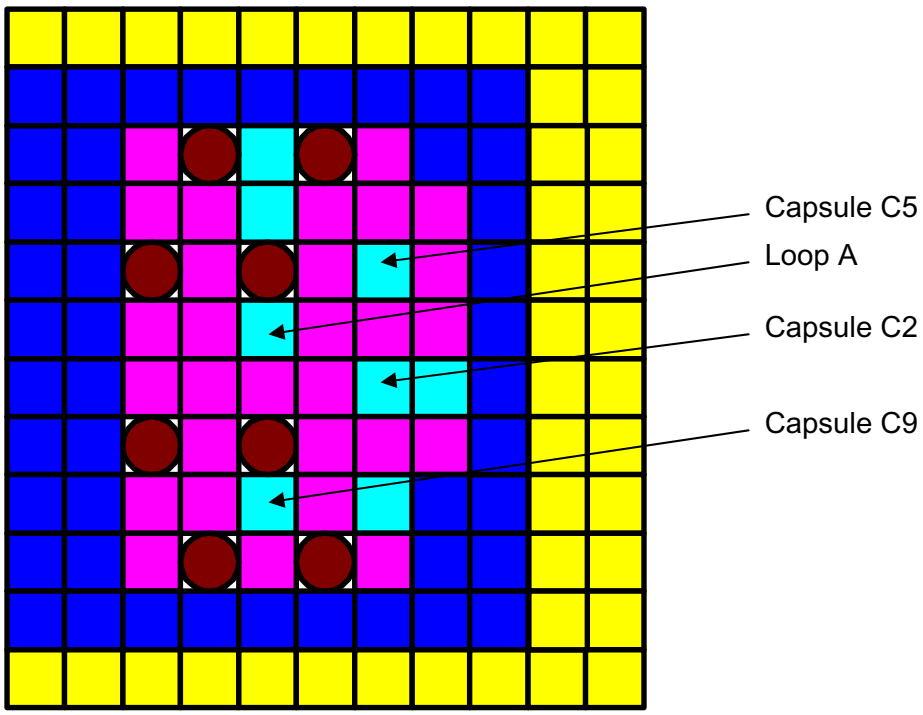

Figure 2 Irradiation devices position in reactor core

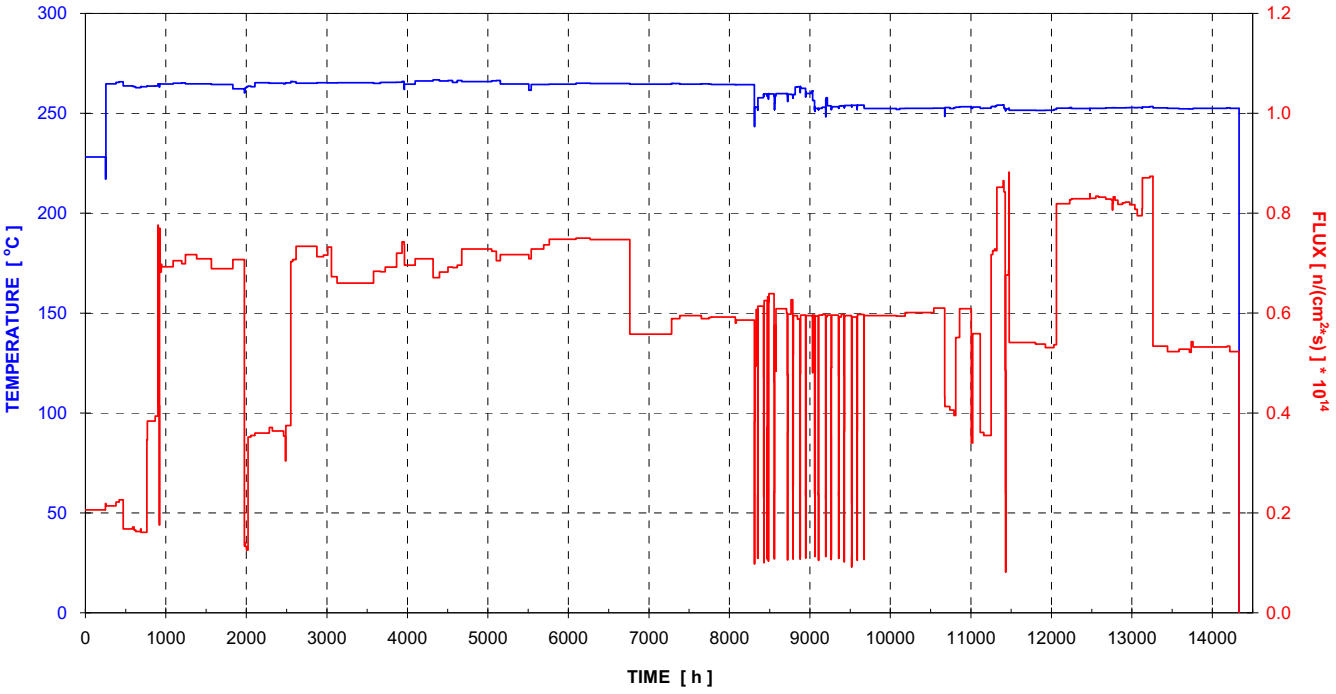

Figure 3 Loop A – Correlation between neutron flux and sample holder temperature

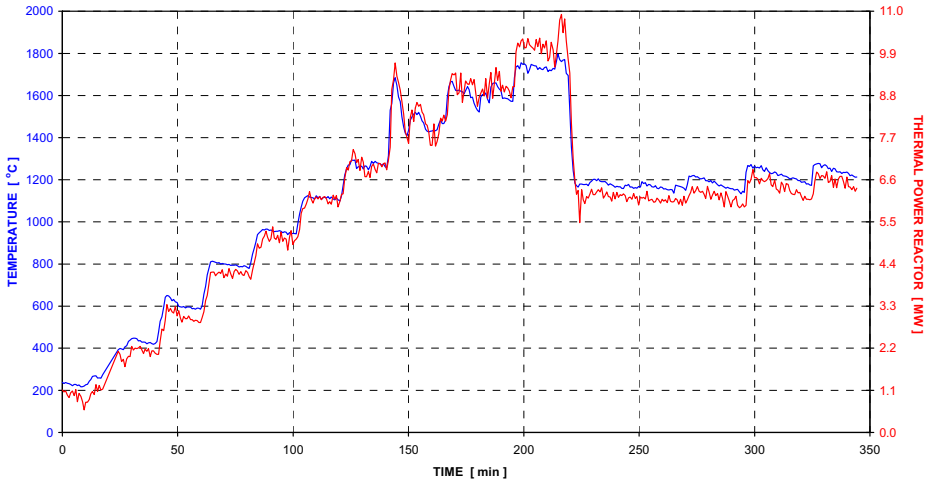

Figure 4 Capsule C2 – Correlation between sample holder temperature and reactor thermal power

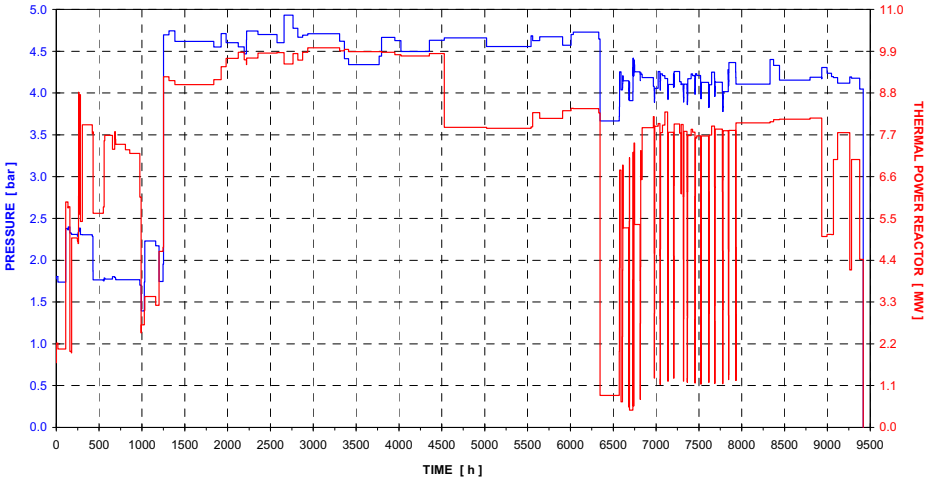

Figure 5 Capsule C5 – Correlation between sample holder pressure and reactor thermal power

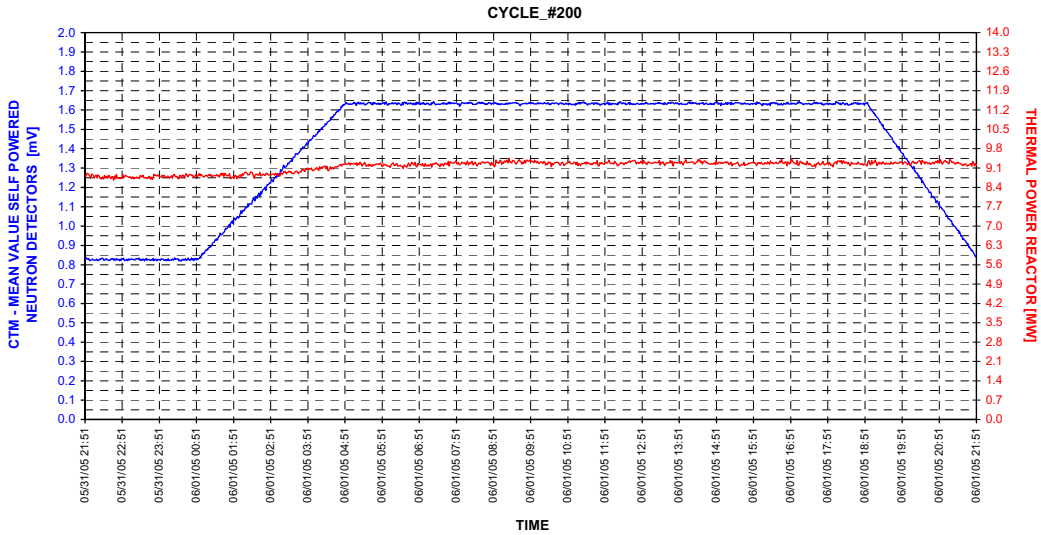

Figure 6 Capsule C9 – Correlation between CTM and reactor thermal power during a power cycle

In 2008 the control-command of primary cooling system was improved and in 2009 the reactor protection and control and monitoring systems were upgraded in cooperation with INVAP Argentina.
The modernization of all the control-command systems, including the reactor operation and safety systems take into account of the operation experience and IAEA guides. The basic requirement for Instrumentation&Control System modification is the separation between safety and operating components in order to decrease the human error consequences and avoid the common cause failures.

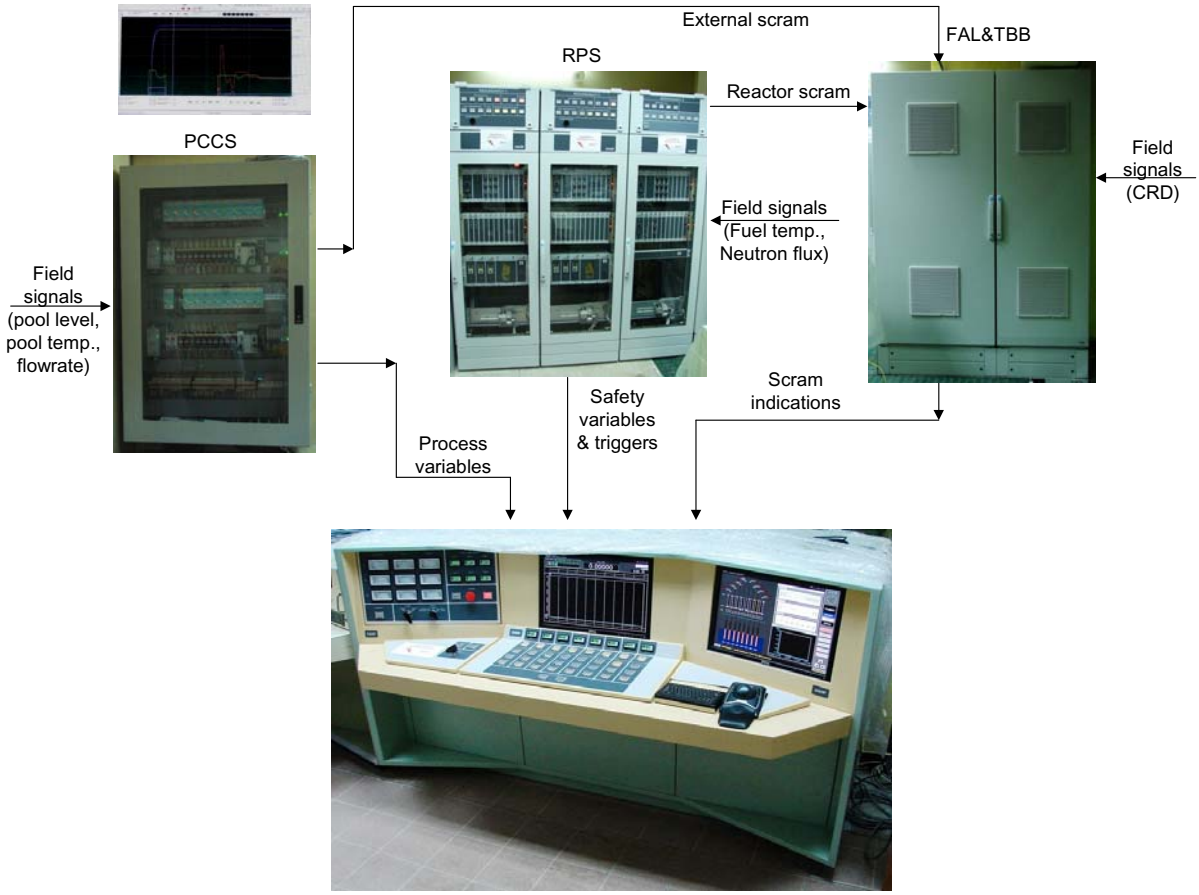

Conclusions

Once these modernization of control-command systems were accomplished we are able to carry out the following activities:
a) In TRIGA SSR 14MW:
- Power cycling on CANDU fuel elements
- CANFLEX fuel irradiation
- BWR fuel irradiation
- PHWR fuel irradiation
- ACR 1000 irradiation
- SEU fuel irradiation
- Irradiation on samples of Zr-2,5%Nb from the pressure tubes of the Cernavoda NPP
- Topaz irradiation
- Power ramp tests
- Irradiation on refabricated fuel
- Radioisotopes production: Ir 192, Co 60, I 129; for Mo 99 the technology under development

b) In ACPR:
- RIA type tests
- Tests on nuclear fuel in transient conditions.

RADIATION SURVEY AND PREPARING FOR THE DECOMMISSIONING OF RESEARCH REACTOR MR, RRC “KURCHATOV INSTITUTE”.

V.G. VOLKOV, A.G. VOLKOVICH, A.S. DANILOVICH, Y.A. ZVERKOV, V.I. KOLYADIN, A.V. LEMUS, V.I. PAVLENKO, S.G. SEMENOV, S.V. SMIRNOV, A.V. CHESNOKOV, A.D. SHISHA

Department «Rehabilitation”, Kurchatov Institute, (10 pt, italics)
Kurchatov Sq., 123182, Moscow, Russia

ABSTRACT

Works for the rehabilitation of nuclear and radioactively contaminated objects of the RRC Kurchatov Institute, continued for several years and now the experts of the center began work to prepare for the decommissioning of research reactor MR. As part of this work is carried out radiation survey radwaste repositories located in its premises, characterization of high-level waste that has accumulated in the storage basin and the extracts of the CPS, a survey of loop reactor facilities. Radiation survey carried out using robotic tools Brokk, equipped with gamma locator for the identification of intense gamma radiation sources. The gamma locator installed on a robotic tool serves for control and gamma vision of the Brokk. Management of the robotic tool and the gamma locator made from a safe place. Transfer of control signals and measurement data of the gamma locator were carried over by radio channel. For the radiation survey of the waste placed in cooling pools and the gateway of the reactor, the clarification and decontamination of water in these reservoirs was carried out. The clarification of the water was not carried out from 1993, when the reactor MR was shot down. Water purification was executed by standard water treatment systems for small basins. Sand coarse filters water collected radioactive particulate matter present in the pools and the gateway. Upon completion of the filter as radioactive waste were sent to long-term storage of Radon enterprise. Use of standard equipment was fully justified in referring to relatively low costs of conducting operations. In 2008 the characterization of the high level radwaste placed at the storages in the reactor hall was executed. For measuring of specific activities of the casks containing the radwaste the gamma locator installed at robot Brokk was used. The gamma locator allowed measuring of distribution of activity along the casks. This works allowed planning of amount of containers for removing of the high level radwaste from the reactor premises.In addition, work carried out on the removal of accumulated spent fuel from research reactors, including reactor MP. Now the project of decommissioning of research reactor MR is prepared and held its state expertise. If it approved at the end of 2009 it’s expected to start work of decommissioning the reactor.

1. Introduction

In 2008, specialists of Research Center “Kurchatov Institute” began work on decommissioning of Center’s research reactors under the Federal Program" Ensuring nuclear and radiation safety of Russia in 2008 and until 2015 ". In 2008-2009, in RRC “Kurchatov Institute” has been developed the project of “Decommissioning research reactors MR and RTF Federal government agencies of Russia Research Center "Kurchatov Institute" [1-4]. An endorsement of the FGA "Glavgosekspertiza Russia" and the endorsement of the State Ecological Expertise were received. This project was approved by the Federal Agency for Science and Innovation. Currently documentation for obtaining a license for the

decommissioning of the reactors MR and RTF is preparing. As part of preparatory activity purchase of the necessary equipment will be entered. According to experts from the RRC "Kurchatov Institute" it should be removed up to 3-4 thousand m^3 of solid waste and extracted and processed about 10 thousand m^3 of radioactively-contaminated soil.
In 2009, major efforts were aimed at obtaining of permits, removal of loop channels of the MR reactor, a survey of reactor storage, currently used as a repository for high level waste, as well as a sluice hatch between the storage pool and reactor pools, the depths of which are ~ 9 and ~ 6 m respectively.

2. Radiation survey of reactors premises and removal of loop installations

In the period after the final shutdown in 1993 at the reactor complex the preparatory activities, mainly aimed at ensuring the necessary level of its nuclear and radiation safety was carried out [2]. In 1996, from the active zone and from the reactor pool-storage working spent fuel and loop fuel assemblies (FA) were unloaded. They were placed in "dry" reactor storage. To date, radiation survey of the MR and RTF reactors and loop installations of MR reactor, which includes more than 600 pieces of equipment located in ~ 70 technological areas, has been done. As a result it was found that the contaminated systems, equipment and piping loop of the reactor and its facilities is mainly due to the inner surfaces of contamination by radionuclides ^{137}Cs, ^{90}Sr and ^{60}Co. Therefore, radiation survey techniques and tools developed to perform remote measurements have aimed on the measuring of radiation of these radionuclides. Levels of specific activity of equipment and building constructions being in the range from 103 Bq/kg and 107 Bq/kg, which determines the range of measured values and requirements of the remote means developed. Now some of the established means are installed on the robotic systems Brock to use of in the works of improving of the radiation situation in the reactor facilities [5].
To assess the current status and planning of engineering systems and technological support for work on the decommissioning of the reactors a radiation survey of systems of radiometric control, ventilation, sewage, water, electricity, heating was carried out. Engineering survey of the reactor building was made.
In order to improve the radiation situation in the reactor hall the work of removing parts of the loop channels over the pool water storage was carried out. Removing of the loop channel items was carried out using robotic «BROKK-330" and "BROKK-180", remotely controlled with the help of the developed video system (Fig. 1). Then with the help of "BROKK-180" cut channel element was placed in a concrete container. Dose rate, measured from the deleted items loop channels, ranged from 2 mSv/h to 0.03 Sv/h. After the segments, protruding elements of loop channels were again placed in the pool-store below the water level. As a result of work background of gamma radiation in the central hall of the reactor above the pool-storage was reduced by more than 20 times (from 0.63 to 0.03 mSv/h), outside the basin storage - 2 times (at 0.04 to 0.02 mSv/h).

3. Radiation survey of the sluice hatch of the reactor MR.

In 2009 radiation survey sluice hatch between the pool and the reactor's cooling pools, in which large quantities of radioactive products has been accumulated during the exploitation of the reactor, was held. There are no events for the purification of these reservoirs has not been since the shutdown of the reactor in 1993. Its transparency was very low and does not allow for visual inspection and survey tools video. Therefore it was decided to hold water clarification to remove the suspension and removal of impurities. Established system of water purification using ion exchange resins, today, demanded the audit and repair.
The work to restore its performance had been scheduled for 2010. Therefore it was decided to hold water clarification using the basin of the mechanical filter with a filling of quartz sand.
After achieving the necessary transparency of water in the gateway was carried out a visual examination of objects under a layer of water, and a detailed inspection of the underwater

area with a special TVsystem. Visual inspection revealed that in the pool sluice hatch organized storage of beryllium and graphite blocks of masonry, propellants rods and control rods. Storage is organized in two tiers. After the preliminary survey of the contents of the pool - the gateway, was detected a number of objects that require a thorough radiation survey. The purpose of the survey was to assess the EDR -radiation of different types of blocks and products, and the definitionγ spectrometric methods the main dose forming nuclides. Based on the study of design documentation it was selected objects for measurements that were in the process of exploitation in the immediate vicinity of the working fuel assembly channels of the reactor - Beryllium blocks of three types, two blocks of displacer and the graphite block.

Fig. 1. Cutting elements of loop channels, using remote-controlled robotic mechanisms «BROKK-180" and «BROKK-330"

For measurements the assembled leak tight canister was hang out into the pool. The detector was placed in the canister at a height of 30 cm from the blocks, located on the lower tier in the sluice hatch, and the distribution of EDR was measured. EDR values ranged from 0,3 to 8,2 mSv/h. For a preliminary assessment of EDR of γ-radiation and the distribution of activity planned for the height measurements of products were extracted from the pool, the staff left the room and measurements were performed remotely using a measuring complex "Gamma-pioneer" in the Brock-90. Simultaneously, the EDR at distance of 1 m was measured by a standard dosimeter (see Fig. 2).
The results of radiation surveys were identified products for spectrometric measurements. Spectrometric measurements were carried out by gamma-spectrometric complex ISO-CART firm ORTES, spectrometer DigiDART, detector GEM40P4.The detector was located outside the reactor hall, at a distance of 14.5 m from the measured object. According to the results of measurements it was found that the main emitting radionuclide is ^{60}Co, in the spectrum of the beryllium block there is radiation 1^{52}Eu and ^{154}Eu.

4. Radiation survey of dry repository.

In preparation for the decommissioning of the reactor MR the spent fuel was removed from dry repository and placed in the repository of SNF of the center (SFR in the building #109). Precise data on the distribution of the spent assemblies and their types were missing. To develop the technology unloading of the dry repository it was needed to store inventory of its content and get the following inputs:

- number of loaded cells.
- type of suspension products in the cell. The presence of protective plugs in the cells.

- characterization of products by their appearance - SFA, canister, open canister, the size of products, weight, presence of markings, etc.
- technical state of items and its pendants - corrosion, breaking of the guy.
- the content of the cells - one or two tiers.
- radiation characteristics – EDR of γ-radiation, measured at a distance of 1 m.
- video recording of done work.

Fig.2. Radiation survey of the objects extracted from the sluice hatch.

The expected dose rate could be hundreds of mSv/h. Therefore it was decided to use for the dry repository revision the measuring complex "Gamma-pioneer", which was mounted on robot Brock-90 [5]. The staff who managed of the Brock-90 and the complex of "Gamma-pioneer" was placed outside the hall and was protected by the biological defense of the thickness of 1,5 m. The Brock-90 with the complex of "Gamma-pioneer" was installed near the dry repository so that the measuring unit of the complex was on distance of 1 m from the investigated object.
During the examination of SFA the radiation characteristics, overall length, diameter of the SFA (to determine the type of hermetic packing), the type of connection SFA to the suspension canister are evaluated. As a result of works the certification of all 30 cells of dry repository was carried out, spent fuel, placed in them, was removed in the main repository of the Center.

5. Development of the project of decommissioning the reactors MR and RTF.

All data obtained during the preparatory phase were used in developing of the design of the MP and RTF reactors decommissioning. As base strategy of design a variant DECON – immediate stage-by-stage dismantle of constructions and the equipment of MR reactor and its loopback installations, including dismantle of the constructions of the RFT reactor is accepted. The validity of the choice confirmed by multivariate analysis and its comparison with other alternatives (SAFSTOR, ENTOMB) [4].
It is planned to use a remotely-controlled means (BROKK), the operator of which can be located in the radiation-safe place and manage these mechanisms, using video monitors. Dose load on the staff at this case will be 10-100 times lower than with traditional methods. All dismantling procedures were divided into three categories, requiring of the similar dismantling technologies.
The first category includes equipment cooling loop and loop facilities, located outside the pool of the reactor MR and pit of the reactor RTF. Dismantling of equipment in this category will be carried out using remote-controlled means, equipped with different attachments. An

increase in openings in the technological areas will require for the delivery of equipment in the premises and removal of containers with radioactive waste.
The second category includes equipment located in the pool of the MR reactor. This equipment will be dismantled in the pool under a layer of water. In this regard, it was proposed the use of remotely-controlled mechanical arm-manipulator mounted on a special platform.
The third category of operations was classified the works executed in the shaft of the RTF reactor. For dismantling works, related to the recovery of the graphite stack and cutting the reactor, the use of remotely-controlled mechanical robotic arm, installed on a specially designed platform, provides. After the removing of the graphite blocks it is planning to dismantle and cut the reactor vessel in the shaft. Then the large pieces of shell and constructions will be subsequently fragmentized in the pool under a water layer to prepare them for the transportation. According to the radiation survey data in the technological rooms of reactor cooling system, loops of the MR reactor and analysis of the weight and dimensions characteristics of equipment estimations of the amount of solid RW resulting from the dismantling operations are made.
In accordance with the classification of solid waste, depending on their specific activity (SPORB-99) with the decommissioning of reactors MR and RTF will form solid waste related mainly to the categories of medium-and low-active, amounting to ~ 300 and ~ 1500 m^3 respectively. Thus the total activity of solid radioactive waste resulting from the dismantling of reactors and loop systems was estimated as ~$1{,}0 \times 10^{14}$ Bq (~2700 Ci).

6. Results and conclusions

During the preparation for the decommissioning of reactors MR and RTF the radiation survey of equipment and their facilities was carried out. The characterization of the high-level waste at the sluice hatch between the storage pool and the pool of the reactor MR was executed. For each cells of the dry reactor repository the type of the object and canister, the object size, weight, presence of markings, the technological status and suspension (the presence of corrosion, violating of the guy), the radiation characteristics of objects were determined. According to the developed regulations the extraction works, repacking of highly active waste and the spent fuel in the made canisters and their moving to special repository of the spent fuel in the Center were executed.
Currently, design of decommissioning of the above reactors is developed, all the necessary allowances are received, documents for obtaining a license for decommissioning are prepare.

7. References:

[1]. Ryazantsev E.P., Kolyadin V.I., Egorenkov P.M. e.a. The decommissioning of nuclear and radiation hazardous objects Kurchatov Institute ". -Nuclear Power, V.87, No.3, 1999, p. 180-189.
[2]. Ryazantsev E.P., Bourkov A.V., Egorenkov P.M. e.a. The first results of the research reactor MR decommissioning. -In: Proc. of Intern. Symp. On Research Reactor Utilization, Safety and Management. Lisbon, Portugal, 6-10 Sept. 1999. Vienna: IAEA, SM-360-39P, 2000, p. 177-179.
[3]. Volkov V.G, Ivanov O.P, Kolyadin V.I, ea, Program of decommissioning for MR research reactor in the Kurchatov Institute,-In: Book of Abstracts of Intern. Conf. Decommissioning Challenges: an Industrial Reality? Avignon, France, 28 Sept. - 2 Oct. 2008, p. 75-76.
[4]. Volkov V.G., Zverkov Y.A., Kolyadin V.I., et al, Preparation for the decommissioning of research reactor in the MR Kurchatov Institute, Atomic energy, v. 104, no. 5, May 2008, p. 259-264. *(in Russian).*
[5]. Smirnov S.V., Radiation surveying robot, Environmental Safety, № 4, 2008, p. 77-79.

CHARACTERIZATION OF BOND STRENGTH OF MONOLITHIC TWO METAL LAYER SYSTEMS

S. DIRNDORFER, W. SCHMID, H. BREITKREUTZ,
R. JUNGWIRTH, H. JURANOWITSCH, W. PETRY

Forschungsneutronenquelle Heinz Maier-Leibnitz (FRM II), Technische Universität München, Lichtenbergstr. 1, 85747 Garching, Germany

C. JAROUSSE
AREVA-CERCA, Les Bérauds, BP 114, 26104 Romans Cedex, France

M. HIRSCH
Lehrstuhl für Umformtechnik und Giessereiwesen (utg), Technische Universität München, Walther-Meissner-Str., 85748 Garching, Germany

ABSTRACT

The in-pile performance of nuclear fuel plates is strongly influenced by the mechanical contact between fuel and cladding. Today, there is not much information available about the bond strength of two layer systems typical for monolithic fuel plates. The bond strength is considered to be a plausible indicator for the quality of the mechanical contact. Using tensile tests, the bond strength of the following material combinations were examined: fuel / cladding, fuel / diffusion barrier and diffusion barrier / cladding. Double layer foils, consisting of uranium-molybdenum alloy with 8 wt.% Mo (DU-8Mo) as fuel surrogate, Al 1050 as cladding and Ti, Nb or Zr as diffusion barrier materials were used. They were produced by sputtering. Beforehand, the behaviour of the adhesive used to mount the samples onto the specimen holders has been examined. Bond strengths of DU-8Mo on Ti and Nb larger than 70 MPa have been achieved.

1. Introduction

The RERTR program (Reduced Enrichment for Research and Test Reactors) aims on developing new fuel forms in order to convert research reactors to use fuel with a lower enrichment preferably LEU. It is well known that the in-pile performance of nuclear fuel plates is strongly influenced by the mechanical contact between fuel / cladding, cladding / diffusion barrier and fuel / barrier. It is therefore important to study their bond strength as this indicates the quality of the mechanical contact between metal layer systems that are suitable for research reactor fuels. The examination of the bond strength is a current point of worldwide investigations and has also been carried out by [4].

2. Experimental Methods and Materials

2.1 Test specimens

Test specimens were fabricated by a DC-magnetron sputtering device [3]. The test specimens consisted of two metal layers, a substrate and a sputtered layer. Specimens consisted of aluminium, niobium, tantalum, titanium and zirconium as substrate and of a

sputtered layer of Ti, Nb or an uranium-molybdenum alloy with 8wt.%Mo which were approximately 8 µm thick. The specimens were circular with a diameter of 25 mm or were quadratic with an edge length of 25 mm. These specimens are considered to represent interfaces to occur eventually in future fuel plates of monolithic type.

2.2 Tensile Tests

Every specimen was mounted on top of a specimen holder, made of stainless steel. The surface of this stainless steel measured 314 mm², which corresponds to the area of the specimens to be loaded. Detailed information about test specimens and preparation can be found in [1]. The adhesive EP-15 of MasterBond needed curing at 200 C° for 90 minutes to achieve the utmost bond strength. SEM analyses of heated specimen showed no negative results due to the applied heat treatment. The bond strength was examined by tensile tests that were executed according to a standardised procedure [2]. The tensile tests were carried out with a universal testing machine, a Zwick Roell Z100. All tensile tests were conducted at room temperature with a constant crosshead rate of 0.5 mm/min. The specimens were loaded until rupture occurred. The following combinations were examined concering their bond strength: substrate/sputtered layer
Al/Ti, Al/Nb, Al(non-polished)/DU-8Mo, Al(high polished)/DU-8Mo, Ta/DU-8Mo, Zr/DU-8Mo, Ti/DU-8Mo, Nb/DU-8Mo

Figure 1: Tensile test machine with specimen holders

3. Results and Discussion

SEM photographs of the fuel-clad interface and the fuel-barrier interface are shown in the figures 2 to 5.
In all the photographs of the specimen no interlayer is apparent. All specimens are compact and there are no visible cracks. In photographs referring to titanium and zirconium substrates a clear uninterrupted line is visible. In contrast to the niobium and aluminium substrates they show an irregular craggy bond line. Due to this, the effective bonding area on niobium and aluminium substrates is larger as it is on titanium and zirconium substrates.
Preliminary tests were made to determine the optimum parameters which resulted in a high degree of bond strength of the adhesive. A bond strength of (70.03 ± 4.91) [MPa] was achieved [1]. As soon as a rupture occurred, the reasons for it were allocated to a specific failure mode, as recommended by ASTM C 633 [2].

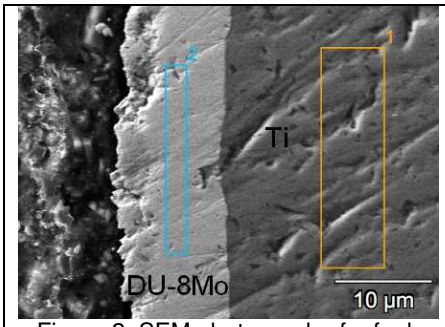

Figure 2: SEM photograph of a fuel-barrier interface Ti/Du-8Mo

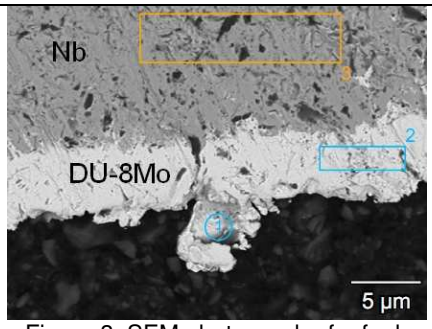

Figure 3: SEM photograph of a fuel-barrier interface Nb/DU-8Mo

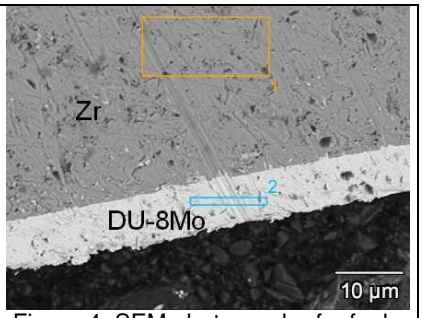

Figure 4: SEM photograph of a fuel-barrier interface Zr/DU-8Mo

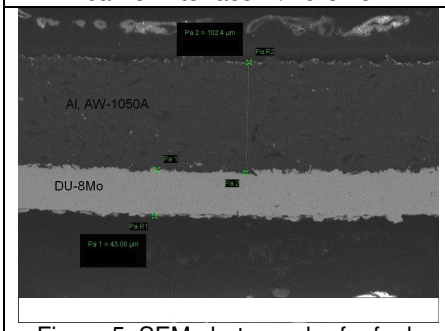

Figure 5: SEM photograph of a fuel-cladding interface Al/DU-8Mo

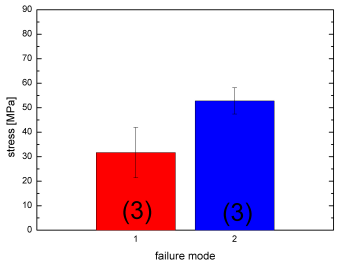

Figure 6: Bond strength of Al(polished)/DU-8Mo, cladding/barrier system

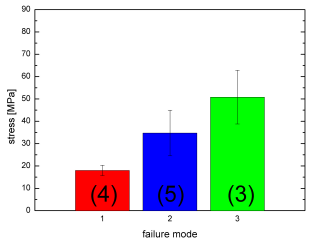

Figure 7: Bond strength of Al/DU-8Mo, cladding/barrier system

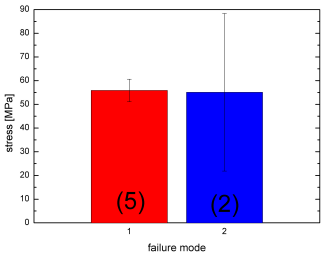

Figure 8: Bond strength of Al/Nb, cladding/barrier system

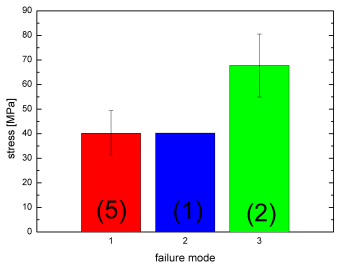

Figure 9: Bond strength of Al/Ti, cladding/barrier system

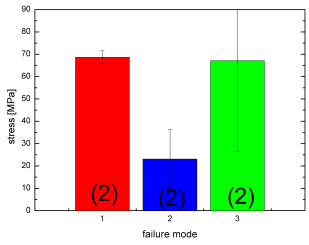

Figure 10: Bond strength of Zr/DU-8Mo, fuel/barrier system

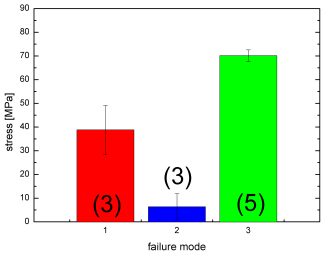

Figure 11: Bond strength of Ti/DU-8Mo, fuel/barrier system

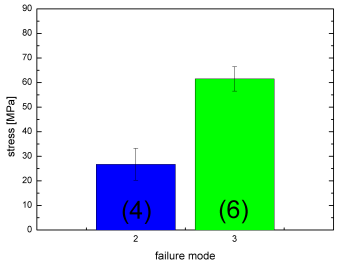

Figure 12: Bond strength of Ta/DU-8Mo, fuel/barrier system

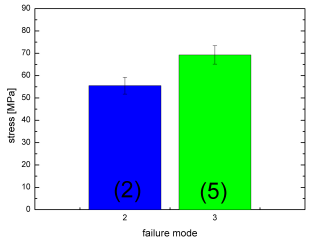

Figure 13: Bond strength of Nb/DU-8Mo, fuel/barrier system

- Failure mode 1
  The sputtered layer separated from the substrate. In this case, the bond strength of the adhesive was stronger than that of the specimen. The real value of the bond strength can be identified. Failure mode 1 is illustrated in red in the figures 6 - 13.
- Failure mode 2
  The rupture occurred between adhesive and specimen holder or adhesive and specimen. This bond strength provides only a lower limiting value of the bond strength of the sputtered layer on the substrate. Failure mode 2 is not as meaningful

as failure mode 3, as the adhesive did not reach the optimum bond strength. Failure mode 2 is illustrated in blue in the figures 6 - 13.

- Failure mode 3
  The failure occurred within the adhesive. The adhesive is visible on both sides, i.e. on the surface of the specimen and the specimen holder. The cohesion failure indicates that the adhesive has reached its maximum bond strength. The cohesion failure happens when the bonding from adhesive to the surfaces is stronger than the cohesion within the adhesive. In failure mode 3 a higher bond strength is present. It is therefore more suitable to estimate the quality of the bonding. Failure mode 3 is illustrated in green in the figures 6 - 13.

The number of experiments associated with each failure mode is presented in parentheses in the plots. Further in table 1, the bond strengths of the different failure modes are presented. The results for Ti/DU-8Mo and Zr/DU-8Mo scatter in a broad range. Three essential reasons for this can be identified. First, the Ti, Zr, Nb and Ta substrates were punched out to get a circular form. Ti and Zr were partially bent by this procedure. This deformation led to a minor bond strength as the adhesive bonding was difficult to achieve. Second, some specimens were affected by crumbs within the sputtering device, that degraded the bonding. Third, as shown by the SEM photographs, the interface of niobium was much better interlocked as it was the case with titanium and zirconium. These reasons explain why failure mode 1 occurred of titanium and zirconium specimens. If failure mode 2 and 3 are coexistent, failure mode 3 provides a better lower limiting value. As for niobium and tantalum no failure mode 1 occurred, a lower limiting value for the bond strength can definitely be stated.

Specimen	Failure mode 1	Failure mode 2	Failure mode 3
Ti/DU-8Mo	(38.81 ± 10.29) [MPa] (3)	(6.38 ± 5.51) [MPa] (3)	(70.13 ± 2.46) [MPa] (5)
Zr/DU-8Mo	(68.67 ± 2.89) [MPa] (2)	(23.10 ± 13.27) [MPa] (2)	(67.17 ± 40.78) [MPa] (2)
Ta/DU-8Mo		(26.74 ± 6.48) [MPa] (4)	(61.50 ± 4.96) [MPa] (6)
Nb/DU-8Mo		(55.51 ± 3.76) [MPa] (2)	(69.27 ± 4.14) [MPa] (5)
Al-non-pol./DU-8Mo	(18.02 ± 2.33) [MPa] (4)	(34.76 ± 10.21) [MPa] (5)	(50.80 ± 12.04) [MPa] (3)
Al-pol./DU-8Mo	(31.68 ± 10.26) [MPa] (3)	(52.78 ± 5.37) [MPa] (3)	
Al/Nb	(55.88 ± 4.75) [MPa] (5)	(55.11 ± 33.25) [MPa] (2)	
Al/Ti	(40.25 ± 9.17) [MPa] (5)	40.28 [MPa] (1)	(67.76 ± 12.83) [MPa] (2)

Table 1: Bond strength according to failure mode of different specimens that were coated with DU-8Mo, Nb or Ti by DC-magnetron sputtering [3], number of experiments for each specimen are in parentheses

The results of the fuel-cladding systems Al/DU-8Mo showed that there exists no significant difference between the non-polished and high polished aluminium specimens. The bond strength of failure mode 2 of the high polished aluminium compared to the bond strength of failure mode three of the non-polished aluminium is at the same level. The uncertainty of the bond strength of those test specimens with aluminium (polished and non-polished) as substrates is too high to estimate whether polishing the substrate improves the bonding between fuel and cladding in a significant way. Up to now, no real improvement by polishing the aluminium substrates can be stated. Al/Ti and Al/Nb specimens showed a mixed

behaviour. Failure of the specimens and of the adhesive occurred, with mode 1 being dominant. Al/Ti and Al/Nb did not reach the bond strength that the barrier/fuel specimens achieved. This result is mainly due to the different substrates. The aluminium used was a commercial product, AW-1050A with a purity of 99.5%. This aluminium foil was either 80 µm (non-polished) or about 450 µm thick. Al 1050 foils had not the same quality standard as the barrier substrates and were more sensitive to deformation. Ta, Ti, Zr and Nb substrates were of the same manufacturer with a thickness of 127 µm and a purity of 99.99%. Finally, DU-8Mo sputtered on the barriers niobium and tantalum showed the best results after the tensile tests. They did not fail in mode 1 and reached a high lower limiting value concerning their bond strength. It has to be emphasised that the maximum load is limited due to the bond strength of the adhesive. Therefore the real bond strength, although not measured in the tensile tests, is higher.
Similar tests were conducted at the INL [4], in examining the bond strength of monolithic specimens produced by HIP (hot isostatic pressing), TLPB (transient liquid phase bonding) or FSW (friction stir welding). For those tests the same adhesive EP-15 was used [5]. The following bond strengths were reported: FSW 6.42 MPa, TLBP 15.4 MPa and HIP 60.3 MPa, whereby in case of HIP an adhesive failure occurred. The sputtered specimens have a larger bond strength than the TLPB or FSW specimens. Compared to the HIP specimen the bond strengths reported in this work are more conclusive. More tests could be carried out and a more effective tensile test machine was available. In contrast to tensile tests of [4] a constant crosshead rate of the tensile test machine could be guaranteed for all bond strengths.

4. Summary

Tensile tests of fuel/cladding, fuel/barrier and barrier/cladding specimens were carried out in order to determine their bond strength. The tests revealed different results and failure modes. It has to be stated that the bond strengths of DU-8Mo on niobium and tantalum were the highest as no rupture of the specimen itself occurred and cohesive failure of the adhesive occurred on level of 70 MPa. A higher bond strength by using high polished substrates could not be proven. As some results varied considerably the sputtering process has to become more reproducible, the couple barrier system sputtered on DU-8Mo has to be tested and further tensile tests are necessary.

5. Acknowledgements

The authors thank Dr. Markus Hölzel and Martin Hirsch for fruitful discussions and technical assistance. This work was supported by a combined grant (FRM0911) from the Bundesministerium für Bildung und Forschung (BMBF) and the Bayerisches Staatsministerium für Wissenschaft, Forschung und Kunst (StMWFK).

6. References

[1] S. Dirndorfer, Tensile Tests on Monolithic two Metal Layer Systems for Research Reactor Fuels, Diplomarbeit, TU München, 2010.
[2] ASTM Designation: C 633 - 01 (Reapproved 2008), “Standard Test Method for Adhesion or Cohesion Strength of Thermal Spray Coatings,” West Conshohocken, USA (2008).
[3] W. Schmid, Sputtering as a Technique for Fuel Plate Production, to be published.
[4] D. E. Burkes, D. D. Keiser, D. M. Wachs, J. S. Larson, M. D. Chapple, Characterization of Monolithic Fuel Foil Properties and Bond Strength, Idaho National Laboratory (INL), March 2007.
[5] D. E. Burkes, Idaho National Laboratory (INL), private communication, 2009.

DEVELOPMENT OF QUALITY ASSURANCE METHODS FOR LOW ENRICHED FUEL ASSEMBLIES

N.E. WOOLSTENHULME*, G.A. MOORE, D.M. PEREZ, D.M. WACHS
Idaho National Laboratory
P.O. Box 1625, Idaho Falls, ID 83415 – USA
**Corresponding Author, Nicolas.Woolstenhulme@inl.gov*

ABSTRACT

As the Reduced Enrichment for Research and Test Reactors (RERTR) fuel development program has furthered the technology of low enriched uranium fuels, much effort has been expended to specify requirements, perform appropriate inspections, and to qualify experimental fuel plates and assemblies for irradiation. A great deal of consideration has been given to generate examinations and criteria that are both applicable to the unique fuel types being developed and consistent with industry practices for inspecting plate-type reactor fuel. Recent developments in quality assurance (QA) methodologies have given a heightened confidence in satisfactory fuel plate performance. At the same time, recommendations are given to further develop a system suitable for the testing and acceptance of production fuel elements containing low enriched uranium fuels.

1. Introduction

The RERTR program has been tasked with developing low-enriched uranium (LEU) nuclear fuels to be used in lieu of high-enriched uranium (HEU) fuels in research reactors worldwide [1]. Specifically, the RERTR Advanced Fuel Development project (RERTR-AFD) has developed LEU fuels with uranium densities that are high enough to enable the conversion of several high power research reactors. The RERTR-AFD project has developed uranium-molybdenum (U-Mo) alloy fuels in both dispersion and monolithic (i.e. foil) forms. As the RERTR-AFD project advances toward qualification of U-Mo fuels and subsequent technology transfer and commercial deployment, much effort has been expended to establish QA practices that are pertinent to these fuel types and consistent with current QA practices for plate-type reactor fuels.

Due to similarity in fabrication technique (i.e. powder blending, fuel core compacting, and cladding via roll bonding) anticipated changes in QA methodology will be minimal for those reactors able to convert using the U-Mo dispersion system. Monolithic fuels, however, differ somewhat in fabrication technique and other characteristics which directly affect QA methodology. Since the higher uranium density of monolithic type fuels will be required for conversion of five US High Power research Reactors (HPR) [1], careful examination of the current QA practices for these five reactors has been performed to avoid the establishment of techniques that are not sensible for commercial fabrication. Accordingly, this document is primarily focused on QA methods pertaining to monolithic type fuel plates.

Although the conversion of these high power research reactors will occur at least a few years from the current time, the institution of commercially suitable QA methods for LEU monolithic fuel assemblies is of immediate concern to the RERTR-AFD project due to the near term schedule of the RERTR Full-size Element (RERTR-FE) demonstration. The RERTR-FE demonstration will consist of the irradiation of driver fuel elements in Idaho National Laboratory's Advanced Test Reactor (ATR). RERTR-FE demonstration elements are planned to be identical to existing ATR driver fuel elements except that 11 of the 19 fuel plates will have LEU fuels cores in place of the current HEU aluminide dispersion fuel. The selected fuel type for use in RERTR-FE monolithic fuel plates is a monolithic foil composed

of U-10Mo (10wt% Mo), coated with a thin zirconium interlayer on both sides, and clad in aluminium alloy 6061 by Hot Isostatic Press (HIP) [2]. Current efforts to define commercially appropriate QA practices are tailored to this fuel system and fabrication process. Unlike any RERTR-AFD irradiation to date, the RERTR-FE demonstration will be performed in driver fuel reactor positions (as opposed to experiment positions) and the monolithic fuel will be required to "drive" the reactor. Consequently, RERTR-FE demonstration elements must conform to a QA system of equivalent rigor as is currently required for commercially produced driver fuel elements.

2. QA Methods

Due to close collaboration with the ATR, much of the QA methodology currently adopted by the RERTR-AFD project has been modelled after existing specifications for ATR driver fuel. Although the majority of QA specifications currently applied to RERTR-AFD experimental monolithic fuel plates are identical to those for ATR driver fuel, there are a few exceptions. These exceptions are primarily attributed to differences in fabrication scale (i.e. research vs. production), status of current technologies and data relating to monolithic fuels, and differences in the fuel type/fabrication method. Figure 1 provides a summary of the fabrication processes for both dispersion and monolithic type fuels. Figure 2 displays a summary of QA inspections and outputs correlating to each respective fabrication stage seen in Figure 1. More detailed information regarding these summaries can be found in references [3], [4], [5], and [6].

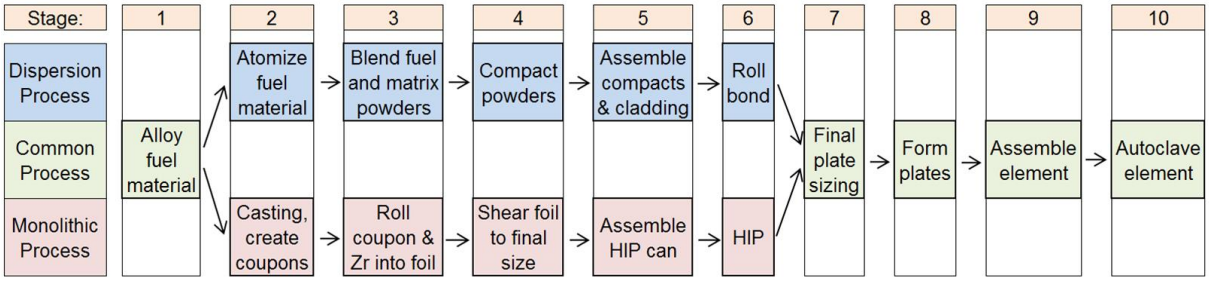

Figure 1: Fabrication Processes Overview

Stage	Dispersion Process	Monolithic Process
1	Isotopic and chemical compositions of feedstocks and alloys	
2	Particle size (sieve analysis)	Coupon dimensions
3	Certification of non-fuel powders	Certification of interlayer material
	Composition of blended powder	
4	Compact (billet) mass	Foil mass and dimensions
5	Certification of cladding materials	
6	Blister test	n/a
7	Immersion density for percent void	Bend test
	Plate dimensions, surface finish, and defects	
	Ultrasonic scan for minimum cladding thickness and bond quality	
	Radiography for stray fuel particles and fuel homogeneity	
	Plate cleanliness and radioactive contamination	
8	None	
9	Inspection and testing of swage joints and welds	
10	Boehmite thickness inspection	
	Element dimensions, surface finish, and defects	
	Element cleanliness and radioactive contamination	

Figure 2: QA Inspections and Outputs

A close look at the summaries in Figure 1 and Figure 2 reveals that monolithic and dispersion fuels differ only somewhat in fabrication and QA methods; particularly in plate and element processing stages. Notable differences occur predominantly in fuel preparation and processing stages (2 through 4) as well as stages 6 and 7. Several of these differences are likely to be inconsequential for industrial fabricators of monolithic LEU fuel. For example, dimensional inspection of cast coupons rather than sieve analysis of atomized powder will not require establishment of novel, complicated, or unproven QA inspections. Some differences, however, may prove to be noticeable departures from current industrial QA practices. These dissimilarities occur primarily in fabrication stages 4, 6, and 7 and are discussed in greater detail in section 3 of this paper.

It is also worth noting that a few deviations from industrial QA methods are practiced by the RERTR-AFD project due to differences in production scale and data evolution rather than fuel nature or fabrication techniques. Other deviations from industrial QA are due to the experimental nature of RERTR-AFD irradiations. For experimental irradiations there are safety driven upper fuel loading limits, but, since these experiments are not required to "drive" the reactor, there are no lower fuel loading limits. As mentioned earlier, upcoming RERTR-FE irradiations will use monolithic fuel in driver positions. Consequently, lower loading limits, as well methods to characterize uranium mass loading, are currently being established. It is also worth noting that radiography for fuel loading homogeneity (i.e. hot/cold spots) may be effectively performed on monolithic foils prior to encapsulation in cladding since the HIP process does not "form" the fuel core like roll bonding processes. This deviation in the sequence of inspection is not noted in Figure 2, but would allow for fabricators to reject suspect foils before further processing and may be of benefit.

3. Discussion and Recommendations

As the technology state of the monolithic LEU fuel departs from laboratory scale and approaches commercial deployment many of the deviations from conventional QA methods for plate type fuel will likely be rectified. For example, established fuel systems, such as the HEU aluminide currently used in the ATR, are fabricated by established formulas via qualified processes [6]. As the processing parameters necessary to produce qualified monolithic fuels become more mature then inspections may be augmented with process controls. In some cases, this will enable inspections to be performed on a statistical sampling basis whereas RERTR-AFD experimental fuel plates are currently qualified on a 100% inspection basis. For example, HIP processing parameters such as time, temperature, and pressure will likely be established as part of a qualified process in a production setting.

The same will be true of QA practices currently driven by incomplete data set for monolithic fuel. As the data set for monolithic LEU fuel approaches completeness, distinct criteria may be deployed. For example, ultrasonic testing (UT) for bond quality on RERTR-AFD plates currently enforces no specific criteria for acceptance over monolithic foils due incomplete data [5]. However, much UT data, such as average signal attenuation through fuel, has been obtained for monolithic fuel plates during recent RERTR-AFD irradiation campaigns. Corresponding criteria will likely be deployed in forthcoming specifications.

Another example of incomplete monolithic data relates to fuel plate forming. The majority of the HPR's that will require monolithic fuel for conversion use fuel plates which are formed to specific curvatures. Current commercial fuel plate qualification processes use UT inspection of fuel plates to determine bond quality and minimum cladding thickness when the fuel plate is in the flat, or pre-formed, condition. Due to the presence of U-Mo foils, the mechanical behaviour of monolithic fuel plates differs somewhat from dispersion fuel plates. As a result, phenomena regarding monolithic fuel plate behaviour under forming (i.e. bending stress) have not yet been entirely quantified. Upcoming RERTR-AFD irradiations will test monolithic fuel plates in curved arrangements [7]. Additionally, fabrication of a UT scanner capable of inspecting curved fuel plates is underway. It is not anticipated that forming will have a

deleterious effect on monolithic fuel plates and that UT of these plates for QA purposes in the flat condition will be sufficient. UT inspection of formed plates will likely elucidate this matter. It is also acknowledged that future RERTR-AFD irradiation will incorporate burnable poisons, such as boron carbide, into monolithic fuel plates. QA methodology for burnable poison homogeneity in monolithic fuel plates will likely be addressed as it is now; by process qualification and intermittent destructive examination of fabricated fuel plates.

As mentioned previously, a handful of QA practices and inspection techniques are unlike industrial practices due to the nature of the monolithic fuel and fabrication methods. These practices have received particular attention in preparation for the RERTR-FE irradiations. The first such item involves massing the fuel core of each plate. In conventional dispersion fuels the matrix, fuel, and poison powders are massed, blended, and compacted before encapsulation in cladding. This method allows for direct measurement of the mass of the fuel material which, in conjunction with chemical and isotopic analysis of fuel materials, can be used to determine uranium 235 (U-235) masses in the fuel plates. In the monolithic system, cast U-Mo coupons are formed into raw monolithic foils and bonded to Zr interlayers as part of the same rolling operation. These raw foils are then sheared to final size and massed. Consequently, the final foil weight cannot be obtained until the thin Zr interlayers are bonded to the U-Mo; making it impossible to mass the U-Mo alone.

Since tolerances for U-235 mass loading can be as rigorous as ± 1% for HPR's [6], it is recommended that a suitable method for inspecting the mass of monolithic fuel cores be established. One such method may involve the use of microscopy to establish the average Zr interlayer thickness based on initial thicknesses, rolling reduction schedule, and other pertinent variables. These thicknesses may then be used to calculate the portion of the monolithic foil mass that is U-Mo. Another method may involve performing immersion density measurements on each monolithic foil, prior to HIP operations, in order to obtain foil volume. This volume may be used, in conjunction with the known physical densities of U-Mo and Zr, to calculate the portion of the monolithic foil mass that is U-Mo. At the present time, immersion density is performed on production HEU dispersion fuel plates to assess void density. Void density measurement will not likely be required for commercially produced monolithic plates, but a similar inspection may be implemented on the foils themselves to quantify foil volume. In either case, chemical and isotopic analysis of U-Mo material may then be used to determine the U-235 mass.

Currently, fuel plates for HPR's are bonded and formed to final thickness by roll bonding; giving a surface finish typical of rolling processes. For monolithic plates, the current fabrication scheme involves machining fuel plates to final thickness. Subsequent to either of these processes, fuel plates are chemically cleaned and treated in an autoclave to create a corrosion resistant aluminium oxide layer in the form of boehmite. Although the surface finish of machined plates can meet current HPR specifications for average roughness, laboratory inspections of the boehmite layer thickness via eddy current instrumentation have shown some sensitivity to different kinds of surface finish (i.e. rolled vs. machined). It is recommended that this matter be investigated more fully and that appropriate standards be developed for machined monolithic fuel plates.

Another concern regarding proposed monolithic QA practices is the practice of blister annealing. Blister annealing is performed on dispersion type plates by holding the plates at an elevated temperature for a prescribed amount of time in order to form raised areas on the plate (blisters) due to the coalescence and expansion of entrapped gases [4]. It has been shown that blister annealing is detrimental to monolithic fuel plates due primarily to differences in thermal expansion coefficients between aluminium 6061 cladding and U-Mo foils, causing two-dimensional out-of-plane bending [8]. It is also proposed that blister annealing treatments are not applicable to HIP'ed monolithic fuel types due to lack of porosity in the fuel core and degas/evacuation steps associated with the HIP method. For this reason, it is recommended that commercial QA regimes for monolithic fuel do not

enforce blister anneal treatments. This recommendation however, will leave something of a schism in the current HEU QA system. It is worth mentioning that, unlike existing industrial HEU QA processes, bend tests are performed on excess cladding strips which are removed from RERTR-AFD experimental fuel plates during final plate sizing [5]. In some ways, this test may be used to compensate for the proposed elimination of blister anneal testing as it is easily performed and can be an effective determination of clad-to-clad bond strength. However, bend testing may not be a suitable substitution for blister annealing in commercial monolithic QA practices since it is a destructive test that cannot be performed on actual plates and it does not inspect for clad-to-fuel bond quality.

For the above reasons, it is recommended that future commercial QA processes for monolithic fuels adopt 100% UT inspection for bond quality on all fuel plates (as opposed to partial scan). It has been shown that UT inspection is capable of detecting bonding defects typical of the monolithic system without blister annealing treatments [8]. Substituting blister annealing with more rigorous UT inspection will likely require investigation of UT methodology and acceptance criteria with particular attention given to monolithic type plates. These considerations might include phenomena such as pronounced edge effect, signal attenuation through monolithic foils, and kissing bonds at bonding surfaces (i.e. bonds that adequately transmit UT signal but are not effectively bonded). In regard to the latter, some research has been performed to non-destructively characterize kissing bonds with ultrasonic techniques [9], [10]. It is recommended that similar techniques be investigated and put into practice as appropriate in the QA methodology of monolithic fuel plates.

4. References

[1] D.A. Wachs, C.R. Clark, R.J. Dunavant, “Conceptual Process Description for the Manufacture of Low-Enriched Uranium-Molybdenum Fuel,” http://www.osti.gov/, February 2010.

[2] M.D. Cook, J.M. Wight, N.E. Woolstenhulme, “Demonstration Control Plan for the RERTR Full-size Element”, INL Internal Document.

[3] “Greenfield Alternative Study LEU-Mo Fuel Fabrication Facility”, www.inl.gov/technicalpublications/Documents/4074868.pdf, January 2010.

[4] J.M. Wight, G.A. Moore, S.C. Taylor, N.E. Woolstenhulme, and S.T. McCormick, “Testing and Acceptance of Fuel Plates for RERTR Fuel Development Experiments,” Proceedings of the RERTR-2008 International Meeting, Washington D.C., USA, October 5 - 9, 2008.

[5] J.M. Wight, N.E. Woolstenhulme, “Fuel Plate Specification for RERTR 11 & 12 Fuel Irradiations in the ATR”, January 2010, INL Internal Document.

[6] “Specification For Advanced Test Reactor Mark VII Zone Loaded Fuel Elements, IN-F-9-ATR, Revision 17” November 2005, INL Internal Document.

[7] D.M. Wachs “RERTR Fuel Development and Qualification Plan,” http://www.osti.gov/, February 2010.

[8] D.M. Wachs, A.M. Phillips, E.L. Shaber, B.H. Rabin, C.R. Clark, A.B. Robinson “RERTR-10A Experiment Discussion” , February 2010, INL Internal Document.

[9] S.E. Kruger, M. Lord, D. Levesque, and A.J. Bakker, “Detection of Kissing Bond in Extruded Aluminum by Laser-Ultrasound,” Review of Quantitative Nondestructive Evaluation, Vol. 27 2008, American Institute of Physics.

[10] T. Kundu, A. Maji, T. Ghosh, K. Maslov, “Detection of kissing bonds by Lamb waves,” Ultrasonics 35 (1998) 573-580.

IN CORE INSTRUMENTATION FOR ONLINE NUCLEAR HEATING MEASUREMENTS OF MATERIAL TESTING REACTOR

C.REYNARD, J. ANDRÉ, J. BRUN, M.CARETTE, A. JANULYTE, O. MERROUN, Y ZEREGA

Laboratoire Chimie Provence LCP UMR 6264 – University of Provence
Centre St Jérôme, Avenue Escadrille Normandie-Niemen bât Madirel,
13397 Marseille cedex 20, France

A. LYOUSSI, G. BIGNAN, J-P. CHAUVIN, D. FOURMENTEL, W. GLAYSE, C. GONNIER, P. GUIMBAL, D. IRACANE, J-F VILLARD

Commissariat à l'Energie Atomique CEA Direction de l'Energie Nucléaire
Centre de Cadarache, 13108 Saint-Paul-Lez-Durance, France

E-mail: abdallah.lyoussi@cea.fr or christelle.carette@univ-provence.fr

Keywords: Gamma heating, Calorimetry, neutron and gamma measurements, Material ageing, MTR

ABSTRACT

The present work focuses on nuclear heating. This work belongs to a new advanced research program called IN-CORE which means "**I**nstrumentation for **N**uclear **r**adiations and **C**alorimetry **O**nline in **RE**actor" between the LCP (University of Provence-CNRS) and the CEA (French Atomic Energy Commission) - Jules Horowitz Reactor (JHR) program. This program started in September 2009 and is dedicated to the conception and the design of an innovative mobile experimental device coupling several sensors and ray detectors for on line measurements of relevant physical parameters (photonic heating, neutronic flux …) and for an accurate parametric mapping of experimental channels in the JHR Core.

The work presented below is the first step of this program and concerns a brief state of the art related to measurement methods of nuclear heating phenomena in research reactor in general and MTR in particular. A special care is given to gamma heating measurements. A first part deals with numerical codes and models. The second one presents instrumentation divided into various kinds of sensor such as calorimeter measurements and gamma ionization chamber measurements. Their basic principles, characteristics such as metrological parameters, operating mode, disadvantages/advantages, ... are discussed.

1. Context

The growing of the energy needs due to the increasing world population associated to the fast development of large emerging countries and coupled to environmental challenge dedicated to the reduction of greenhouse gas production has contributed to the acknowledgement of the nuclear energy.

In Europe this kind of energy corresponds already to an important part of the energy mix. But an improvement of the performances of nuclear power reactors is constantly required. For instance concerning the existing Generation II reactors, the question of their lifespan represents a real interest as well for safety as economical stake. Consequently, the increasing of their lifetime requires research works focusing in particular on their structure materials. The scientific aims are to better understand and to anticipate behavior of these materials under nuclear irradiation in order to determine their durability and to reach their optimization.

Experimental studies on accelerated ageing of materials are carried out by means of MTR (Material Testing Reactor). The existing European MTRs, such as OSIRIS in France, BR2 in Belgium, or Halden in Norway were built principally in the sixties. Consequently they are ageing and new MTRs with higher performances are necessary. The construction of Jules Horowitz material testing Reactor (JHR) is registered in this context [1]. This MTR will succeed OSIRIS. It will be a major European research infrastructure to perform screening, qualification and safety experiments on material and fuel behaviour under irradiation for the

coming decades [2, 3]. It will contribute to the safety studies and to the optimization of existing or coming nuclear power reactors as well as the developments of the future ones (Generation IV reactor). The JHR core will offer specific experimental operating conditions such as high fast neutron flux to study structural material ageing and high thermal neutron flux for fuel experiments. The JHR will allow typically ~ 20 simultaneous experiences in the core and in the reflector. As of the beginning, the first experiments in the JHR will have to be performed with a high level of quality under new severe conditions. This high level will be obtained only if different criteria are respected.

For instance, the first one concerns the online monitoring of the operating conditions. A real time measurement of these conditions with lowest possible uncertainty will lead to enhance accuracy and contribute to make signal interpretation more comfortable. . Then the second one deals with the ability to perform specific experimental conditions such as thermal conditions in order to avoid the influence of complex physical phenomena interferences on the experimental setup . Thus quantifying nuclear heating and especially gamma heating is of a great importance in order to design the thermo-hydraulic system, the shielding materials and structures of the reactor and of the experimental device housing the experimental load according to safety requirements and according the aim to control the temperature gradient or the stationary temperature of samples during irradiation processes.

Consequently to reach this high level targeted which will guarantee the scientific quality of the conducted research programs, new experimental devices have to be designed including innovative instrumentation and associated advanced measurement methodologies[4]. According to this a new advanced research program between the LCP (University of Provence-CNRS) and the CEA (French Atomic Energy Commission) - Jules Horowitz Reactor (JHR) program deals with such scientific and technological challenge. This program called IN-CORE (Instrumentation for Nuclear radiations and Calorimetry Online in REactor) will lead to an innovative mobile device focusing to the online parametric mapping of the JHR core channels. The device will be composed by several sensors dedicated to measurements of relevant physical parameters (photonic heating, neutronic flux …).

Actually in-pile instrumentation in MTRs concerns the measurements of temperature (thermocouples), dimensions (LVDT, strain gauges, hyper frequency resonant cavities), fission gas release (pressure sensor or analytical devices in laboratory), neutron flux (self powered neutron detectors, fission chambers) and gamma heating (calorimeter and gamma thermometers) [5].

In this paper we focus especially on one of relevant parameters: nuclear heating. The origin of nuclear heating will be described. Recent numerical works will be discussed. And finally, a brief state of the art related to direct and indirect measurement methods of nuclear heating phenomena in research reactor in general and MTR in particular such as calorimetry, gamma thermometer measurements, gamma ionization chamber measurements will be presented.

2. Nuclear heating and numerical models

A nuclear reactor core is a place to a wide variety of nuclear reactions such as interactions of neutrons and radiations with matter. Each interaction releases an important quantity of energy that appears mainly in kinetic energy of product particles and emission of gamma rays. This energy can be absorbed locally by charged particles or transported by neutron-photons offsite of reactions and deposited in shielding material. The energy lost is transformed into thermal energy called nuclear heat. The largest part of nuclear heating of irradiated samples in a reactor core is due to gamma rays. They are created mainly by fission, capture and inelastic neutron interactions with various target nuclides. The induced gammas interact with matter via three principal modes of interaction: i) photo-electric, ii) Compton and iii) pair production effects. Thus, they communicate their energy to electrons of the medium which cede this energy in matter by ionization and excitation. This phenomenon contributes to heating which causes the temperature rises of the material exposed to radiations. This depends essentially on the materials constituting the samples and the radiation intensity to which they are exposed [6].

The process of calculating gamma heating is based firstly on determining the different gamma rays sources and the associated produced electrons following their interactions with matter. Secondly, one should determine the gamma flux by resolving the Boltzmann particle transport equation. The transport of electrons can be neglected if geometrical dimensions of the problem studied are larger than electron mean free path [7]. Hence, their energy is calculated at the place of their creation. Knowing that gamma heating level is proportional to gamma flux, the gamma heating rates can be obtained by multiplying gamma-ray flux by KERMA factor which represents the ratio between the energy deposited, in a given material, of incident and outgoing gamma rays. Various numerical codes or models are developed to accurately determine gamma heating as the Monte Carlo radiation transport codes: MCNPX [8] and TRIPOLI [9] and could be improved with local experimental data or the point kernel approach used in the MERCURE-5 code and the GHRRC code developed to estimate the gamma heating of small samples inside the GRR-1 research reactor core [10].

However, whatever the approach and the physical model approximation of the particle transport used, heating simulation constitutes a difficult task because various key parameters affect the computational results. Uncertainties can be induced by variance and statistics of Monte Carlo calculations but important uncertainties (about 30% (2σ)) are coming from the gaps, or the gamma emission data present in the libraries of basic nuclear data [11]. Furthermore the omission of some heating mechanisms as the case of the study done by Varvayanni can affect rigorously results [10]. In other to specify and quantify these uncertainties, a set of experimental programs have been conducted for gamma heating measurements as ADAPh in the EOLE and MINERVE critical assemblies at the CEA Cadarache facility [11]. Different TLD and micro-ionization chamber for measuring the integral prompt and delayed gamma ray dose have been used in the UO2 core of MINERVE research reactor. Monte Carlo computational results obtained via TRIPOLI4-PEPIN2 are underestimated in comparison to measurements due to the lack of information concerning the data libraries used for gamma-ray emission. A Bayesian method of adjustment has been developed in order to re-estimate the principal components of the gamma heating. The studies made in this context, and detailed in the references [11, 12], seems to be promising and enhancing the possibility to reduce significantly the uncertainties on the determination of the gamma heating from 30% to 15% (2σ).

Consequently, the constant improvement in modeling and simulation coupled to the requirements of new irradiation programs dedicated to fuel or material behavior characterization for various reactors (HTR [13], Gen IV systems, fusion [14]) leads to a need of a high-quality in-pile instrumentation.

3. Nuclear heating Instrumentation and measurement methods

In the future Jules Horowitz Reactor in order to reduce the uncertainties in the knowledge of the experimental conditions, a selection of the most appropriate sensors for neutron and nuclear heating measurements is necessary, as well as an improvement of their performances. Nuclear heating can be measured by different methods : direct method such as calorimetry, gamma thermometer and indirect method such as gamma and neutron measurements by ionization chambers. The direct measurement of the nuclear heating in the most powerful research reactors relies on the use of calorimeters.

3.1 Calorimetry

Since many years calorimetry has become a technique usually employed. On one hand for example, old scientific journals decide to change or extend their title to show their growing interest in calorimetry such as the journal created in 1969 under the name "Journal of Thermal Analysis," which in 1998 became "Journal of Thermal Analysis and Calorimetry"[15]. On the other hand various developments and research about calorimetry are performed in many different scientific fields in addition to the nuclear field such as

chemistry, medicine or pharmacology for the determination of thermodynamic parameters or characterization of physical phenomena [16, 17, 18].

In nuclear sciences and technologies Gunn divided radiometric calorimetry in four categories such as *radionuclide calorimeters*, *beam calorimeters*, *local absorbed dose calorimeters*, and *in-reactor calorimeters* [19, 20, 21]. The fourth category is devoted to studies of energy deposition in specific samples for engineering purposes of structural materials [22,23] or for local measurements of nuclear heating in reactor.

This paper section discusses this fourth category.

In nuclear reactor environment the instrumentation design is directly impacted by specific properties in addition to usual metrological characteristics such as sensitivity, low uncertainty. One of the important specific characteristic imposed by the restricted available space is the sensor compactness. In-pile calorimeters must have low dimensions (a few centimeter diameter in general) contrary to large volume calorimeters developed for radioactive element quantification such as tritium especially used in the military nuclear activities [24]. Consequently the calorimeter has also a simple robust design with few cables. In fact the calorimeter can be composed by a single cell (a core containing the material sample, a jacket and sometimes shields) [20, 22, 25] or by a twin cell (a body containing a sample cell and an empty identical cell with or without a pedestal) [21]. The sample choice leads directly to the sensor selectivity (for example graphite) because according to the core material, a specific separation of neutron- and gamma- effects (nuclear heating, gamma heating (mostly) or neutronic heating) is possible.

The robustness and the reliability lead to the choice of an operating mode not requiring an auxiliary system or complex electronic supporting radiations. Various operating modes exist such as adiabatic mode, permanent mode, [21, 26]… but the adiabatic one is more complicated to be implemented because it needs a pumping system to ensure a high vacuum in the inner volume to reach a good thermal isolation. Moreover with this kind of mode a lower power range can be tested by performing instantaneous measurements. Thus the heat flow operating mode based on heat transfers between the radiation absorber sample and its surroundings is preferred [22]. In fact the main calorimeters used in MTRs are pseudo-adiabatic calorimeters which have the advantage of small sizes and easy implementation (So-called Gamma-Thermometers belong to this category) and the differential calorimeters (discussed in the following paragraph).

The last characteristic presented is the simplicity of the measurement method to determine the nuclear heating. On one hand, the energy deposited in the sample is determined by measuring its temperature rise with only thermocouples embedded in specific location. On second hand the calorimeter allows abstaining of the different constant's employment, hardly determinable such as thermal resistance and the nuclear heating can be determined straightforwardly thanks to an electrical calibration curve (for example a second order polynomial curve which occurs when convective and radiative heat transfers increase [22]). The heat transfer of the calorimeter under the irradiation condition is simulated with an electric heating. The relationship between the temperature difference versus the heating power due to Joule effect is used to define the nuclear heating from the temperature difference measurement during the irradiation. In the case of a differential calorimeter based on the differential measurement of the heating in a twin cell, the signal delivered can be directly proportional to the nuclear heating in the sample. Another advantage of a differential calorimeter consists on the uncertainty reduction or a sensitivity improvement. Its accuracy can be even increased by using in-situ calibration with miniaturized electric heaters. These kinds of calorimeters are largely used in MTRs for nuclear heating measurements up to 15 W/g.Another calibration method can be based on a heating curve corresponding to the irradiated step and on a cooling curve corresponding to the calorimeter removal [25

Figure 1: assembly of a differential calorimeter used in OSIRIS reactor for nuclear heating measurements (external diameter is about 20mm)

3.2 Ionisation Chambers

Intense neutron flux can be measured online in MTRs using Self Power Neutron Detectors (SPND) or fission chambers.

An SPND is made of a cylindrical emitter (for example in rhodium, cobalt, silver, vanadium, etc.) surrounded by an electric insulation (for example alumina) and a metallic body, which acts as collector. The dominant process in SPNDs is the neutron induced generation of high-energy electrons in the emitter that cross the insulator, resulting in an externally measurable current between emitter and collector. Depending on the material chosen of the emitter, a distinction between two kinds of SPNDs can be made:

- prompt SPNDs, in which neutron capture gammas generate Compton and photoelectric effects,
- delayed SPNDs, in which neutron capture generates short-lived isotopes emitting βrays.

Figure 2: rhodium SPND for thermal neutron flux measurements (external diameter is 3mm)

A fission chamber is an ionisation chamber designed for the detection of neutrons by their interaction with a solid fissile material. Most commonly, a cylindrical construction is used where the fissile material is applied as a coating on one (or both) electrodes contained in a selected filling gas. In operation, a bias voltage (in the order of hundreds of volts) is applied to the electrodes. Neutrons induce fissions in the fissile material and the high energy ionising fission products result in the generation of an electric signal between the electrodes, which is, in first approximation, linear with the neutron flux level.

Different operating modes can be used for fission chambers. Among them, the Campbelling mode or Mean Square Voltage (MSV) mode allows to minimize the gamma background contribution in the signal [27].

Figure 3: sub-miniature fission chamber (external diameter is 1.5mm)

Among the recent progresses in the field of neutron measurement, one can notice the development of a unique instrumentation for the online determination of the fast neutron flux, using a miniature fission chamber with ^{242}Pu deposit and a specific data processing [28], [29,30].

4. Conclusion

Finally, main and central aim of IN-CORE project is a better assessment of the neutron and photon contributions in the nuclear heating in MTRs. Consequently, the instrumentation and measurement methodologies to be used in this program should allow to perform the online and simultaneous determination of nuclear heating, gamma flux, but also fast and thermal neutron flux. Different kinds of usual or innovative sensors will be selected and combined in a scanning system. This system coupled with an appropriated analytical approach of data analysis provided by direct and indirect measurements will improve the knowledge of the experimental conditions in the future Jules Horowitz Reactor and hence reducing uncertainties and enhancing accuracy of physical relevant parameters.

5. References

1. Materials subjected to fast neutron irradiation,Jules Horowitz Reactor: a high performance material testing reactor, D. Iracane, P. Chaix, A. Alamo, C. R. Physique 9 (2008) 445–456
2. Experimental material Irradiation in the Jules Horowitz Reactor, S. Carassou, G. Panichi, F. Julien, P. Yvon, M. Auclair, S. Tahtinen, P. Moilanen, S. Maire, L. Roux, TRTR-2005 / IGORR-10 Joint meeting, September, 12-16, 2005
3. Neutronic study regarding transmutation fuel research at Jules Horowitz Reactor, T. Stummer, Y. Peneliau, C. Gonnier, Research Reactor Fuel Management (RRFM) Transactions 2009
4. Developments status of irradiation devices for the Jules Horowitz Reactor, C. Gonnier, D. Parrat, S. Gaillot, J.P. Chauvin, F. Serre,G. Laffont, A. Guigon, P. Roux, Research Reactor Fuel Management (RRFM) Transactions 2008
5. Innovative in-pile instrumentation developments for irradiation experiments in MTRs, J-F. Villard, IGORR 2005
6. Ibrahim, M.A., 2002. Heat generation and corresponding rise in temperature due to absorption of thermal neutrons in several shielding materials. Annals of Nuclear Energy, 29 : 1131–1136
7. Development and validation of gamma-heating calculational methods for plutonium-burning fast reactors. Anton LÜTHI, 1998. Doctoral thesis. Ecole polytechnique federal de Lausane.
8. MCNPX, April 2008. 3-D Monte Carlo radiation transport code. Los Alamos National Laboratory.
9. T. TRIPOLI: A general Monte Carlo code, present state and future prospects, Nimal, J.C., Vergnaud, Progress in Nuclear Energy. 24, 195-200.
10. A point kernel model for the energy deposited on samples from gamma radiation in a research reactor core, Varvayanni, M., Catsaros, N., Antonopoulos-Domis, M., 2008. Ann. Nucl. Energy 35, 2351–2356.
11. Qualification of a gamma-ray heating calculation scheme for the future Jules Horowitz material testing reactor (RJH), Blanchet, D., Huot, N., Sireta, P., Serviere, H., Boyard, M., Antony, M., Laval, V., Henrard, P., 2008. Ann. Nucl. Energy 35, 731–745.
12. Développement méthodologiques et qualification de schémas de calcul pour la modélisation des échauffements photoniques dans les dispositifs expérimentaux du futur réacteur d'irradiation technologiques Jules Horowitz (RJH). Blanchet, D. Doctoral thesis. June 2006. Université Blaise Pascal.
13. Nuclear heating measurements for SS-316, copper, graphite, tungsten, chromium, beryllium in a copper centered assembly bombarded with 14 MeV neutrons and analysis, Y. Ikeda, F. Maekawa, M. Wada, Y. Kasugai, C. Konno, Y. Uno, A. Kumar, M.Z. Youssef b, M.A. Abdou, Fusion Engineering and Design 42 (1998) 289–297
14. Graphite irradiation testing for HTR technology at the High Flux Reactor in Petten J.A. Vreeling , O. Wouters, J.G. Van Der Laa, Journal of Nuclear Materials 381 (2008) 68–75
15. 40-years anniversary, Simon, J. (2009), *Journal of Thermal Analysis and Calorimetry* 95(1), 3.
16. A survey of the year 2007 literature on applications of isothermal titration calorimetry, Bjelic, S. & Jelesarov, I. (2008), *Journal of Molecular Recognition* 21(5), 289--312.
17. Application des microcalorimètres aux mesures thermiques, L. Élégant, J. Rouquerol, R3010 Techniques de l'Ingénieur.
18. A review of analytical applications of calorimetry, H.F. Fergusona, D.J. Fruripb, A.J. Pastorb, L.M. Peereyb, L.F. Whitingc, Thermochimica Acta 363 (2000) 1-21
19. 'Radiometric calorimetry: A review', Gunn, S. (1964), *Nuclear Instruments and Methods* 29(1), 1 - 24.
20. 'Radiometric calorimetry: A review (1970 supplement)', Gunn, S. (1970), *Nuclear Instruments and Methods* 85(2), 285 - 312.

21. 'Radiometric calorimetry: A review: 1976 supplement', Gunn, S. (1976), *Nuclear Instruments and Methods* 135(2), 251 - 265.
22. Measurements of Nuclear Heating Rate and Neutron Flux in HANARO CN Hole for Designing the Moderator Cell of Cold Neutron Source, M-S. Kim, S-Y. Hwang, H-S.Jung and K-H. Lee, Proceedings of IGORR 2005
23. Benchmark of heat deposition measurement techniques in the SAFARI-1 reactor using MCNP5, B.M Makgopa, M. Belal, Research Reactor Fuel Management (RRFM) Transactions 2009
24. Mathonat, C.and Mauger, J. (2007), *Large volume and high sensitivity calorimetry for nuclear materials investigations*. ESARDA
25. Simulation of the In-Core Calorimeter Experiment in the SAFARI-1 Reactor, B.M Makgopa, M. Belal, ANIMMA International Conference, 7-10 June 2009, Marseille, France
26. Differential calorimeter based on the heat leak principle. Biltonen et al. March 1981. US Patent References: 4255961.
27. Experimental Verification of the Fission Chamber Gamma Signal Suppression by the Campbelling Mode, *L. Vermeeren, M. Wéber, L. Oriol, S. Breaud, P. Filliatre, S. Normand, B. Lescop*, ANIMMA 2009 Conference, Marseille, June 7-10 2009
28. Innovations for in-pile measurements in the framework of the CEA-SCK•CEN Joint Instrumentation Laboratory, J-F Villard, M. Schyns., ANIMMA 2009 Conference, Marseille, June 7-10 2009.
29. Reasons why Plutonium 242 is the best fission chamber deposit to monitor the fast component of a high neutron flux *P. Filliatre a,c,_, L. Oriol a,c, C. Jammes a,c, L. Vermeeren,* Nuclear Instruments and Methods in Physics Research A 593 (2008) 510– 518
30. Joint estimation of the fast and thermal components of a high neutron flux with a two on-line detector system, P. Filliatre, L. Oriol, C. Jammes, L. Vermeeren, Nuclear Inst. and Methods in Physics Research, A, 603 (3), p.415-420, May 2009

European Nuclear Society

Rue Belliard 65, 1040 Brussels, Belgium
Telephone +32 2 505 30 54, Fax + 32 2 502 39 02
rrfm2010@euronuclear.org - www.euronuclear.org